A TUNED MASS DAMPER DESIGN BASED ON EDDY CURRENT DAMPING

BURGAÇ AKIMI İLE SÖNÜMLEMEYE DAYANAN BİR AYARLI KÜTLE SÖNÜMLEYİCİ TASARIMI

YUNUS GÖKHAN SAK

ASSOC. PROF. DR. BİLSAY SÜMER

Supervisor

Submitted to

Graduate School of Science and Engineering of Hacettepe University

as a Partial Fulfillment to the Requirements

for the Award of the Degree of Master of Science

in Mechanical Engineering

September 2023

ABSTRACT

A TUNED MASS DAMPER DESIGN BASED ON EDDY CURRENT DAMPING

Yunus Gökhan SAK

Master of Science Degree, Department of Mechanical Engineering

Supervisor: Assoc. Prof. Dr. Bilsay SÜMER

June 2023, 76 Pages

All dynamic structures encounter vibration during their operation. A structure experiences the vibration load in an amplified manner at structure's natural frequencies. If the amplitude of vibration load is high enough, this may damage the structure. Tuned mass dampers (TMD's) are one of the passive vibration control methods to prevent mechanical failure.

A TMD, which has good applicability in space applications, is designed in this study. Reliability is chosen as the key concept of the design since the TMD is going to operate at space, where maintenance is not an option. A literature survey is carried out to find the best concept for the application. It is found that a passively controlled classical TMD with eddy current damping (ECD) mechanism is the best candidate for the application.

In ECD, a permanent magnet which moves in proximity of a conductive material creates eddy currents within the conductor. These eddy currents create electromagnetic force on the magnet and this force tries to counter act to the motion of the magnet. Therefore, damping is achieved which is analogues to the viscous damping. ECD is created by placing a permanent magnet inside of a conductive tube in this thesis.

After the system architecture of the damping mechanism is determined, analytical model of the TMD is prepared. This model consists of mass, damping coefficient and stiffness of the TMD. It is found in the literature that as the frequency of the excitation increases, damping coefficient of the ECD decreases. This phenomenon is called as the skin effect. A dynamic damping coefficient model which includes the skin effect is found. Although the effect of the skin effect on the ECD is known, it seems that there is no detailed study related to couple the skin effect with the damping coefficient in a scenario where a magnet is moving inside of a conductive tube.

In order to observe the effect of the TMD, a test structure is required in which the dynamic characteristics around its natural frequency are to be controlled. This structure is chosen to be a simple cantilever beam which has a rectangular cross section. Fundamental natural frequency of this cantilever beam is chosen to be controlled. Analytical model of this cantilever beam is prepared. Then, coupling of the TMD and cantilever beam is modeled to simulate the assembly of the TMD to the cantilever beam. Afterwards, response of this system is modeled. In order to observe the effects of the TMD, response of the cantilever beam alone is also modeled. These responses are modeled under a harmonic sweep forcing excitation.

The design of the TMD is optimized to have maximum ECD possible. After the design of the TMD, two dedicated experimental setups are designed to measure steady-state damping coefficient and the system response. It is shown that the experimental results are found to be consistent with respect to theoretical results. Therefore, it can be concluded that a TMD based on ECD was successfully designed, analyzed and tested.

Keywords: Tuned Mass Damper, Electromagnetic Damping, Eddy Current Damping, Passive Vibration Control

ÖZET

BURGAÇ AKIMI İLE SÖNÜMLEMEYE DAYANAN BİR AYARLI KÜTLE SÖNÜMLEYİCİ TASARIMI

Yunus Gökhan SAK

Yüksek Lisans, Makine Mühendisliği Bölümü

Tez Danışmanı: Doç. Dr. Bilsay SÜMER

Haziran 2023, 76 Sayfa

Tüm dinamik yapılar faaliyetleri sırasında titreşime maruz kalırlar. Yapı doğal frekanslarında uygulanan titreşim yüküne artırılmış olarak maruz kalır. Bu artırılmış titreşim yükünün seviyesi yeteri kadar yüksekse, bu durum yapıya zarar verebilir. Ayarlı kütle sönümleyiciler (AKS) mekanik arızayı önlemek için kullanılan pasif titreşim kontrol yöntemlerinden biridir.

Bu çalışmada uzay uygulamaları için uygulanabilirliği olan bir AKS tasarlandı. Uzay ortamında bakım çalışmaları mümkün olmayacağı için AKS tasarımında anahtar konsept olarak güvenilirlik seçildi. Bu kapsamda en iyi konseptin bulunması için literatür araştırması yapıldı. Pasif olarak kontrol edilen ve burgaç akımı ile sönümlemeye (BAS) dayanan AKS'nin en iyi aday olduğu görüldü.

BAS konseptinde iletken bir malzemenin yakınında hareket eden bir kalıcı mıknatıs iletken içinde burgaç akımlarının oluşmasını sağlar. Bu burgaç akımları mıknatıs üzerinde elektromanyetik kuvvet yaratır ve bu kuvvet mıknatısın hareketini durduracak şekilde etki gösterir. Bu şekilde viskoz sönümlemeye benzer sönümleme elde edilir. Bu tezde BAS kalıcı bir mıknatısın iletken bir tüp içine yerleştirilmesi ile elde edilmiştir.

Sönümleme mekanizmasının sistem mimarisinin belirlenmesinin ardından AKS'nin analitik modeli hazırlandı. Bu model AKS'nin kütle, sönümleme katsayısı ve sertliğini içermektedir. Literatürde uyarımın frekansı arttıkça BAS'nin sönümleme katsayısının azaldığı bulundu. Buna sebep olan fenomen deri etkisidir. Deri etkisini içeren dinamik bir sönümleme katsayısı modeli bulundu. Deri etkisinin BAS üzerindeki etkisi bilinmesine rağmen, mıknatısın iletken tüp içinde hareket ettiği bir senaryoda sönümleme katsayısı ile deri etkisini ilişkilendiren detaylı bir çalışma bulunamamıştır.

AKS'nin etkisini gözlemleyebilmek için doğal frekansı civarındaki dinamik karakteristik özelliklerinin AKS tarafından kontrol edileceği bir test yapısı gerekmektedir. Bu yapı olarak dikdörtgen bir kesite sahip olan basit bir konsol kiriş seçildi. Bu konsol kirişin ilk doğal frekansının kontrol edilmesi belirlendi. Konsol kirişin analitik modeli hazırlandı. Sonrasında, AKS ve konsol kirişin ilişkilendirilmesi AKS'nin konsol kirişe montajını simüle etmek için modellendi. Ardından, sistemin tepkisi modellendi. AKS'nin etkisini görebilmek için yalnızca konsol kirişin tepkisi de modellendi. Bu tepkiler harmonik tarama altında modellendi.

AKS tasarımı maksimum BAS'yi elde edecek şekilde en iyileştirildi. AKS tasarımının sonrasında, AKS'nin durağan durum sönümleme katsayısını ve sistem tepkisini ölçmek için iki özel deney düzeneği tasarlandı. Deneysel sonuçların teorik sonuçlar ile uyumlu olduğu gösterildi. Dolayısıyla, BAS'ye dayalı bir AKS'nin başarıyla tasarlandığı, analiz edildiği ve test edildiği sonucuna varılabilir.

Anahtar Kelimeler: Ayarlı Kütle Sönümleyici, Elektromanyetik Sönümleme, Burgaç Akımı ile Sönümleme, Pasif Titreşim Kontrolü

ACKNOWLEDGEMENTS

I would like to express my appreciation to my supervisor, Assoc. Prof. Dr. Bilsay SÜMER for his guidance throughout this thesis work.

I would like to express my gratitude to my mentor, Dr. Taner KALAYCIOĞLU for sharing his technical expertise and recommendations throughout the testing part of this thesis study. I would also like to thank him for his guidance throughout my career to improve me as an engineering professional.

I would like to express my gratitude to Dr. Güvenç CANBALOĞLU for sharing his technical expertise and recommendations throughout the testing part of this study.

I would also like to express my gratitude to Mustafa KARAKOÇ and Umutcan ERHAN for their support throughout the procuring, manufacturing and assembling the test setups.

I would like to thank my managers and ASELSAN Inc. for giving me the opportunity to use the capabilities of the company throughout this thesis work.

I am especially thankful to my wife Yasemin KABASAKAL SAK, for her love, support and encouragement throughout this thesis work.

I would like to express my huge appreciation to my dear mother Derya SAK and my aunt Assoc. Prof. Dr. Hanaslı GÜR for their support, trust and encouragement throughout this thesis work and my life.

TABLE OF CONTENTS

LIST OF FIGURES

LIST OF TABLES

LIST OF SYMBOLS AND ABBREVIATIONS

LIST OF SYMBOLS

σ	: Conductivity of the conducting material
$\vec{B}$	: Magnetic flux density
$\vec{v}$	: Velocity
$\vec{J}$	: Current density
$d\vec{B}$	: Magnetic flux density
μ_0	: Permeability of free space
B_0	: Residual magnetic flux density of the magnet
M_0	: Magnetization
$\vec{R}_1$	: Vector from source point to field point
$d\vec{l}$	: Vector of infinitesimal strip
b	: Radius of the circular magnet
y	: Radius of the circular magnet in y direction
z_1	: Distance in the z direction
h	: Length of the magnet
$\vec{F}_d$	: Electromagnetic force created by eddy current damping
δ	: Thickness of the conductive tube
c_d	: Damping coefficient for the steady-state
W	: Weight of the magnet
m	: Mass of the magnet
g	: Gravity
t	: Time
f	: Frequency (Hz)
μ	: Permeability of the conductor
μ_r	: Relative permeability of the conductor
f_{limit}	: Limit frequency
$\vec{F}_{d_{dynamic}}$	: Damping force created by the dynamic loadings
$c_{d_{dynamic}}$	: Dynamic damping coefficient
m_1	: Mass of the main structure
c_1	: Damping coefficient of the main structure
k_1	: Stiffness of the main structure
m_2	: Mass of the TMD
c_2	: Damping coefficient of the TMD
k_2	: Stiffness of the TMD
F_1	: External force applied on the main structure from the fixed end
b_{beam}	: Width of the beam
h_{beam}	: Height of the beam
L	: Length of the beam
ρ	: Density of the material which is used to manufacture the beam
m_{beam}	: Mass of the beam
$m_{beam_{lumped}}$	: Lumped mass of the beam

E : Young's Modulus
I : Moment of inertia of the beam
k_{beam} : Stiffness of the beam
c_{beam} : Damping coefficient of the beam
ζ_{beam} : Damping ratio of the beam
$w_{n_{beam}}$: Natural frequency of the beam (rad/s)
$w_{d_{beam}}$: Damped natural frequency of the beam (rad/s)
d : Wire diameter of the spring
D : Mean coil diameter of the spring
G : Torsional modulus of elasticity
N : Number of active coils
N_s : Number of springs that are used in the system
$k_{one-spring}$: Stiffness of one spring
$k_{spring-system}$: Stiffness of the spring system
$m_{TMD_{sprung}}$: Sprung mass of the TMD
$w_{n_{TMD}}$: Natural frequency of the TMD (rad/s)
c_{TMD} : Damping coefficient of the TMD
$w_{d_{TMD}}$: Damped natural frequency of the TMD
ζ : Damping ratio
$m_{TMD_{unsprung}}$: Unsprung mass of the TMD
α_{beam} : Transmissibility of the beam
r_{beam} : Ratio of frequency to natural frequency of the beam
m_{acc} : Mass of the accelerometer
C_{fa} : Coherence of accelerance FRF
G_{fa} : Cross power spectral density of force and acceleration
G_{af} : Cross power spectral density of acceleration and force
G_{ff} : Auto power spectral density of force
G_{aa} : Auto power spectral density of acceleration
H_R : Real part of the FRF
H_P : Whole part of the FRF with real and imaginary parts
Im_{rec} : Imaginary peak of receptance FRF
Im_{acc} : Imaginary peak of accelerance FRF
ζ_{qi} : Modal damping ratio
k_{qi} : Modal stiffness
m_{qi} : Modal mass
c_{qi} : Modal damping coefficient

LIST OF ABBREVIATIONS

TMD	: Tuned Mass Damper
CTMD	: Composite tuned mass damper
DTMD	: Distributed tuned mass damper system
MDOF-TMD	: Multiple degree of freedom tuned mass damper system
ECD	: Eddy current damping
DC	: Direct current
AC	: Alternating current
FEM	: Finite Element Method
FRF	: Frequency Response Function
MIF	: Mode Indicator Function

1. INTRODUCTION

All dynamic structures encounter vibration during their operation. A structure experiences the vibration load in an amplified manner at structure's natural frequency due to resonance. If the amplitude of vibration load is high enough, this may damage the structure. Tuned mass dampers (TMD's) are used as a vibration control strategy in order to prevent this.

A TMD which has good applicability in space applications is going to be designed in this thesis work. Environmental effects of the space other than the mechanical loadings are out of context of this thesis. Only dynamic mechanical loadings are going to be considered and assessed.

A TMD designed to be used in the space applications must be highly reliable, because it operates in an environment which is hard to reach. That's why, main concern in the TMD design is going to be reliability.

Literature survey about fundamentals of the TMD and types of TMD's are going to be given in Chapter 0. A suitable concept of TMD for space applications is going to be selected in Chapter 0. Also, modeling of the selected TMD and modeling of the tests are going to be given in Chapter 2 as well. Afterwards, design of the TMD and experimental setups to test the TMD are going to be given in Chapter 3. Then, theoretical results of the designed TMD are going to be given in Chapter 0. Afterwards, experiments are going to be performed and theoretical results are going to be validated by experimental results in Chapter 5. At the end, discussion and conclusion of the study are going to be given in Chapter 6.

2. LITERATURE SURVEY

TMD is a vibration control device which is tuned to the natural frequency of the host structure to be controlled. A TMD typically consists of mechanical components which can modeled as spring, mass and damper elements. Ideally mass and spring elements are enough to control a structure's dynamic behavior. But in reality, this system without a damper element is very sensitive to mistuning of the tuning frequency. Therefore, damper elements are added to the device in order to decrease the sensitivity to mistuning. Adding damper elements also results in increasing the effective bandwidth of the TMD around the tuning frequency [1]. Simple schematic of a TMD is shown in Figure 2.1. Adding a TMD to a single-degree-of freedom (SDOF) modelled structure makes the lumped model as two-degree-of freedom (2-DOF) system, where the frequency response typically gives two peaks with decreased amplitude compared to the original model as shown in Figure 2.2. Systems given in Figure 2.2 are taken from Chapter 4.4 of this study.

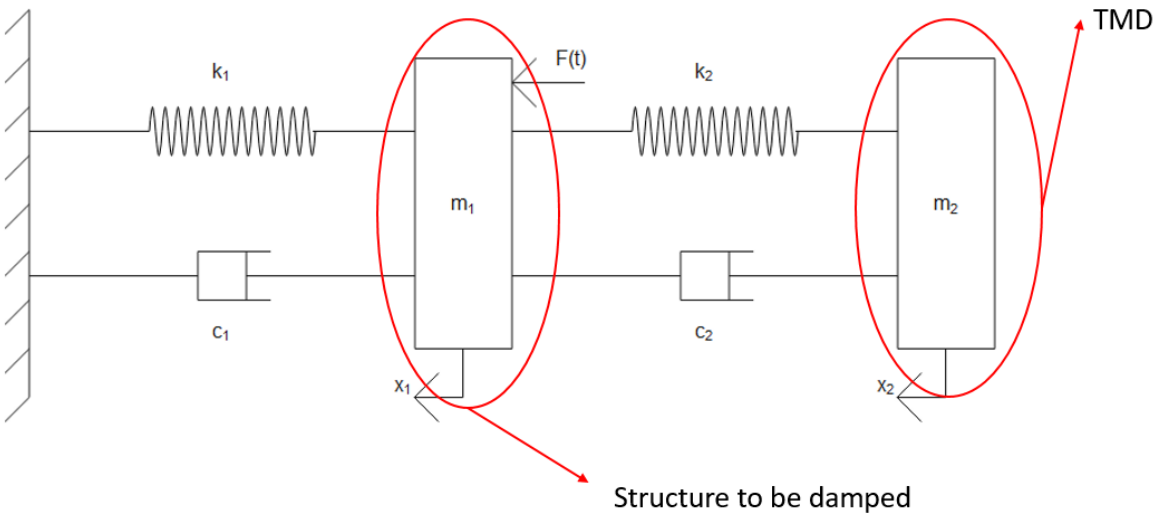

Figure 2.1 Schematic of a simple TMD

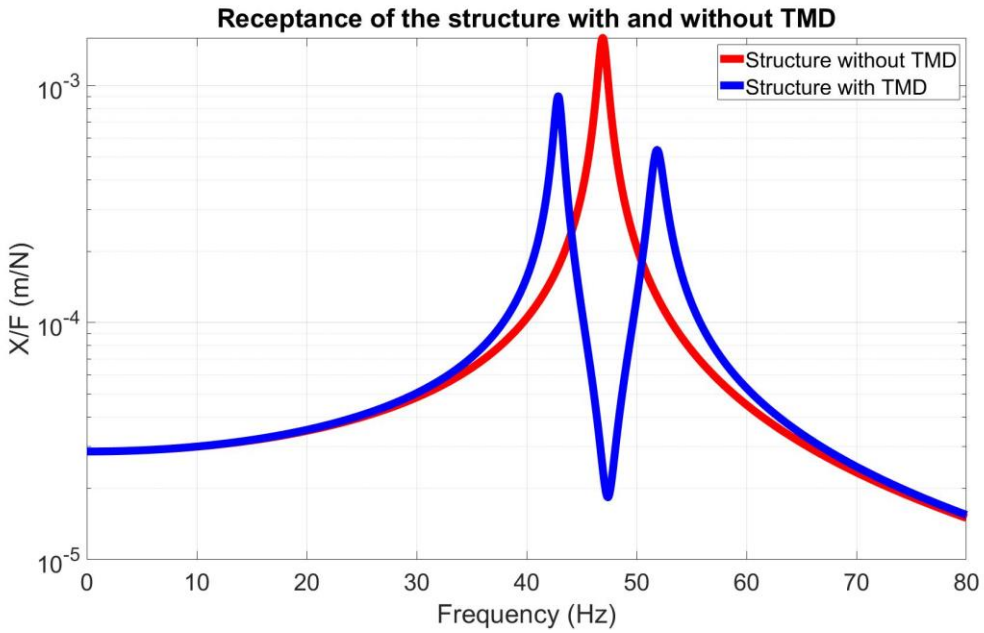

Figure 2.2 Effect of a TMD on a structure

2.1 Types of TMD's

TMD's are studied excessively on literature [1]. There are different configurations, control strategies and technologies, which are used in TMD's. Classification of the different configurations of TMD's are given in Figure 2.3.

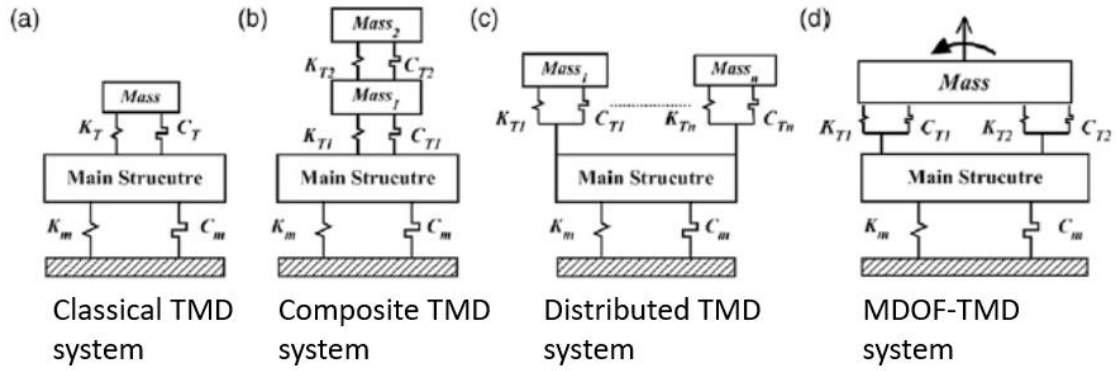

Figure 2.3 Different configurations of TMD's. [1]

The different configurations of TMD's are designed to control the different types of dynamic characteristics of the structures. A classical TMD system is sufficient to control the single vibration mode of a structure [2,3]. A composite TMD system also controls a single vibration mode of a structure but with improvements on performance [4,5]. A distributed TMD system can control many modes of a structure [6,7]. A MDOF-TMD system can control modes related to displacement and rotary degrees of freedom [8,9]. In

this thesis, a classical TMD system configuration is going to be investigated because of its simplicity.

There are three control strategies which are typically used in TMD's. These strategies are given in Figure 2.4.

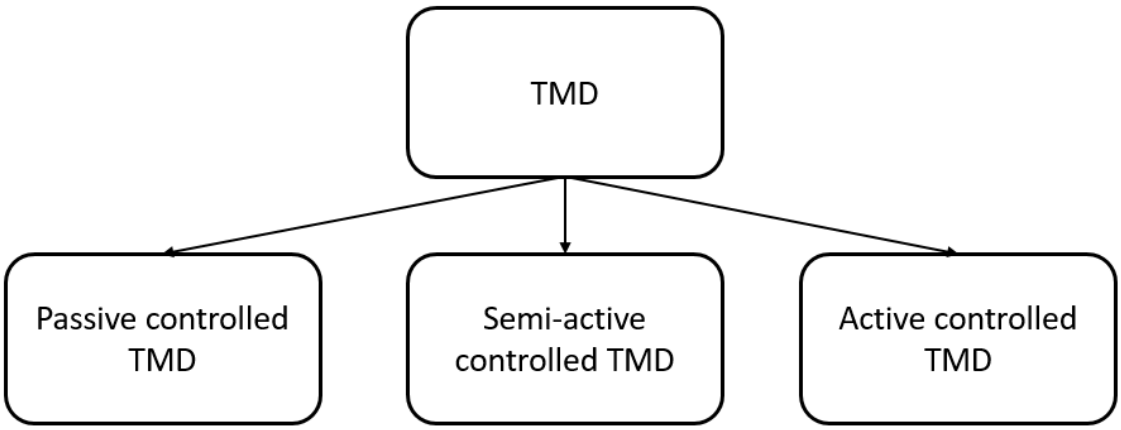

Figure 2.4 Control strategies used in TMD's [1].

Passive controlled TMD's are simple devices because they do not have any means of an active control element. They are tuned to their operating natural frequency and their damping characteristics are pre-determined before their operational use. They do not require any external power source to operate. They are highly reliable and they require low maintenance because of aforementioned properties. Besides these advantages, they have narrower frequency band than the semi-active and active controlled TMD's since there isn't any active control element available in the system [1]. But because of its simplicity and high reliability, passive controlled TMD's are widely used in the vibration reduction applications.

Semi-active and active TMD's have broader frequency band than passive controlled TMD's. Semi-active TMD's work by changing stiffness or damping ratio of the added structure. Active TMD's work by directly opposing the vibration of the controlled structure. They are more complex devices to design and control, they require external power to operate. Because of these properties, they are less reliable and they require more maintenance [10]. They are used in more sophisticated and demanding applications in which these disadvantages can be ignored. High reliability is the key factor in a product

that is going to be used in space applications. Therefore, a passive controlled TMD is going to be used in this thesis because of its simplicity and high reliability.

There are three main types of damping concepts in passive controlled TMD's. They are given in Figure 2.5.

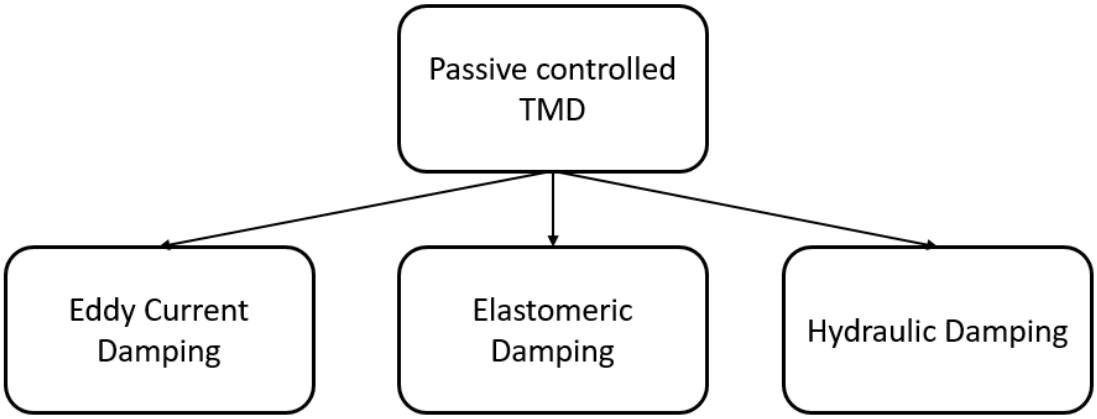

Figure 2.5 Types of damping concepts that are used in passive controlled TMD's.

In eddy current damping (ECD), damping is realized by electromagnetic forces in a non-contact, non-fluidic manner. Because of this nature, electromagnetic damping is highly reliable and it does not have any sealing or packaging problems [11].

In elastomeric and hydraulic damping, damping is realized by friction forces. Because of this nature of these concepts, they are less reliable than the eddy current damping. Also, fluidic nature of hydraulic damping can cause sealing and packaging problems. Eddy current damping concept is going to be investigated in this thesis because of its high reliability.

2.2 TMD Based on Eddy Current Damping

The damping mechanism of the ECD should be understood well to design a TMD based on ECD. The damping is realized in ECD by the electromagnetic forces. Eddy currents are created within the conducting material by relative motion of the permanent magnet near a conductive material. This creates a magnetic field and a repulsive electromotive force. This force generates the damping effect. The induced currents in the conductive material are dissipated into heat because of the conductive material's internal electrical resistance and the energy is removed from the system [11].

There are two types of geometry which are commonly used for ECD applications [12,13], which are given in Figure 2.6.

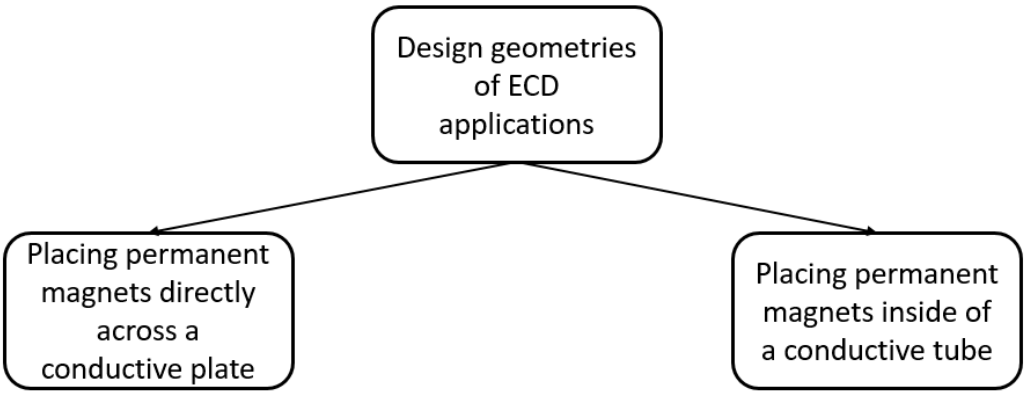

Figure 2.6 Two different designs which are commonly used in ECD based TMD's.

Schematics of these two types are given in Figure 2.7 and Figure 2.8.

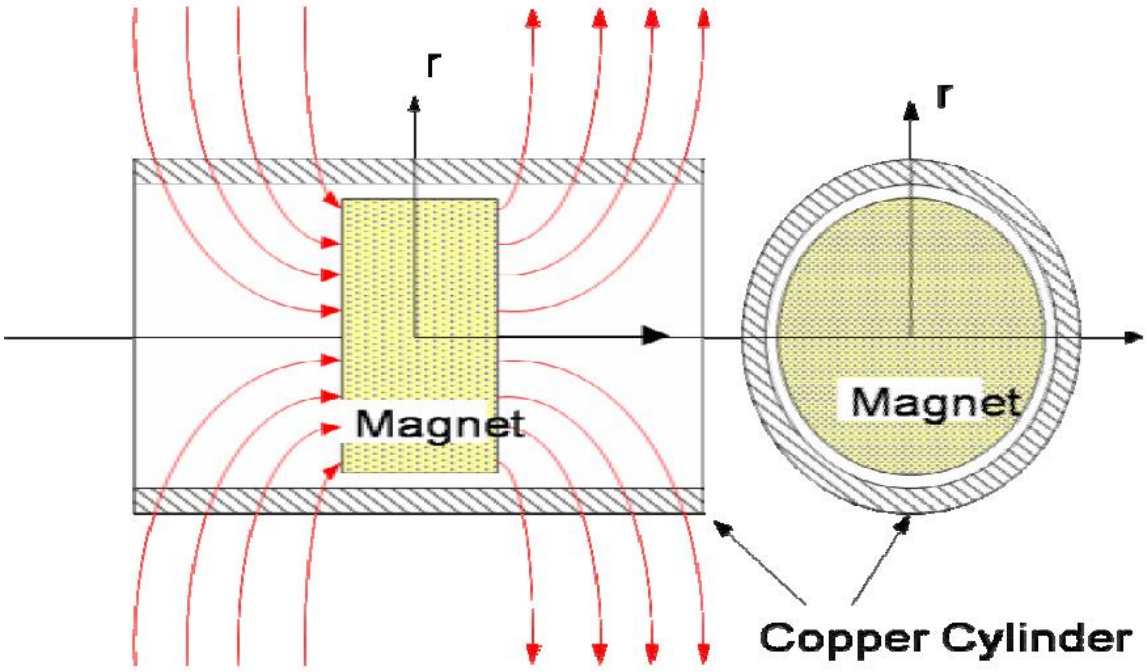

Figure 2.7 Permanent magnet inside of a conductive tube [12]

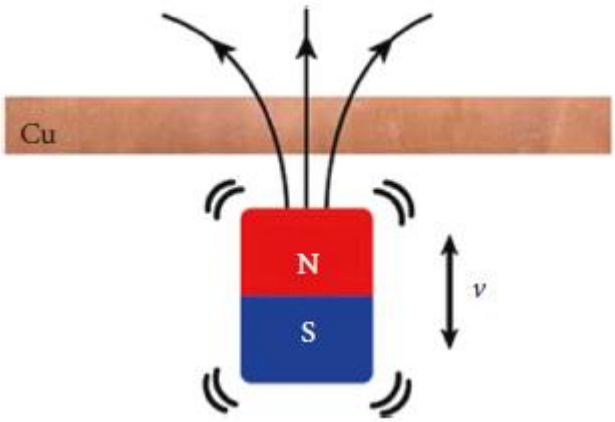

Figure 2.8 Permanent magnet across a conductive plate [11].

In this thesis, the design of placing permanent magnets inside of a conductive tube is chosen. Because a tube as conductor is more suitable and robust than using a plate as conductor for a TMD application. Utilizing a tube as a conductor, the magnet is in close proximity of the conductive material during the whole motion of the magnet since it always vibrates within the conductive tube. On the other side, distance between conductive plate and magnet changes as the magnet vibrates if a plate is used as conductor. Because of this conceptual difference between two approaches, more damping effect can be created by using a tube rather than by using a plate as conductor.

In several studies [12,14–16], a damping model for the steady-state response of the ECD case is studied. To find the damping, free fall of a magnet through a conductive tube is modeled. It is assumed that magnet reaches terminal velocity almost instantly and therefore falling of the magnet is interpreted as a steady-state problem. However, in real life situations TMD is going to operate against dynamic loadings. Therefore, a dynamic model to estimate the dynamic damping coefficient is required in order to consider the real-life situations. In [12], frequency effect on the damping coefficient is assessed experimentally. In [13] a theoretical background of the frequency on the ECD is given. However, the system analyzed in this work uses a plate as a conductor. Therefore, approach given in [13] is not directly going to be used, but the theoretical background related to frequency effect on the damping coefficient is going to be used.

Firstly, a damping coefficient model for the steady-state response is going to be found in the following chapters. These equation are taken from [12]. Then, the effect of the forcing

frequency is going to be added to the damping coefficient model. This is going to result in a model that can be used for dynamic loadings.

2.2.1 Damping Coefficient for Rigid Body Motion

Current density created within conducting tube by movement of a magnet which has a velocity of $\vec{v}$ is shown in Equation (2.1) [12]. σ is conductivity of the conducting material and $\vec{B}$ is the magnetic flux density.

$$\vec{J} = \sigma(\vec{v}\ x\ \vec{B}) \tag{2.1}$$

Schematic includes the coordinate system that are used in this and following equations can be seen in Figure 2.9.

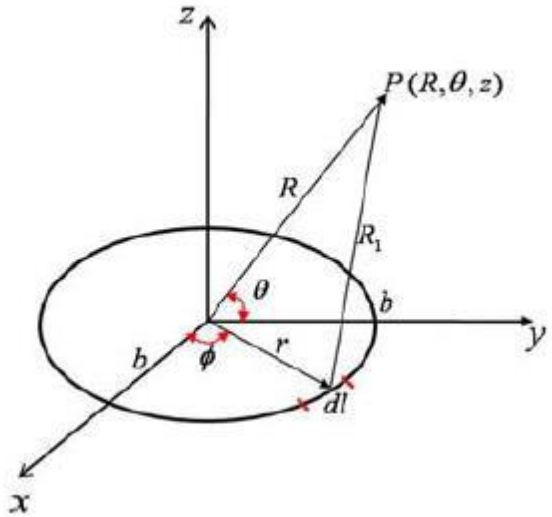

Figure 2.9 Coordinate systems that are used to find damping coefficient [12]

Magnetic flux density can be expressed by Equation (2.2) by applying Biot-Savart law. μ_0 is permeability of free space, M_0 is magnetizaion, $\vec{R}_1$ is vector between source and field points and $d\vec{l}$ is vector of infinitesimal strip. Formula for M_0 can be seen in Equation (2.3). B_0 is the residual magnetic flux density of the magnet. Formulas for $\vec{R}_1$ and $d\vec{l}$ are given between Equation (2.4) and Equation (2.7). b is the radius of the cylindrical magnet. Other parameters can be seen in Figure 2.9.

$$d\vec{B} = \frac{\mu_0 M_0}{4\pi} \frac{d\vec{l}\ x\ \vec{R}_1}{R_1^2} \tag{2.2}$$

$$M_0 = \frac{B_0}{\mu_0} \tag{2.3}$$

$$\vec{R}_1 = \vec{R} - \vec{r} \tag{2.4}$$

$$\vec{R} = y\vec{a}_y + z\vec{a}_z \tag{2.5}$$

$$\vec{r} = b\cos\emptyset\,\vec{a}_x + b\sin\emptyset\,\vec{a}_y \tag{2.6}$$

$$d\vec{l} = -b\sin\emptyset\,d\emptyset\vec{a}_x + b\cos\emptyset\,d\emptyset\vec{a}_y \tag{2.7}$$

Magnet's velocity is in z direction in Figure 2.9. Therefore, magnetic flux density that contributes to the current density is in x or y direction. Formula of this magnetic flux density is given in Equation (2.8). $I_1$is the elliptic integral.

$$dB_y(y,z) = \frac{\mu_0 M_0 bz}{4\pi}\int_0^{2\pi}\frac{\sin\emptyset}{(b^2+y^2+z^2-2by\sin\emptyset)^{\frac{3}{2}}}d\emptyset \tag{2.8}$$

$$I_1(b,y,z) = \int_0^{2\pi}\frac{\sin\emptyset}{(b^2+y^2+z^2-2by\sin\emptyset)^{\frac{3}{2}}}d\emptyset \tag{2.9}$$

Magnetic flux density created by the magnet can be found by integrating Equation (2.8). Formula of this magnetic flux density is given in Equation (2.10). z_1 is distance along z axis from center of the magnet and h is length of the magnet.

$$B_y(y,z,z_1) = \frac{\mu_0 M_0 b}{4\pi}\int_{\frac{-h}{2}}^{\frac{h}{2}}(z-z_1)I_1(b,y,z-z_1)dz \tag{2.10}$$

The electromagnetic force created by eddy current can be expressed as in Equation (2.11) and Equation (2.12). δ is the thickness of the conductive tube.

$$\vec{F} = \int\left(\vec{J}\,x\,\vec{B}\right)dV \tag{2.11}$$

$$\vec{F}_d = v2\pi\sigma\delta y\int B_y^2(y,z,z1)dz \tag{2.12}$$

Equation (2.13) given below is used to find damping coefficient for steady-state.

$$c_d = 2\pi\sigma\delta y \int B_y^2(y,z,z1)dz \tag{2.13}$$

The analytical integral operations in the given equations are hard to solve analytically. Therefore, it is suggested to solve them by using numerical integration methods [12].

Dropping of a magnet inside of a conductive tube is simulated in order to find the steady-state damping coefficient. Formulations of displacement and velocity of magnet are shown by Equation (2.14) to Equation (2.16).

$$W - F_d = mg - c_d v = m\frac{dv}{dt} \tag{2.14}$$

$$v(t) = \frac{mg}{c_d}(1 - e^{\frac{c_d}{m}t}) \tag{2.15}$$

$$x(t) = \frac{m^2 g}{{c_d}^2}\left(1 - e^{\frac{c_d}{m}t}\right) + \frac{mg}{c_d}t \tag{2.16}$$

2.2.2 Damping Coefficient for Dynamic Loadings

Damping coefficient for the rigid body motion response of the ECD is found in previous chapter. However, in real life applications, the oscillations can have steady-state and transient components and have a dynamic behavior. Many frequencies contributed to the dynamic response. As the case changes from quasi static to dynamic, eddy currents created within the conductor changes from DC to AC. As the frequency of the loading increases, thickness of the conductive tube that can be effectively used to create eddy currents decreases. This effect is defined as the skin effect [17]. Effective thickness that can be used is defined as skin depth. Visualization of the skin depth can be seen in Figure 2.10.

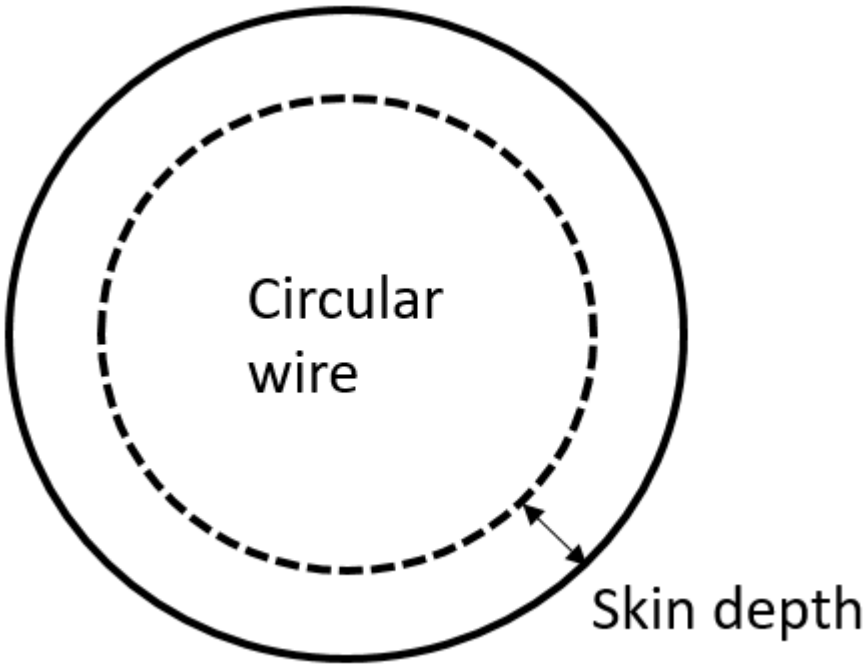

Figure 2.10 Skin depth of a conductor

Formula for the skin depth is given in Equation (2.17). f is the frequency in Hz, μ is the permeability of the conductor. μ_r in Equation (2.18) is the relative permeability of the conductor.

$$\delta = \frac{1}{\sqrt{\pi f \mu \sigma}} \tag{2.17}$$

$$\mu = \mu_0 \mu_r \tag{2.18}$$

Proposed TMD geometry contains a hollow cylinder as conductive tube. This hollow tube has a thickness. By using that thickness, a limit frequency can be defined from Equation (2.17). This frequency defines the limit forcing frequency which dynamic effects become relevant. Formula for this limit frequency is given in Equation (2.19).

$$f_{limit} = \frac{1}{\pi \delta^2 \mu \sigma} \tag{2.19}$$

It is given in Equation (2.17) that, as frequency increases skin depth decreases. The electromagnetic force created by eddy current and damping coefficient for dynamic loading cases can be found by combining Equation (2.17) with Equation (2.12) and Equation (2.13). Their formulas are given in Equation (2.20) and Equation (2.21).

$$\vec{F}_{d_{dynamic}} = v2\pi\sigma\delta(f)y \int B_y^2(y,z,z1)dz \tag{2.20}$$

$$c_{d_{dynamic}} = 2\pi\sigma\delta(f)y \int B_y^2(y,z,z1)dz \tag{2.21}$$

2.3 Modeling of the System

A classical TMD system is going to be investigated in this study. There are two structures in a classical TMD setup. First structure is the structure which is intended to be controlled. In this study, this structure is going to be called as the main structure. Second structure is used to control the first structure which is the TMD. Schematic of a classical TMD is given in Figure 2.11. At first the main structure is going to be modeled alone, without TMD to find its wide frequency band dynamic characteristics. Then, in order to see the effect of the TMD in a narrower frequency band, main structure and TMD are going be modeled as lumped structures.

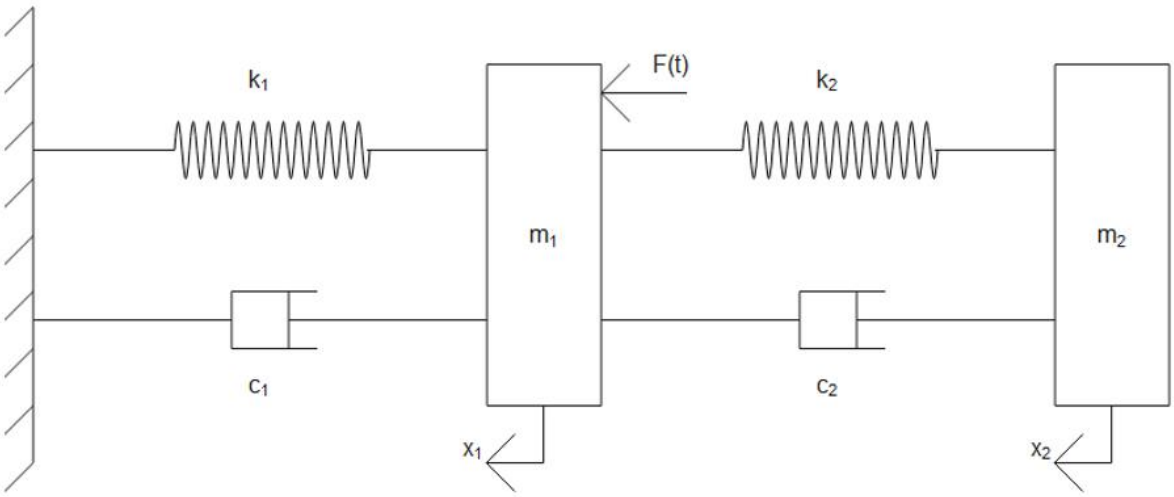

Figure 2.11 A classical TMD system

In Figure 2.11, m_1, c_1 and k_1 are the mechanical components of the main structure. Main structure to be investigated in this thesis is a cantilever beam which has a rectangular cross section. m_2, c_2 and k_2 are the parameters of the TMD. TMD is going to be used to control the fundamental natural frequency of the cantilever beam. Therefore, it is going to be placed at the free end. F is the excitation force applied on the main structure.

The governing equation for the damping coefficient (c_2) of the TMD is already found in the previous chapters. Other parameters of the system are going to be found in the following sub-chapters.

2.3.1 Modeling of the Beam with Rectangular Cross Section

The mass of the beam, which has a rectangular cross section, is given in Equation (2.22). In this equation, b_{beam} is the width and h_{beam} is the height of the rectangular cross section, L is the length and ρ is density of the beam material Schematic illustration of the beam is shown in Figure 2.12.

$$m_{beam} = \rho b_{beam} h_{beam} L \tag{2.22}$$

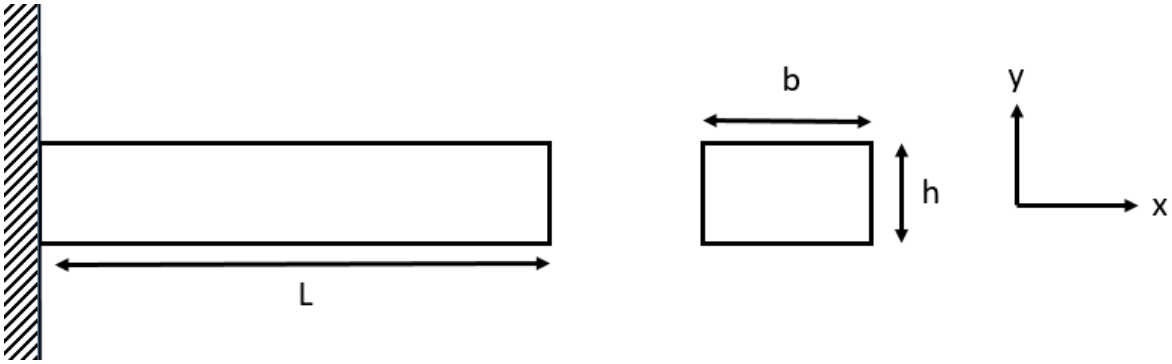

Figure 2.12 Schematic illustration of a cantilever beam with rectangular cross section

The stiffness of a constant-cross section cantilever beam with a fixed-free boundary condition in transverse direction is given in Equation (2.23) [18]. In this equation, E is the Young's modulus, I is the moment of intertia of the beam and L is length of the beam. Formula of the I is given in Equation (2.24).

$$k_{beam} = \frac{3EI}{L^3} \tag{2.23}$$

$$I = I_{xx} = \frac{b_{beam} {h_{beam}}^3}{12} \tag{2.24}$$

Numerical methods are going to be used in order to find frequency response of the beam Natural frequencies and related mode shapes are going to be found up to 5 kHz.

After acquiring cantilever beam's wide frequency band dynamic characteristics, lumped element model of the beam can be made to focus around the first bending mode of the cantilever beam.

Since the beam is going to be modeled as a lumped element, mass found in Equation (2.22) is not going to be directly used. Equivalent mass of the beam is going to be used in the lumped parameter model. Formula for the lumped mass of a cantilever beam can

be found in Equation (2.25) [18]. Schematic of a cantilever beam modeled with lumped mass can be seen in Figure 2.13.

$$m_{beam_{lumped}} = m_{beam}(\frac{33}{140}) \tag{2.25}$$

Figure 2.13 Schematic illustration of a cantilever beam that is modeled with lumped mass.

Damping coefficient of the beam is given in Equation (2.26). In this equation, ζ_{beam} is the damping ratio, k_{beam} is the stiffness of the beam and $m_{beam_{lumped}}$ is the mass of the beam.

$$c_{beam} = 2\zeta_{beam}\sqrt{k_{beam}m_{beam_{lumped}}} \tag{2.26}$$

Natural frequency of the beam is given in Equation (2.27). Since there is damping involved in the beam, damped natural frequency should also be a concern. Damped natural frequency of the beam is given in Equation (2.28).

$$\omega_{n_{beam}} = \sqrt{\frac{k_{beam}}{m_{beam_{lumped}}}} \tag{2.27}$$

$$\omega_{d_{beam}} = \omega_{n_{beam}}\sqrt{1 - \zeta_{beam}{}^2} \tag{2.28}$$

2.3.2 Modeling of the TMD

TMD utilizes ECD mechanism as it is previously discussed. In order to have ECD, there is a moving magnet within the system. Movement of the magnet creates the damping

effect on the system. Damping coefficient is created because of this damping effect, which is already found in Equation (2.21). Mass and stiffness of the TMD is going to be found in the following discussions.

Stiffness of the TMD is going to be created mainly by springs that are attached in a parallel arrangement in this work. Detailed design of the springs is going to be presented in the following chapters. Stiffness of one spring is given in Equation (2.29) [19]. In this equation, d is the wire diameter of the spring, G is the torsional modulus of elasticity of the spring, D is the mean coil diameter of the spring and N is the number of active coils in the spring. Stiffness of the springs that are attached in a parallel arrangement is given in Equation (2.30) [19]. In this equation, N_s is the number of springs that are used in the system.

$$k_{one-spring} = \frac{d^4 G}{8D^3 N} \tag{2.29}$$

$$k_{spring-system} = N_s k_{one-spring} \tag{2.30}$$

Mass of the TMD should be investigated in two parts. These parts are named as sprung and unsprung mass. Sprung mass is the mass that is carried by the springs. This mass includes magnet and magnet carrier parts. Magnet carrier parts are the parts that are used to create a mechanical interface between the magnet and the springs. Unsprung mass is the remaining mass of the TMD. Then the natural frequency of the TMD is given in Equation (2.31).

$$\omega_{n_{TMD}} = \sqrt{\frac{k_{spring-system}}{m_{TMD_{sprung}}}} \tag{2.31}$$

Since there is damping involved in the beam, damped natural frequency should also be a concern. In order to find damped natural frequency of the TMD, damping ratio of the TMD must be found first. Damping ratio of the TMD is given in Equation (2.32).

$$\zeta_{TMD} = \frac{c_{TMD}}{2\sqrt{k_{spring-system} m_{TMD_{sprung}}}} \tag{2.32}$$

Damped natural frequency of the beam is given in Equation (2.33).

$$\omega_{d_{TMD}} = \omega_{n_{TMD}}\sqrt{1-{\zeta_{TMD}}^2} \tag{2.33}$$

2.3.3 Coupling TMD with Cantilever Beam

Modeling of the cantilever beam and TMD is already presented in the previous chapters. Illustration for the assembled system is shown in Figure 2.14.

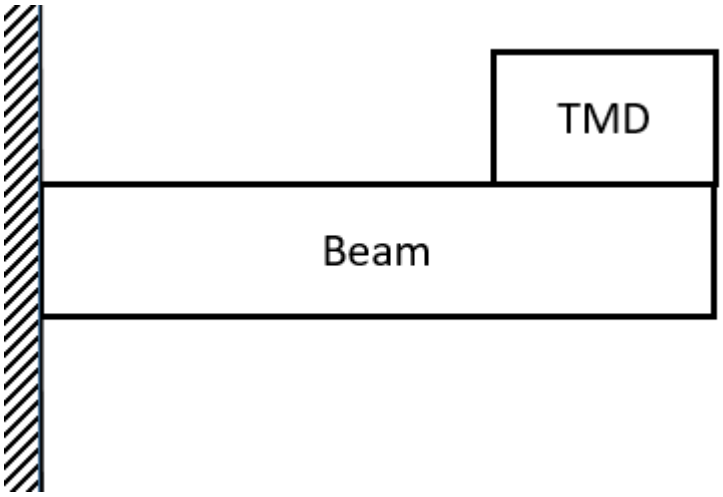

Figure 2.14 Assembled rectangular beam and TMD system

The TMD's mass is separated into two parts, which are sprung and unsprung masses. Besides this, the cantilever beam's mass modeled as a lumped mass. Since unsprung mass of the TMD is not carried by TMD's springs, it behaves as a mass that is attached to the beam. In order to model the system correctly, unsprung mass of TMD should be added to lumped mass of beam. Equivalent mass is given in Equation (2.34).

$$m_{eq_{beam}} = m_{beam_{lumped}} + m_{TMD_{unsprung}} \tag{2.34}$$

2.3.4 The Mechanical Vibration Response of the System

The equation of motion of the system should be determined in order to find the mechanical vibration response of the system. These equation are taken from [20]. Equation of the motion of the 2-DOF system given in Figure 2.11 is given in Equation (2.35).

$$\begin{bmatrix} m_1 & 0 \\ 0 & m_2 \end{bmatrix}\begin{bmatrix} \ddot{X}_1 \\ \ddot{X}_2 \end{bmatrix} + \begin{bmatrix} c_1 + c_2 & -c_2 \\ -c_2 & c_2 \end{bmatrix}\begin{bmatrix} \dot{X}_1 \\ \dot{X}_2 \end{bmatrix} + \begin{bmatrix} k_1 + k_2 & -k_2 \\ -k_2 & k_2 \end{bmatrix}\begin{bmatrix} X_1 \\ X_2 \end{bmatrix} = \begin{bmatrix} F_1 e^{iwt} \\ 0 \end{bmatrix} \tag{2.35}$$

By assuming a harmonic form for the solution Equation (2.35) becomes Equation (2.36).

$$\left[-\omega^2\begin{bmatrix}m_1 & 0\\ 0 & m_2\end{bmatrix}+i\omega\begin{bmatrix}c_1+c_2 & -c_2\\ -c_2 & c_2\end{bmatrix}+\begin{bmatrix}k_1+k_2 & -k_2\\ -k_2 & k_2\end{bmatrix}\right]\begin{bmatrix}X_1\\ X_2\end{bmatrix}e^{i\omega t} = \begin{bmatrix}F_1e^{i\omega t}\\ 0\end{bmatrix} \tag{2.36}$$

Equation (2.36) can be rewritten in generic case as Equation (2.37).

$$\left[-\omega^2[m]+i\omega[c]+[k]\right]\left[\vec{X}\right]e^{i\omega t} = \left[\vec{F}\right]e^{i\omega t} \tag{2.37}$$

After this point, complex matrix inversion method can be used. In order to use this method, Equation (2.37) should be rewritten as Equation (2.38) [20].

$$[A]\left[\vec{X}\right]e^{i\omega t} = \left[\vec{F}\right]e^{i\omega t}$$

$$[A] = \begin{bmatrix}a_{11} & a_{12}\\ a_{21} & a_{22}\end{bmatrix} = \begin{bmatrix}-\omega^2m_1+i\omega(c_1+c_2)+(k_1+k_2) & -i\omega c_2-k_2\\ -i\omega c_2-k_2 & -w^2m_2+i\omega c_2+k_2\end{bmatrix} \tag{2.38}$$

After this arrangement, displacement can be found as in Equation (2.39) by using complex matrix inversion method [20].

$$\left[\vec{X}\right] = [A]^{-1}\left[\vec{F}\right]$$

$$[A]^{-1} = \frac{1}{|A|}\begin{bmatrix}a_{22} & -a_{12}\\ -a_{21} & a_{11}\end{bmatrix} = \frac{1}{(a_{11}a_{22}-a_{12}a_{21})}\begin{bmatrix}a_{22} & -a_{12}\\ -a_{21} & a_{11}\end{bmatrix} = \begin{bmatrix}\alpha_{11} & \alpha_{12}\\ \alpha_{21} & \alpha_{22}\end{bmatrix} \tag{2.39}$$

Four components of the inverted A matrix given in Equation (2.39) are given in Equation (2.40) to Equation (2.43).

$$\alpha_{11} = \frac{-\omega^2m_2+i\omega c_2+k_2}{|A|} \tag{2.40}$$

$$\alpha_{12} = \frac{i\omega c_2+k_2}{|A|} \tag{2.41}$$

$$\alpha_{21} = \frac{i\omega c_2 + k_2}{|A|} \tag{2.42}$$

$$\alpha_{22} = \frac{-\omega^2 m_1 + i\omega(c_1 + c_2) + (k_1 + k_2)}{|A|} \tag{2.43}$$

After finding the components of the inverted A matrix, displacements can be written as in Equation (2.44).

$$\begin{bmatrix} X_1 \\ X_2 \end{bmatrix} = \begin{bmatrix} \alpha_{11} & \alpha_{12} \\ \alpha_{21} & \alpha_{22} \end{bmatrix} \begin{bmatrix} F_1 \\ 0 \end{bmatrix} \tag{2.44}$$

Using Equation (2.44), X_1 and X_2 can be found as in Equation (2.45) and (2.46).

$$X_1 = \alpha_{11} F_1 \tag{2.45}$$

$$X_2 = \alpha_{21} F_1 \tag{2.46}$$

As it can be seen from above, these four components represent the transmissibility of the system.

Transmissibility of a system, which contains only a cantilever beam, should also be found in order to compare the system with TMD to a system only contains a cantilever beam. Transmissibility of a system, which only contains a cantilever beam, is given in Equation (2.47). k_{beam} is the bending stiffness of the beam, r_{beam} is ratio of frequency to natural frequency of the beam and ζ_{beam} is damping ratio of the beam.

$$\alpha_{beam} = \frac{1}{k_{beam}} \sqrt{\frac{1}{(1 - {r_{beam}}^2)^2 + (2\zeta_{beam} r_{beam})^2}} \tag{2.47}$$

3. DESIGN OF THE TMD AND THE EXPERIMENTAL SETUPS

Modeling of the TMD based on ECD was given in previous chapters. Design of the TMD and experimental setups to test the TMD is going to be given in this chapter. Thesis work includes design of the TMD and two different experiments. This requires three different designs and results with three design chapters. These design chapters are going to be divided into two sub-chapters. These chapters are material selection and mechanical design. Material selection involves consideration throughout the material selection of the TMD and the experimental setups. Mechanical design involves mechanical architecture of the TMD and the experimental setups.

3.1 Design of the TMD

All considerations in the context of TMD design regarding material selection and mechanical design are going to be given in the following sub-chapters.

3.1.1 Material Selection for the TMD

TMD consists of the three main parts. These are called the magnet, conductive tube and other supporting structures.

3.1.1.1 Material Selection for the Magnet

Main consideration for the selection of the material of the magnet is to have high magnetic flux density. The permanent magnets, which are made of NdFeB and SmCo, are used in ECD applications because of their high magnetic quality [11]. NdFeB has the higher magnetic flux density between these two materials, as it is given in Table 3.1.

Table 3.1 Magnetic flux density of the SmCo and NdFeB magnets [21,22]

Material	Magnetic Flux Density (T)
SmCo	0.81-1.13
NdFeB	1.03-1.41

NdFeB magnets are chosen for the design since they have higher magnetic flux density. There are many types of NdFeB magnets available in the market where NdFeB N35 is the most common type of the NdFeB magnets. Therefore, NdFeB N35 is going to be used in the experiment. Magnetic flux density of the NdFeB N35 is given in Table 3.2.

Table 3.2 Magnetic flux density of the NdFeB N35 magnets [22]

Material	Magnetic Flux Density (T)
NdFeB N35	1.17

3.1.1.2 Material Selection for the Conductive Tube

Main consideration for the selection of the material of the conductive tube is to have high electrical conductivity. The copper and aluminum are most commonly used material in ECD applications because of their high electrical conductivity [11]. Copper in general has higher electrical conductivity between these two materials and is chosen as the conductive tube material, as it is given in Table 3.3.

Table 3.3 Electrical conductivity of the aluminum and copper [23–27]

Material	Electrical Conductivity (S/m)
Aluminum	2.5×10^7
Copper	5.8×10^7

Therefore, copper is chosen for the design since it has higher electrical conductivity. There are many types of copper available in market. UNS C10100, C10200, C10910 and C11000 are some of the most common types of copper. UNSC10100 copper is going to be used in the experiment.

3.1.1.3 Material Selection for Other Supporting Structures

Magnet and conductive tube create the damping in the TMD by using electromagnetic forces as it is discussed in Chapter 2.2. Other supporting structures have to be made from material which has no magnetic properties and have low electrical conductivity. In order not to create any undesired electromagnetic forces. The best candidate of the related properties in aerospace application is found to be Titanium (Ti). Ti has no magnetic properties and low electrical conductivity relative to the other materials. Besides these attributes, Ti has low density and high strength. These additional properties make the Ti material the best candidate for other supporting structures. Related material properties of the titanium can be seen in Table 3.4.

Table 3.4 Properties of Titanium [28,29]

Property	Value (Unit)
Magnetic Flux Density	0
Electrical Conductivity	1.9×10^6 S/m

3.1.2 Mechanical Design of the TMD

TMD includes three main parts that are described in Chapter 3.1.1. Mechanical design of the TMD which includes these three main parts includes the following sub-structures;

- A titanium base part which is used as a mounting interface between TMD and any other structure which the TMD is going to be installed.
- Titanium spring carriers which carry the springs and fixed to the titanium base part at one end.
- Titanium springs which are attached to the titanium spring carriers and to the titanium magnet carrier. These springs are used to make the unsprung structure's damped natural frequency equal to the structure's damped natural frequency which is to be controlled.
- Titanium magnet carriers which are attached to titanium springs at one end and carry the magnet.
- A NdFeB N35 magnet which is attached to the titanium magnet carriers at one end and relatively moves in the hollow copper conductive tube.
- A hollow copper conductive tube which is fixed to a titanium tube carrier at one end and in which a NdFeB N35 magnet relatively moves.
- A titanium tube carrier which fixes the hollow copper conductive tube and which is fixed to the outer titanium tube.
- An outer titanium tube which is used to enclose and assemble the system.
- Titanium nuts and screws which are used to assemble the system.

The mechanical design of the TMD is given in Figure 3.1, Figure 3.2 and Figure 3.3. All technical drawings are made on PTC Creo Parametric 9.0 software.

The most important geometrical parameters for the TMD design are given in Table 3.5 and Table 3.6.

Table 3.5 Important geometric parameters of the magnet for TMD design

Geometric Parameters	Value (mm)
Diameter	10
Height	10

Table 3.6 Important geometric parameters of the conducting tube for TMD design

Geometric Parameters	Value (mm)
Inner Diameter	11
Outer Diameter	18
Thickness	3.5

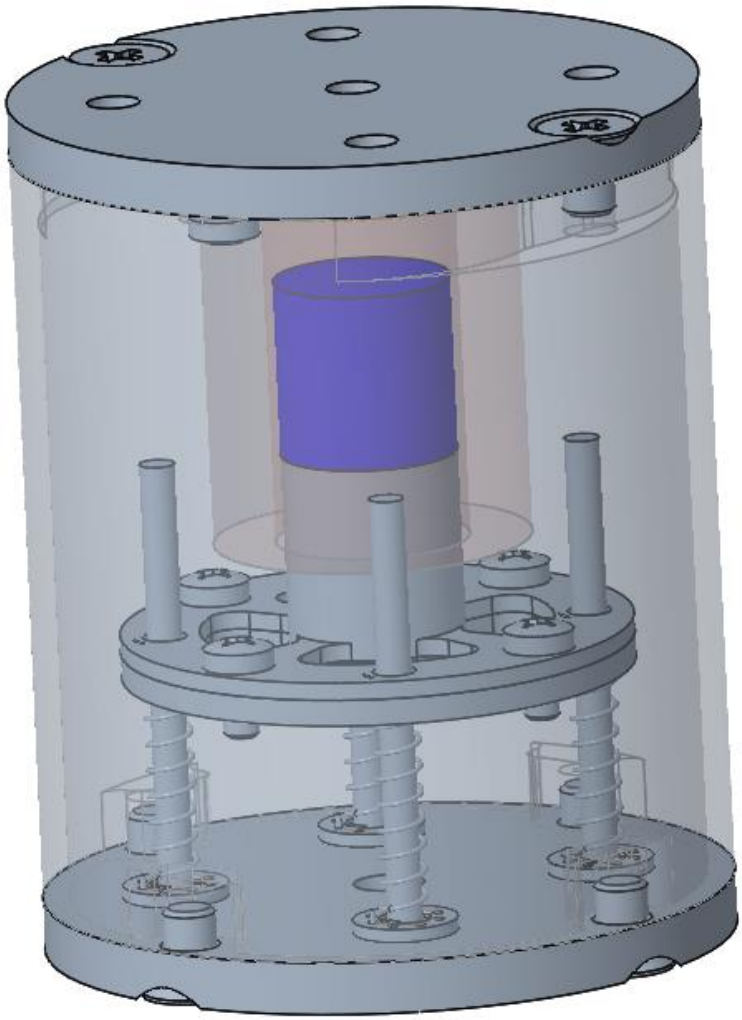

Figure 3.1 Three-dimensional (3D) computer-aided design (CAD) of the ECD based TMD (Side view).

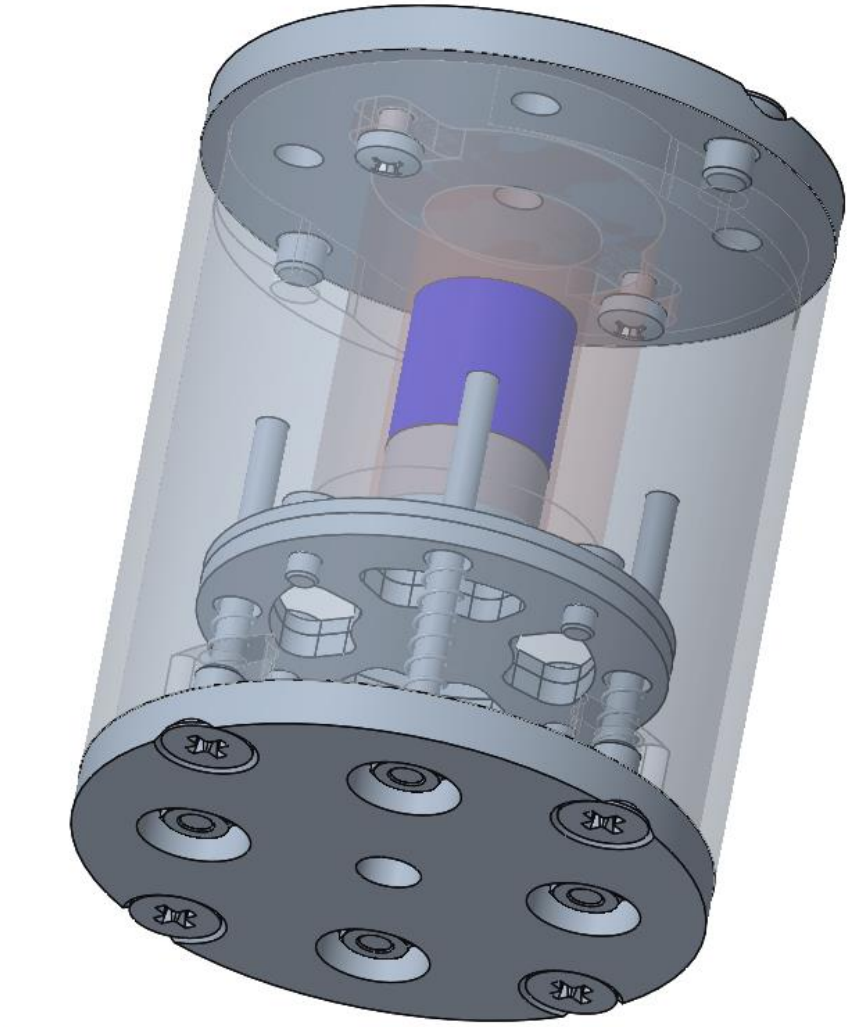

Figure 3.2 Three-dimensional (3D) computer-aided design (CAD) of the ECD based TMD (Bottom view).

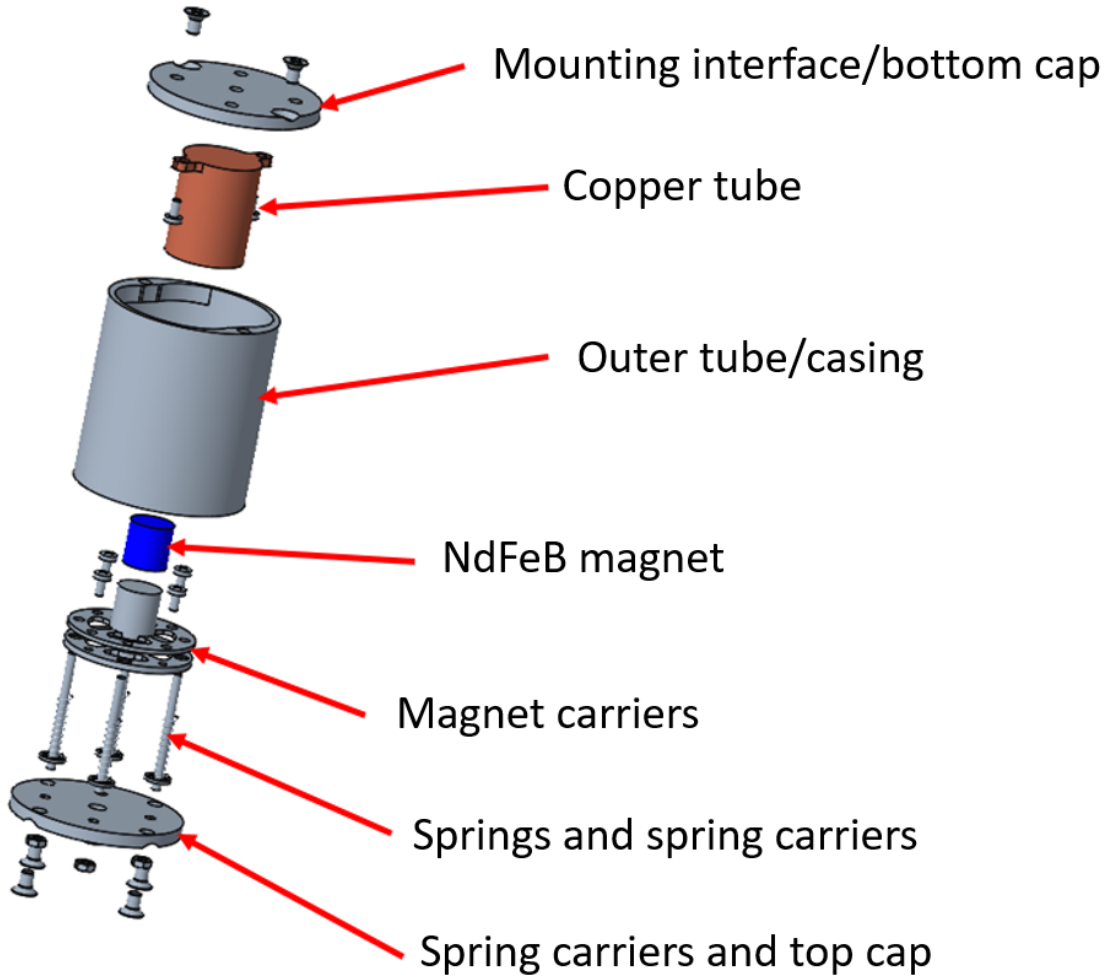

Figure 3.3 Exploded view of the ECD based TMD.

3.2 Experimental Setup for the Steady-State Damping Coefficient Test

In this experiment, a magnet is going to be dropped inside of a hollow conductive tube. All considerations in the context of this drop test design regarding material selection and mechanical design are going to be given in the following sub-chapters.

3.2.1 Material Selection for the Steady-State Damping Coefficient Test

Steady-state damping coefficient test is used to experimentally validate the TMD which's design is stated in Chapter 3.1. Therefore, same materials which are used for the TMD are going to be used in the test. Magnet material is going to be NdFeB N35 and hollow conductive tube material is going to be copper.

3.2.2 Mechanical Design of the Steady-State Damping Coefficient Test

Mechanical design of the steady-state damping coefficient test is fairly simple. It includes a hollow copper conductive tube and a NdFeB N35 cylindrical magnet. Conductive tube is placed vertically on a surface and magnet is dropped inside of the tube.

The most important geometrical parameters for the steady-state damping coefficient test design are given in Table 3.7 and Table 3.8.

Table 3.7 Important geometric parameters of the magnet for steady-state damping coefficient test design

Geometric Parameters	Value (mm)
Diameter	10
Height	10

Table 3.8 Important geometric parameters of the conducting tube for steady-state damping coefficient test design

Geometric Parameters	Value (mm)
Inner Diameter	11
Outer Diameter	18
Thickness	3,5
Height	150

Design of the steady-state damping coefficient test is given in Figure 3.4.

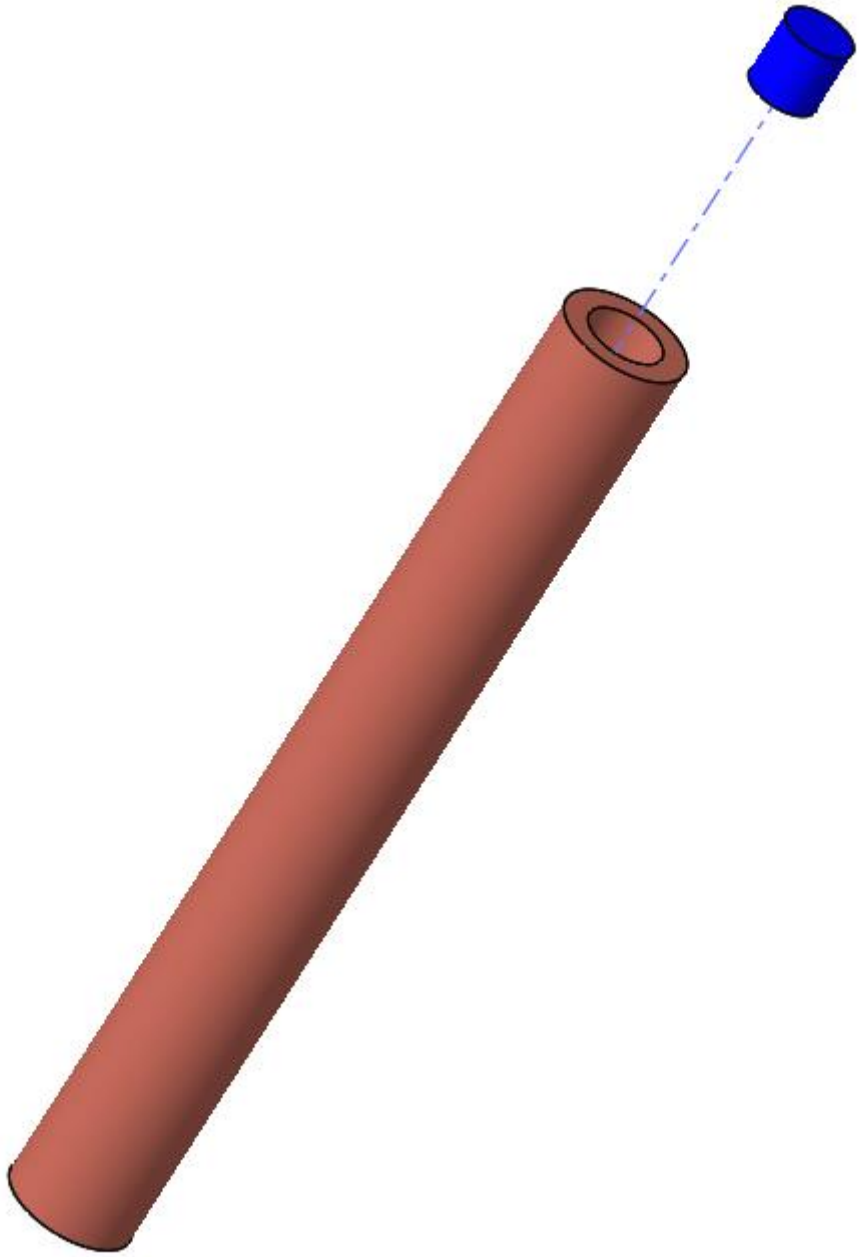

Figure 3.4 An overview of the steady-state damping coefficient test.

3.3 Design of the System Test

System test is going to be used to experimentally validate a system's response which includes the TMD, a cantilever beam, a test stand. TMD designed in Chapter 3.1 is going to be used directly. All other considerations in the context of this system test design regarding material selection and mechanical design are going to be given in the following sub-chapters.

3.3.1 Material Selection for the System Test

Since the TMD in Chapter 3.1 is going to be used directly, material selection for the system test only includes material of the cantilever beam and the test stand. Material for these structures is chosen to be Aluminum (Al) since it is the most commonly used material in aerospace applications. Screws near the TMD are going to be made of titanium. Other screws are going to be made of stainless steel.

3.3.2 Mechanical Design of the System Test

Mechanical design of the dynamic system test includes the following structures (Figure 3.5);

- A test stand which is used to fix the cantilever beam to its fixed end and also is attached to the fixture,
- Cantilever beam which is fixed at one end to the test stand and which has TMD placed at the free end,
- Accelerometer on the cantilever beam's free end to measure the acceleration response of the cantilever beam.

The most important geometrical parameters for the system test design are cantilever beam's parameters. These parameters are shown in Table 3.9.

Table 3.9 Important geometric parameters of cantilever beam for system test design.

Geometric Parameters	Value (mm)
Width	40
Height	20
Length	547

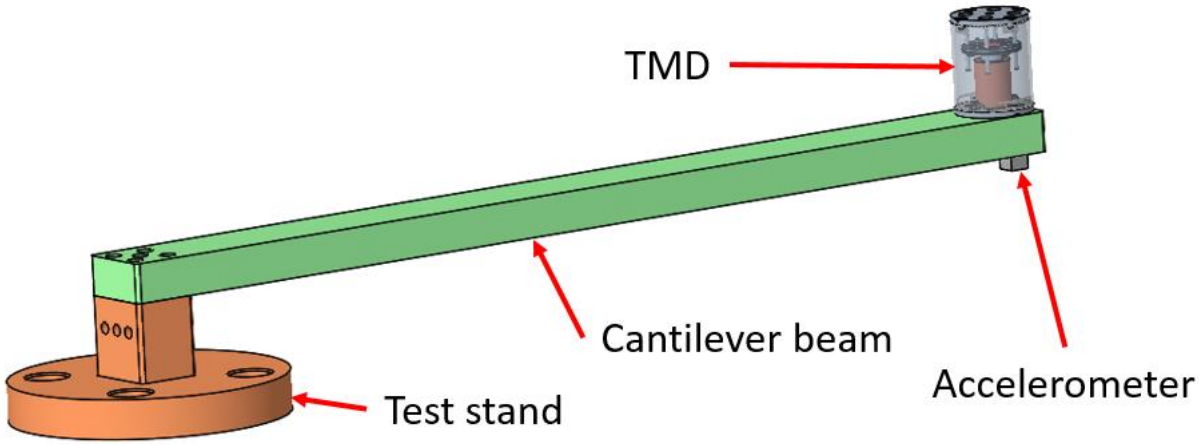

Figure 3.5 Mechanical design of the system test.

4. THEORETICAL RESULTS

In this chapter, the cantilever beam, TMD and system which is made of TMD and cantilever beam is going to be analyzed by the analytical approaches given in Chapter 0 and also using the numerical methods. MATLAB codes are written in order to find the analytical results. Steady-state and dynamic damping coefficients are going to be found in the following sub-chapters. Then, the ECD based TMD system's vibration response is going to be found.

4.1 Theoretical Results of the Steady-State Damping Coefficient

Equation (2.13) and its preceding equations are used in order to find the theoretical result for the steady-state damping coefficient. Following properties and their values given in Table 4.1 are used in order to be able use Equation (2.13) and its preceding equations.

Table 4.1 Properties that are used to find steady-state damping coefficient

Property	Symbol	Value (Unit)
Conductivity of the conductive material	σ	5.8×10^7 S/m
Permeability of free space	μ_0	$4\pi 10^{-7}$ H/m
Radius of the cylindrical magnet	b	5 mm
Height of the cylindrical magnet	h	10 mm
Thickness of the conductive tube	δ	3.5 mm
Radius of the magnet in y direction	y	5 mm
Residual magnetic flux density	B_0	1.17 (T)

By using these values steady-state damping coefficient is found. Result is given in Table 4.2.

Table 4.2 Found value of the steady-state damping coefficient

Property	Symbol	Value (Unit)
Steady-State Damping Coefficient	c_d	2.39684 Ns/m

Dropping of a magnet inside of a conductive tube is simulated to find steady-state damping coefficient. Displacement and velocity of magnet in this scenario is shown in Figure 4.1.

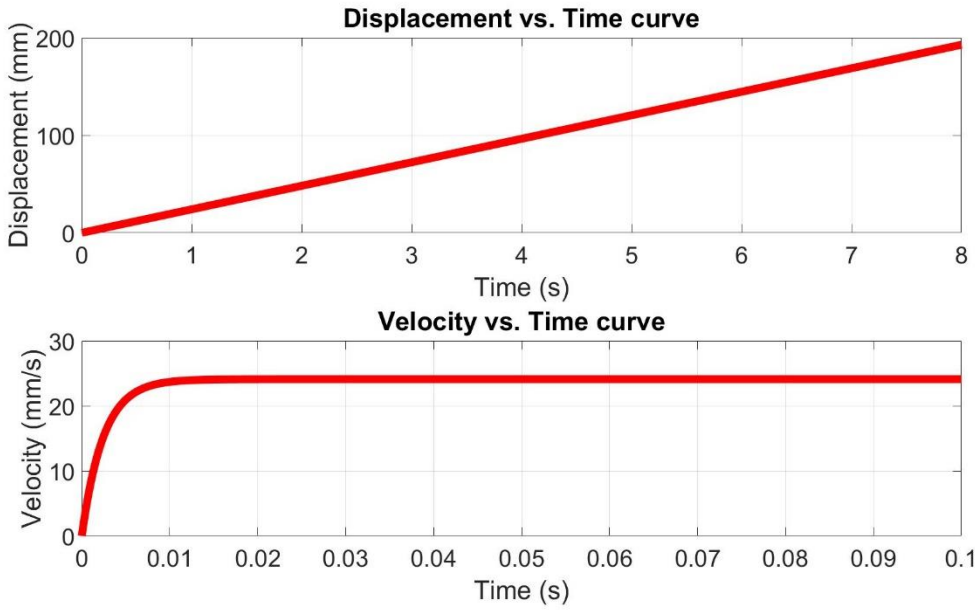

Figure 4.1 Displacement and velocity curves of dropping magnet inside of a conductive tube.

4.2 Theoretical Results of the Dynamic Damping Coefficient

Equation (2.21) and its preceding equations are used in order to find the theoretical result for the dynamic damping coefficient. In addition to properties given in relative permeability of the conductive material is also required. This property is given in Table 4.3.

Table 4.3 Properties that are used to find dynamic damping coefficient

Property	Symbol	Value
Relative permeability of conductive material	μ_r	0.999994

In order to find dynamic damping coefficient, skin effect on the conductive material must be found. Equation (2.17) is used to find the skin effect on the copper. Frequency bandwidth of 0-500 Hz is chosen for the solution. Skin effect on the copper can be seen in Figure 4.2. Skin effect becomes relevant when skin depth of conductive material is less than the thickness of structure. Limit frequency for this to occur is found to be 357 Hz by using Equation (2.19). Dynamic damping coefficient is found by using this value. It is shown in Figure 4.3.

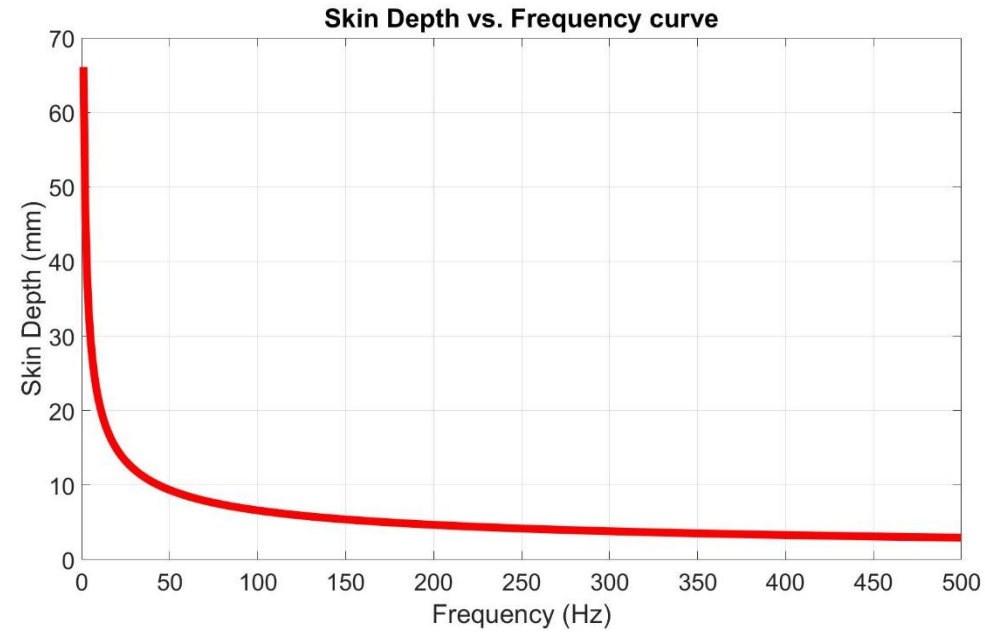

Figure 4.2 Skin effect on the copper: Skin depth (mm) versus the frequency (Hz)

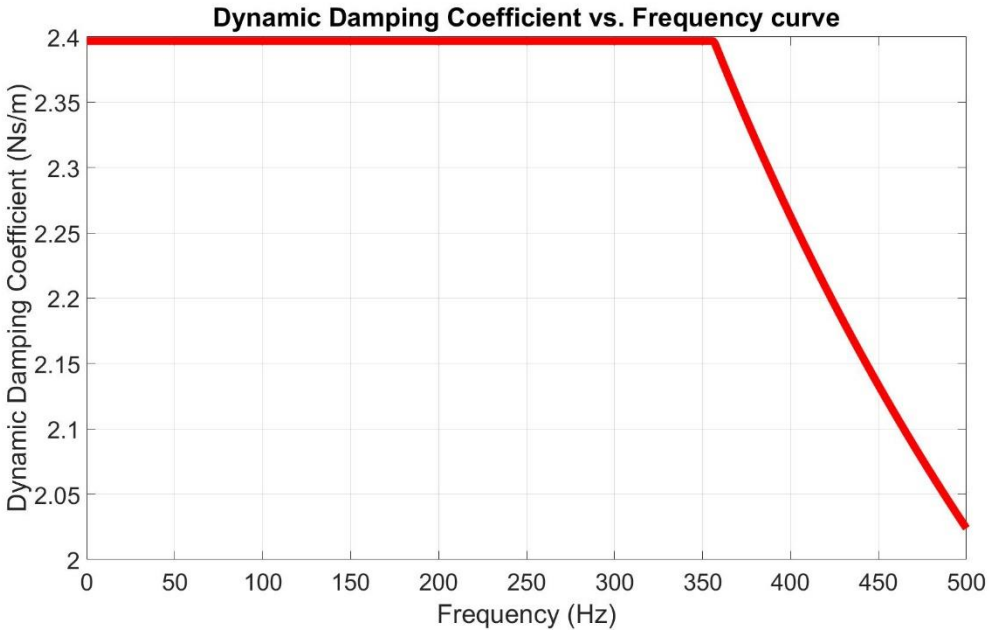

Figure 4.3 The change of the dynamic damping coefficient (Ns/m) with the frequency (Hz)

4.3 Theoretical Results of the Modes and Mode Shapes of the Cantilever Beam

Finite element model (FEM) of the cantilever beam is prepared to find modes and mode shapes of the cantilever beam. ANSYS R23 software is used for the analyses. In this model, beam is fixed at one end by using the counterbore holes that are modeled. Fixed support is given in Figure 4.4.

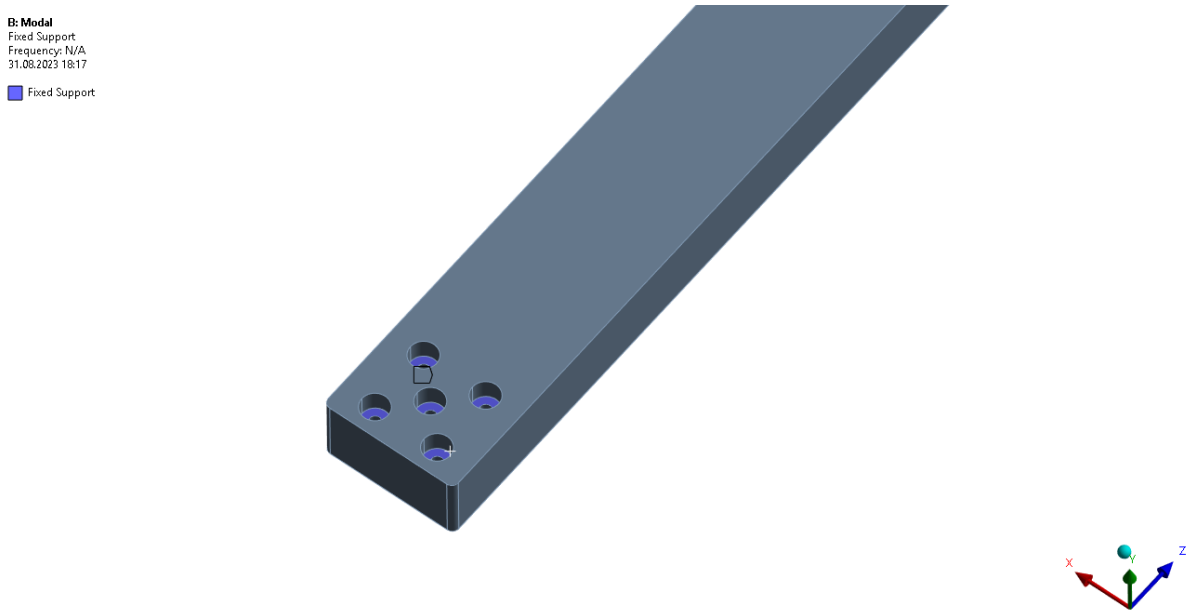

Figure 4.4 Fixed support defined at ANSYS

Afterwards, a modal analysis is made and natural frequencies up to 5 kHz and related mode shapes are found. Results are given in Table 4.4. Modes that have bending mode shape are shown with bold writing.

Table 4.4 FEM results of modes of the cantilever beam

Mode #	Natural Frequency (Hz)	Mode Shape Type	Ratio of Effective Mass to Total Mass in Bending Direction
1	**57.526**	**Bending**	**0.6000**
2	115.19	Lateral	1.30E-09
3	**359.25**	**Bending**	**0.1832**
4	704.87	Lateral	2.9700E-09
5	**998.34**	**Bending**	**0.0618**
6	1110.3	Torsion	4.0800E-08
7	1904	Lateral	1.0900E-06
8	**1932.5**	**Bending**	**0.0308**

9	2373.4	Longitudinal	5.0600E-05
10	**3148.1**	**Bending**	**0.0182**
11	3331.5	Torsion	2.91E-08
12	3557.6	Lateral	1.68E-11
13	**4613.4**	**Bending**	**1.19E-02**

Mode shapes associated with given modes are given in Figure 4.5-4.10.

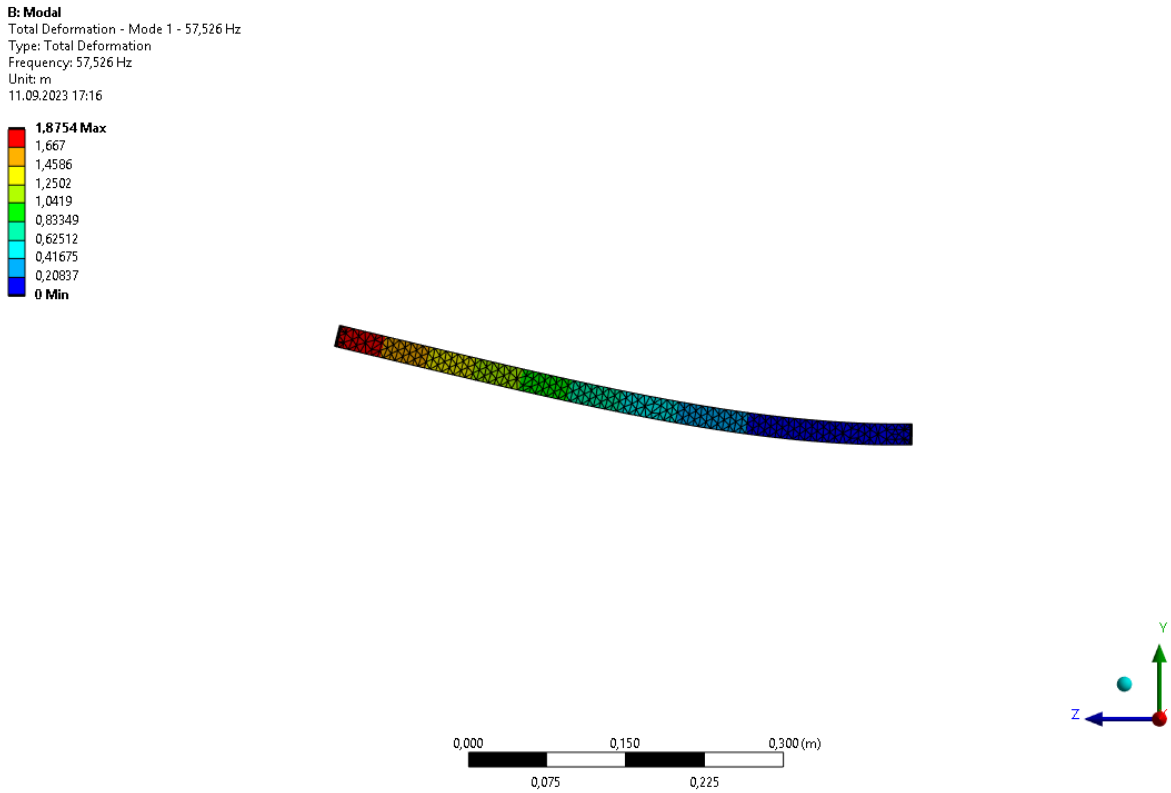

Figure 4.5 FEM result for 1st bending mode shape

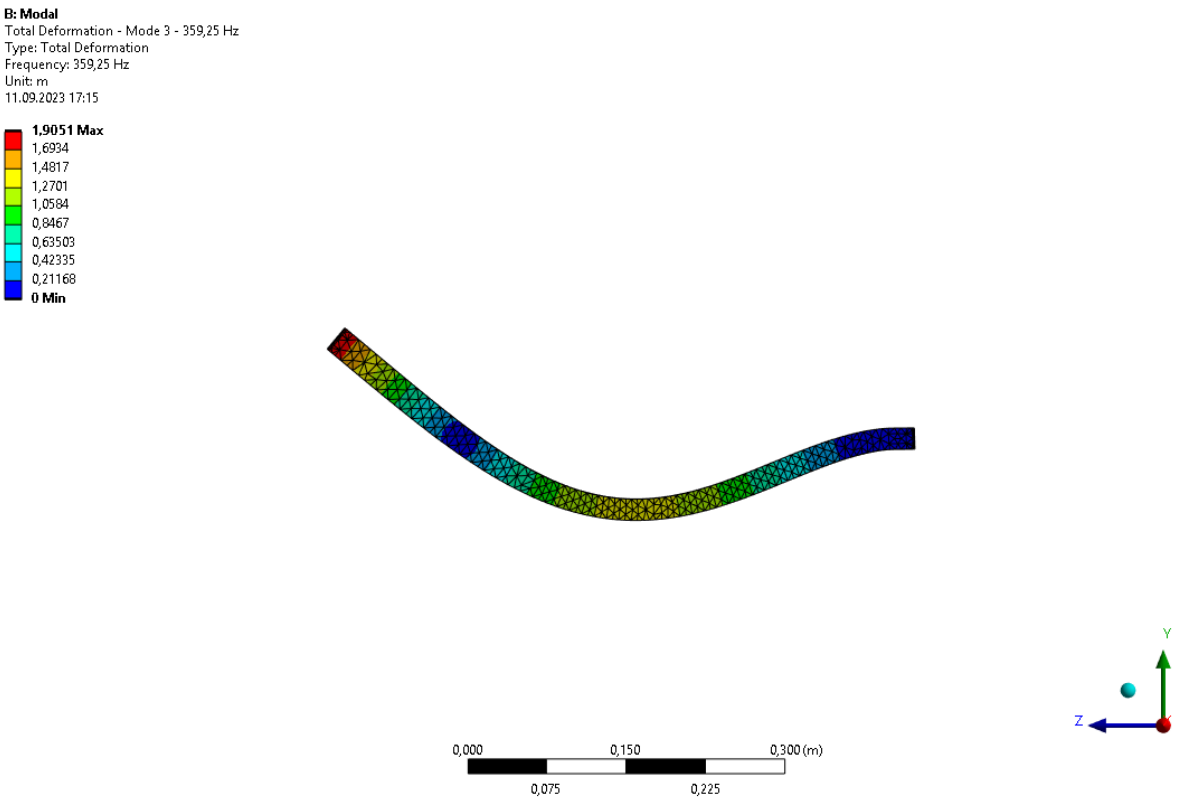

Figure 4.6 FEM result for 2nd bending mode shape

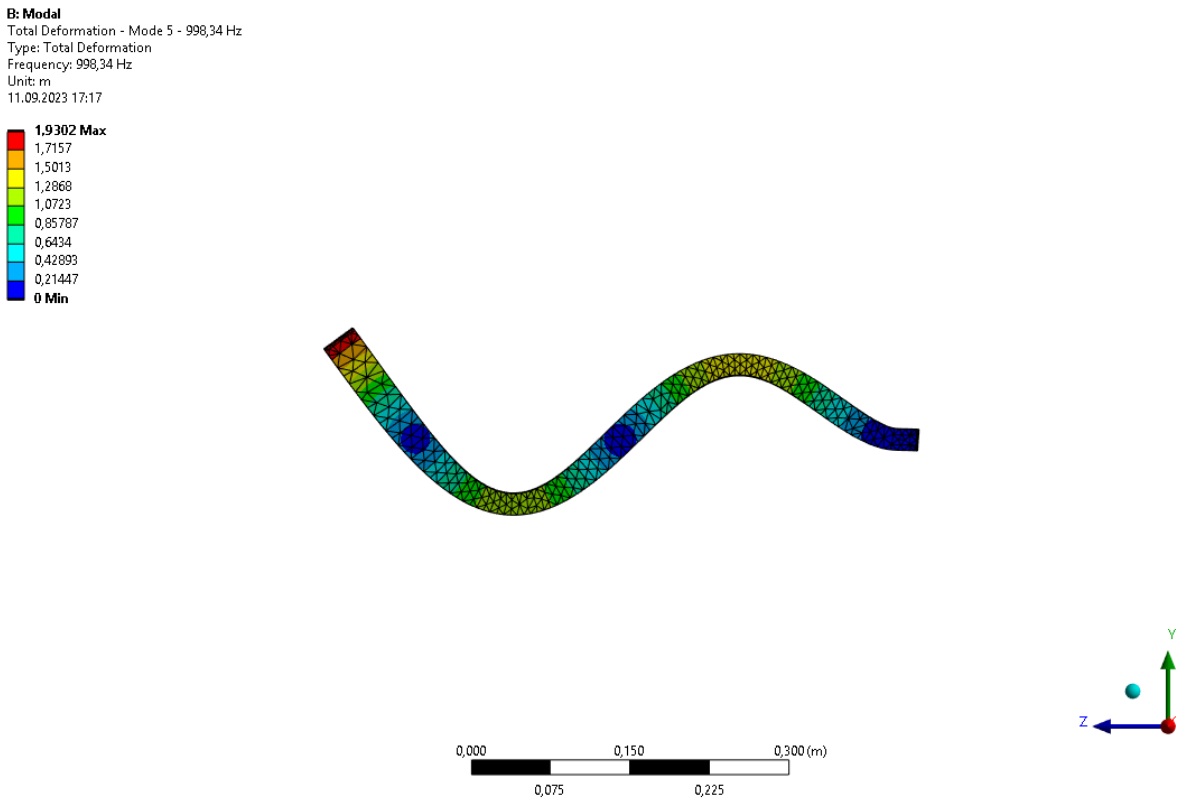

Figure 4.7 FEM result for 3th bending mode shape

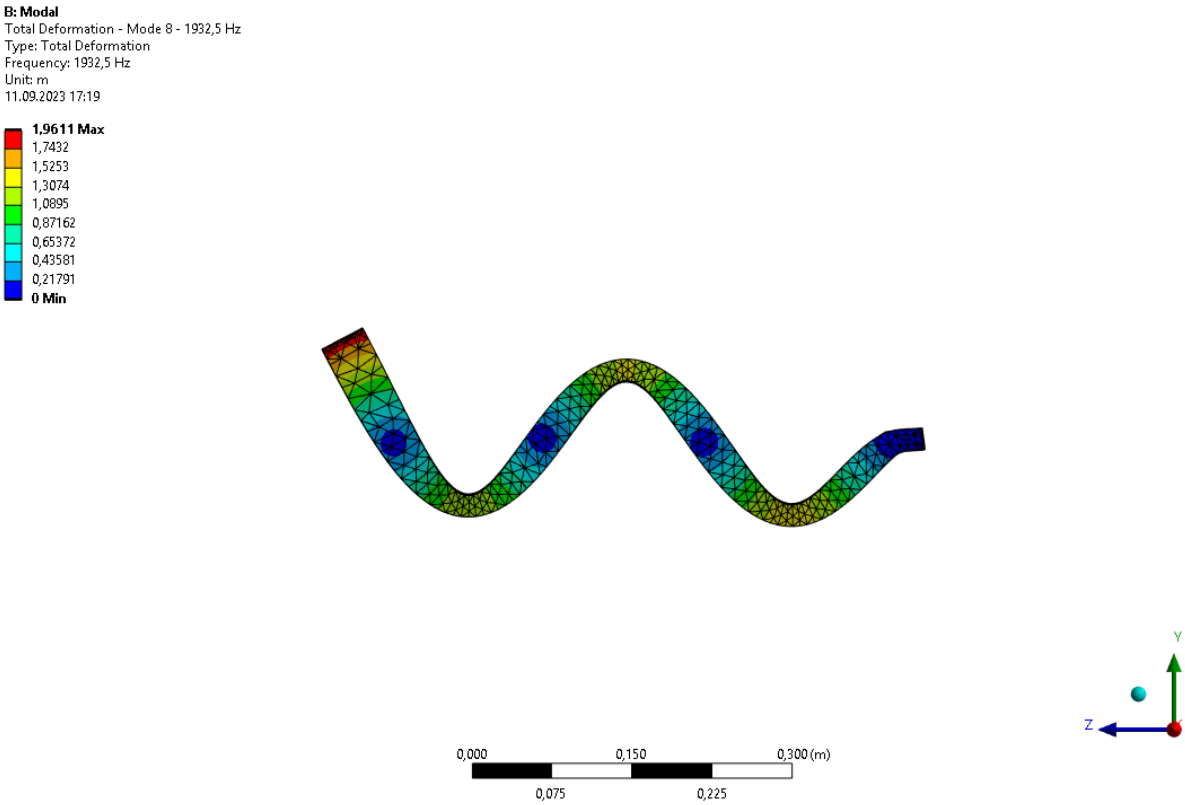

Figure 4.8 FEM result for 4th bending mode shape

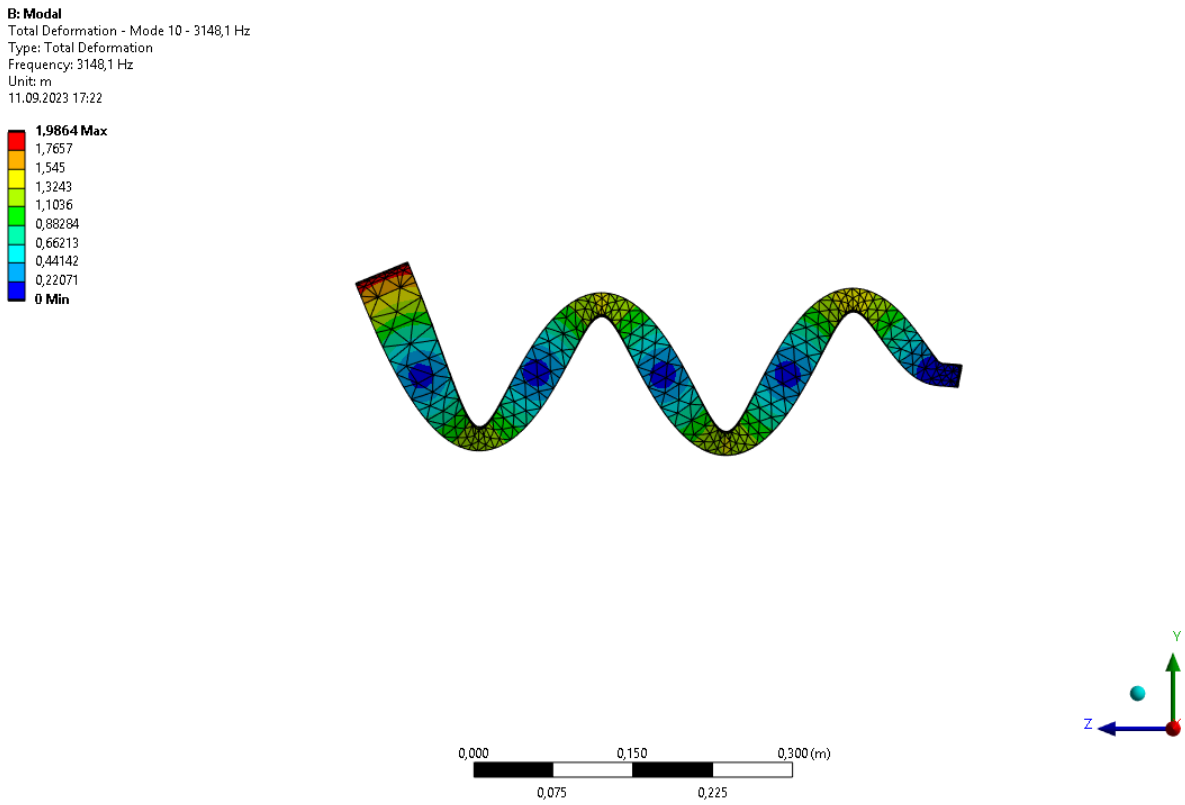

Figure 4.9 FEM result for 5th bending mode shape

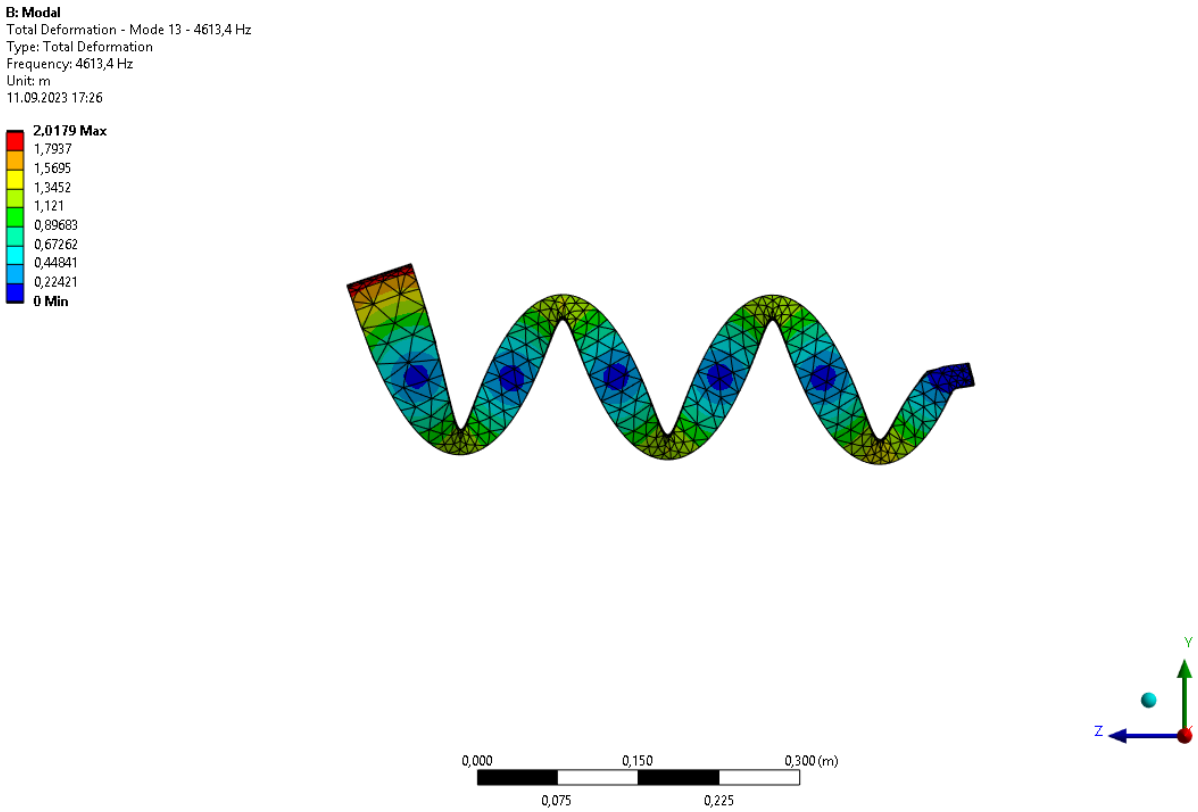

Figure 4.10 FEM result for 6th bending mode shape

4.4 Theoretical Results of the System Response

Equations given in Chapter 2.3.4 are used in order to find the theoretical result for the system response. Following properties given in Table 4.5 are used.

Table 4.5 Properties that are used to derive main properties

Property	Symbol	Value (Unit)
Wire diameter of the spring of TMD	d	0.3 mm
Mean coil diameter of the spring of TMD	D	2.5 mm
Torsional modulus of elasticity of the spring of TMD	G	44 GPa
Number of active coils of the spring	N	9
Number of springs in the system	N_s	4
Sprung mass of the TMD	$m_{TMD_{sprung}}$	14.3 gr
Unsprung mass of the TMD	$m_{TMD_{unsprung}}$	100.2 gr
Width of the cantilever beam	b_{beam}	40 mm
Height of the cantilever beam	h	20 mm
Length of the cantilever beam	L	547 mm
Density of the cantilever beam	ρ	2700 kg/m3
Young's modulus of the cantilever beam's material	E	69 GPa
Mass of the accelerometer	m_{acc}	4.4 gr

System response as receptance for different damping ratio values for the cantilever beam are found and plotted in Figure 4.11, while the TMD is off and on. Same colored curves mean the same damping ratio is fed to the simulation. Straight lines are the cases in which TMD is off and dashed lines are the cases in which TMD is on. Reduction of receptance with different damping ratios of the beam can be seen in Table 4.6. It can be seen that as the cantilever beam's damping ratio decreases, reduction of receptance increases. System without TMD's receptance is more sensitive to decrease of the damping ratio of beam then system with TMD.

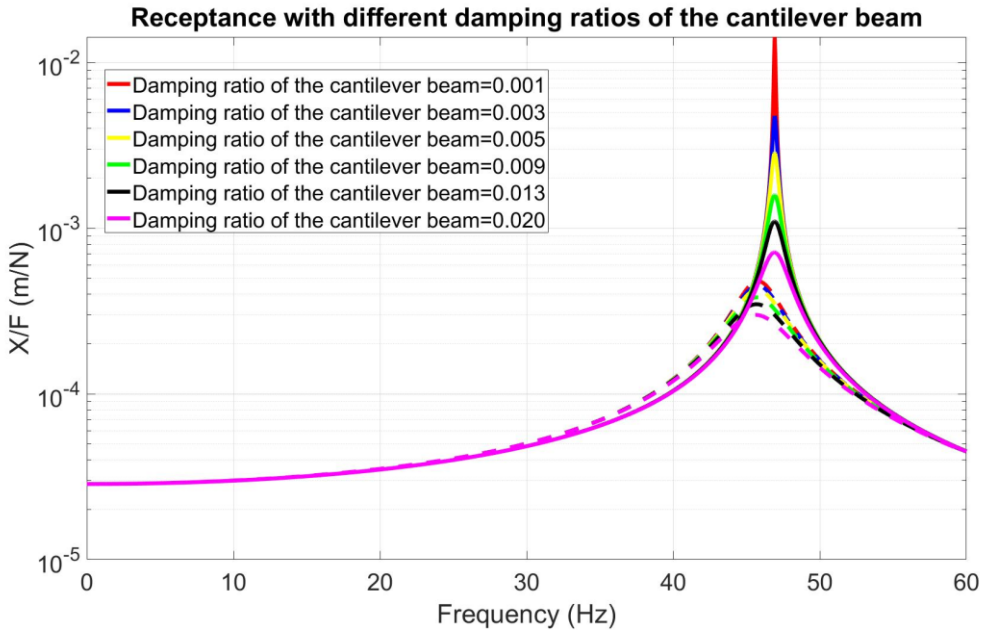

Figure 4.11 Frequency response function with different damping ratios of the cantilever beam

Table 4.6 Reduction of receptance with different damping ratios of the beam

Damping Ratio of the Cantilever Beam	Reduction of Receptance
0.001	29.1 to 1
0.003	10.4 to 1
0.005	6.6 to 1
0.009	4 to 1
0.013	3.1 to 1
0.02	2.4 to 1

System response as receptance for different damping coefficient of the TMD are found and plotted in Figure 4.12 while TMD is off and on. Magenta colored straight line represents the case while the TMD is off. Dashed lines are the cases while the TMD is on. Blue dashed line has the least amount of damping coefficient and magenta dashed line has the highest amount of damping coefficient. It can be seen in blue dashed line curve that receptance is the lowest amount of any case at natural frequency of the beam, but there are two peaks which have high receptance. As the damping coefficient increases, two peaks disappear and the system configuration with the TMD converges to the system without the TMD. Reduction of receptance at natural frequency with different damping coefficient of the TMD can be seen in Table 4.7.

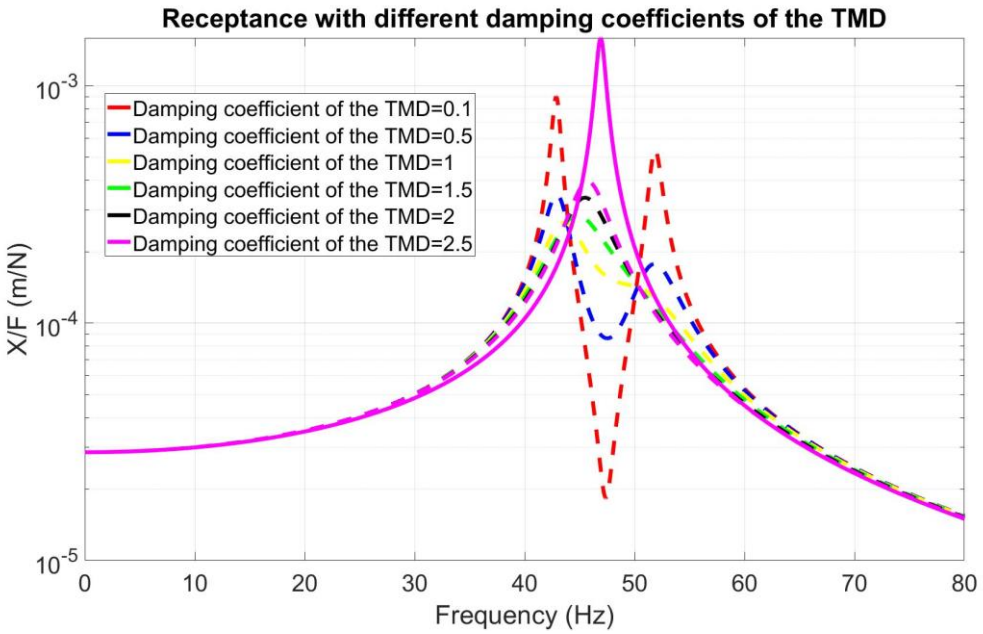

Figure 4.12 System response with different damping coefficients of the TMD

Table 4.7 Reduction of receptance with different damping coefficients of the TMD

Damping Coefficient of the TMD (Ns/m)	Reduction of Receptance
0.1	86.73 to 1
0.5	18.42 to 1
1	6.01 to 1
1.5	5.59 to 1
2	4.19 to 1
2.5	4 to 1

5. EXPERIMENTAL RESULTS

Theoretical results of the system are given in Chapter 0. In this chapter, TMD and the system which is made of TMD and cantilever beam is going to be validated experimentally. In order to do so, two experiments are designed. Design of this experiments are given in Chapter 3.2 and 3.3. Details about the experiment setups and results of the experiments are going to be given in the following sub-chapters.

5.1 Experimental Results of the Steady-State Damping Coefficient

In order to measure steady-state damping coefficient, a NdFeB N35 magnet is dropped inside of a hollow copper conductive tube. It can be seen in Figure 4.1 that magnet reaches terminal velocity almost instantly. Therefore, it is assumed that while magnet is free falling gravity acting on the magnet is equal to the drag force created by the ECD on the magnet. This equilibrium can be seen in Equation (5.1). c_d can be found by using Equation (5.2). Mass of the magnet can be weighed and velocity of the magnet can be found indirectly by dividing the height of the tube to time passed as the magnet drops within the tube. In order to find the velocity, time is measured as the magnet drops within the tube.

$$mg = c_d v \tag{5.1}$$

$$c_d = \frac{mg}{v} \tag{5.2}$$

Mass of the magnet and height of the tube are measured. Their values are given in Table 5.1.

Table 5.1 Material and geometric properties of steady-state damping experiment

Property	Value (Unit)
Mass of the magnet	5.80 gr
Height of the tube	150.04 mm

Velocity of the magnet as it drops within the tube is measured by the chronometer. 10 measurements are made and results of these measurements are given in Table 5.2. True error is found relative to theoretical result which is found in Chapter 4.1.

Table 5.2 Results of the 10 measurements

Experiment Number	Measurement (s)	Damping Coefficient (Ns/m)	True Error (%)
1	5.46	2.10	12.4

2	4.94	1.90	20.7
3	5.1	1.96	18.1
4	4.9	1.89	21.4
5	5.14	1.98	17.5
6	5.17	1.99	17.0
7	4.96	1.91	20.4
8	5.07	1.95	18.6
9	4.91	1.89	21.2
10	4.97	1.91	20.2

Average values from these 10 experiments are taken to determine the steady-state damping coefficient experimentally. Results are given in Table 5.3. The error may be caused by the manufacturing errors of the parts and human error while measuring the past time.

Table 5.3 Results of the average of 10 measurements

Average Measurement (s)	Damping Coefficient (Ns/m)	True Error (%)
5.06±0.17	1.95±0.06	18.8±2.59

5.2 Experimental Results of the Cantilever Beam Characterization

After theoretical analyses, the beam is manufactured and tested for its natural frequencies, mode shapes and modal parameters. Before the tests, beam's mass and geometric properties are measured. Results are given in Table 5.4.

Table 5.4 Mass and geometric properties of the beam

Property	Value (Unit)
Mass	1.218 kg
Length	547.2 mm
Width	40.3 mm
Height	20.2 mm

Afterwards, test setup is prepared to characterize the beam. Test equipment that are used in the tests are given in Figure 5.1. List of the equipment that are used is given in Table 5.5.

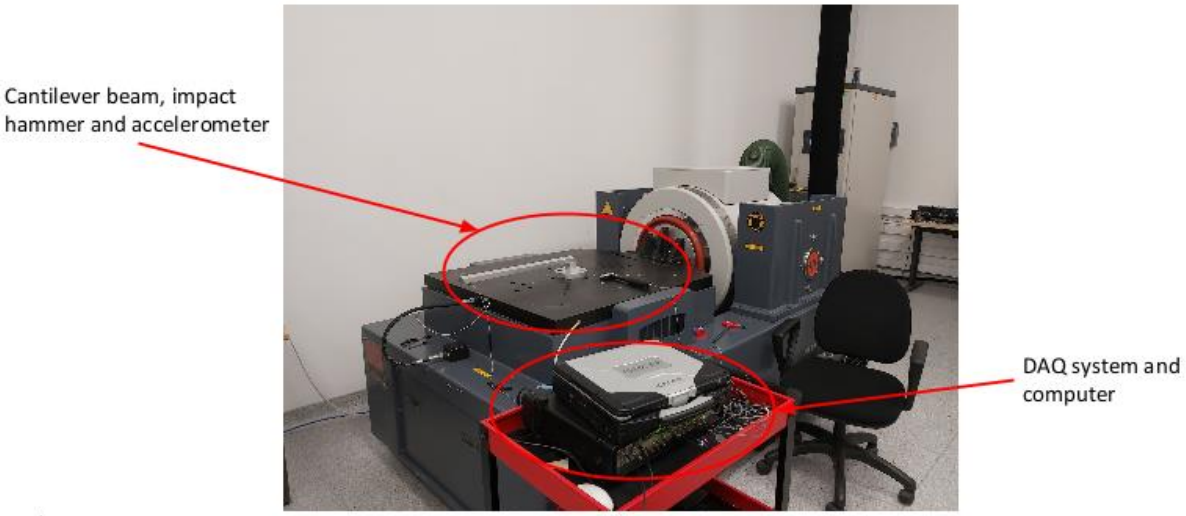

Figure 5.1 Cantilever beam characterization test setup

Table 5.5 Cantilever beam characterization test equipment

Equipment	Equipment Name
Impact Hammer	Brüel & Kjaer 8202
Accelerometer	Brüel & Kjaer 4507 (Single Axis)
DAQ System	PULSE IDA 3560-C Front End
Software	Pulse LabShop Release 20

In order to characterize the cantilever beam, the beam is excited near its free-end three times and FRF of these excitations are gathered. An impact hammer with hard tip which can be seen in Figure 5.2 is used in these excitations to excite a wide frequency band. These FRF's and average FRF are given in Figure 5.3.

Figure 5.2 Impact hammer with hard tip

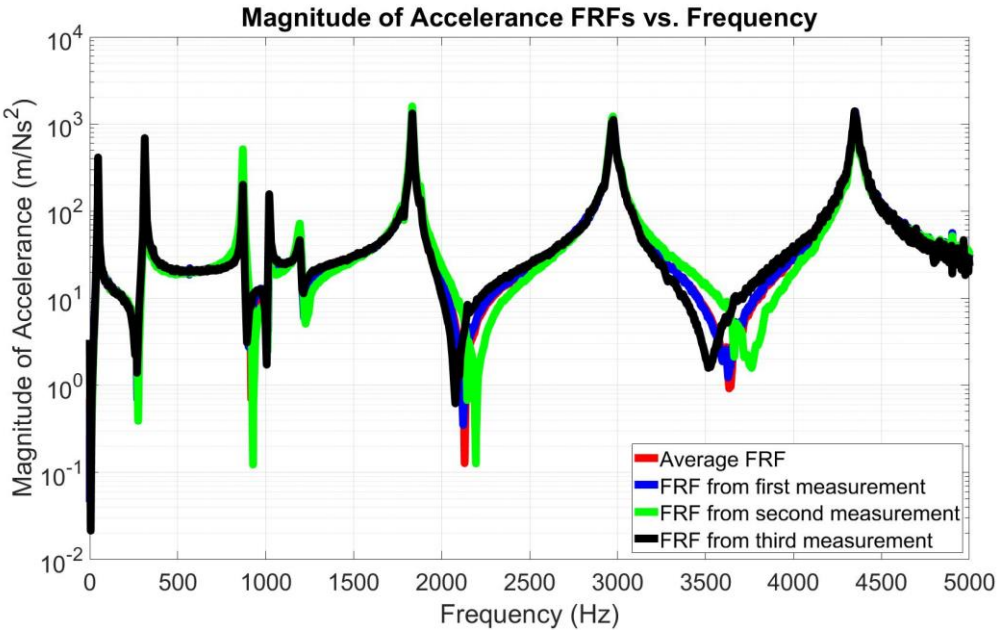

Figure 5.3 Magnitude of accelerance FRFs vs. Frequency of the cantilever beam

It can be seen that all FRF's are close in value except anti-resonances. In order to check this further and comment on repeatability of the measurements, coherence is found.

Coherence formulation can be seen in Equation (5.3). G_{fa} and G_{af} are cross power spectral densities of force and acceleration FRF's and G_{ff} and G_{aa} are auto power spectral densities of force and accelereation FRF's [30]. Coherence and average FRF is plotted together in Figure 5.4. Also, natural frequencies are shown in red circles. Values of these natural frequencies are given in Table 5.6.

$$C_{fa} = \frac{G_{fa}G_{af}}{G_{ff}G_{aa}} \tag{5.3}$$

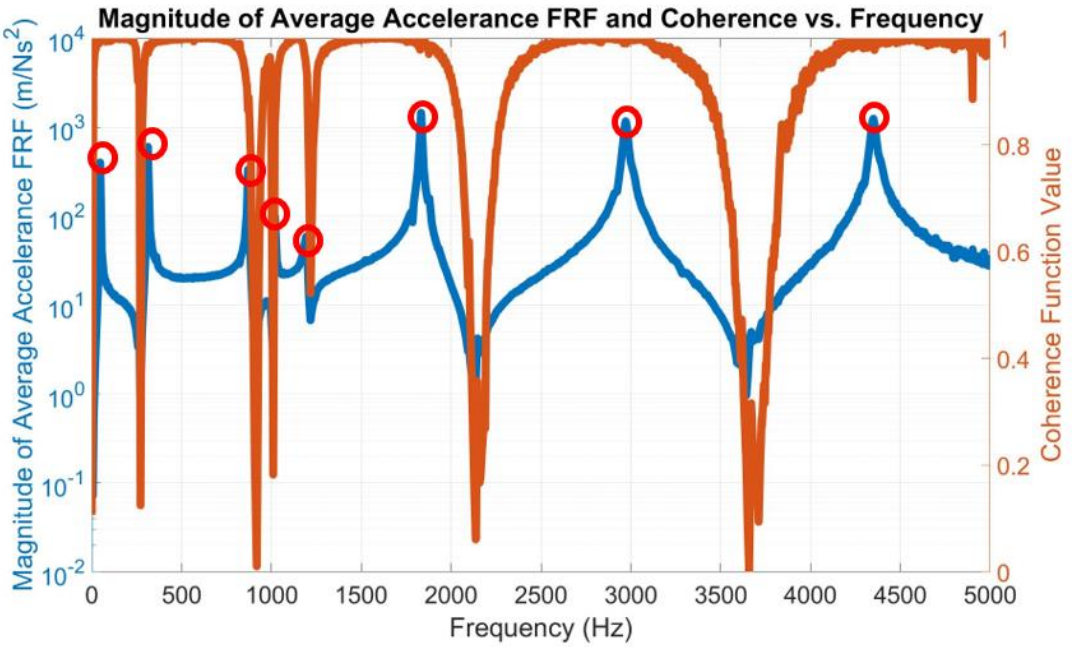

Figure 5.4 Magnitude of Average Accelerance FRF and Coherence vs. Frequency. Natural frequencies are marked in red circle

Table 5.6 Test results for modes of cantilever beam

Mode #	Natural Frequency (Hz)
1	46.9
2	312.6
3	870.2
4	1020
5	1194

6	1833
7	2970
8	4350

It can be seen from FEM results that there are 6 bending modes below 5 kHz. But there are 8 modes found by the tests. In order to see that all found modes in FRF are in fact modes of the structure, MIF is applied. MIF formulation can be seen in Equation (5.4). H_R is the real part of FRF and H_P represents the whole FRF with real and imaginary parts [31]. MIF plot can be seen in Figure 5.5.

$$MIF(f) = \frac{H_R(f)}{H_P(f)} \tag{5.4}$$

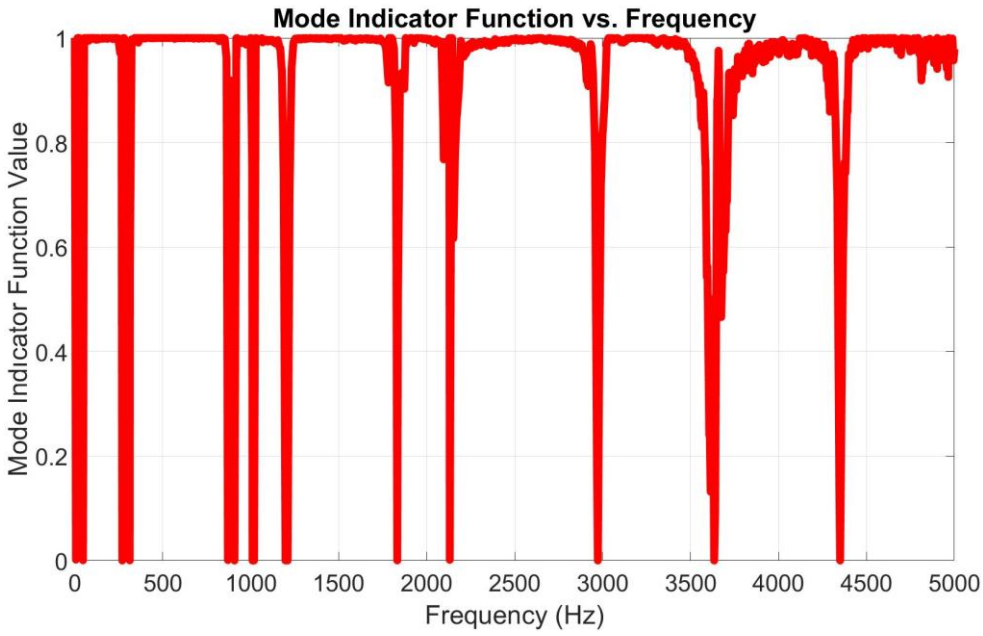

Figure 5.5 MIF vs. Frequency of cantilever beam

It can be seen from MIF plot that besides 8 modes from average FRF, anti-resonances of the FRF are shown as well. Appearing of anti-resonances in MIF is a regular phenomenon, since they represent a local minimum on the plot as well. Therefore, it is concluded that all 8 modes are modes of the structure. After founding the modes, corresponding mode shapes are found. In order to do that, cantilever beam is excited at several locations along the beam and at the free end with an impact hammer while an accelerometer is placed at the free end. Impact locations along the beam is shown in

Figure 5.6. Then, direct and cross FRF's are found to find mode shape of the cantilever beam.

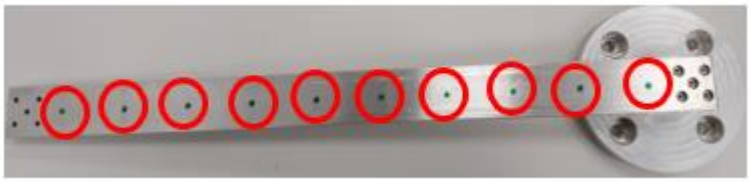

Figure 5.6 Impact locations along the beam

In order to find the mode shape of a mode, receptance FRF's imaginary peaks at natural frequencies are used as maximum displacement. Measurements are made by accelerometer and therefore found FRF's are accelerance. However, accelerance and receptance are related by square of the natural frequency. Equation (5.5) is used to find receptance imaginary peaks at every natural frequency for every direct and cross FRF measured. For a natural frequency, plotting data points which include receptance data and the impact location vs. beam length and curve fitting or interpolating the data points results with the mode shape at that natural frequency.

$$Im_{rec} = \frac{Im_{acc}}{{w_n}^2} \tag{5.5}$$

Found mode shapes of cantilever beam are shown in-between Figure 5.7 and Figure 5.16.

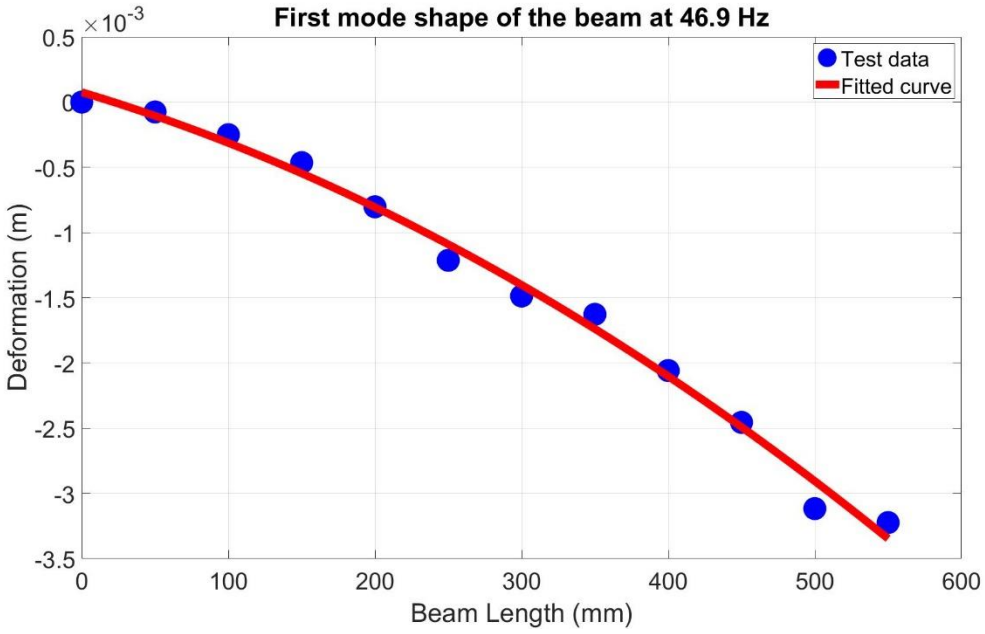

Figure 5.7 Test result for 1st mode shape

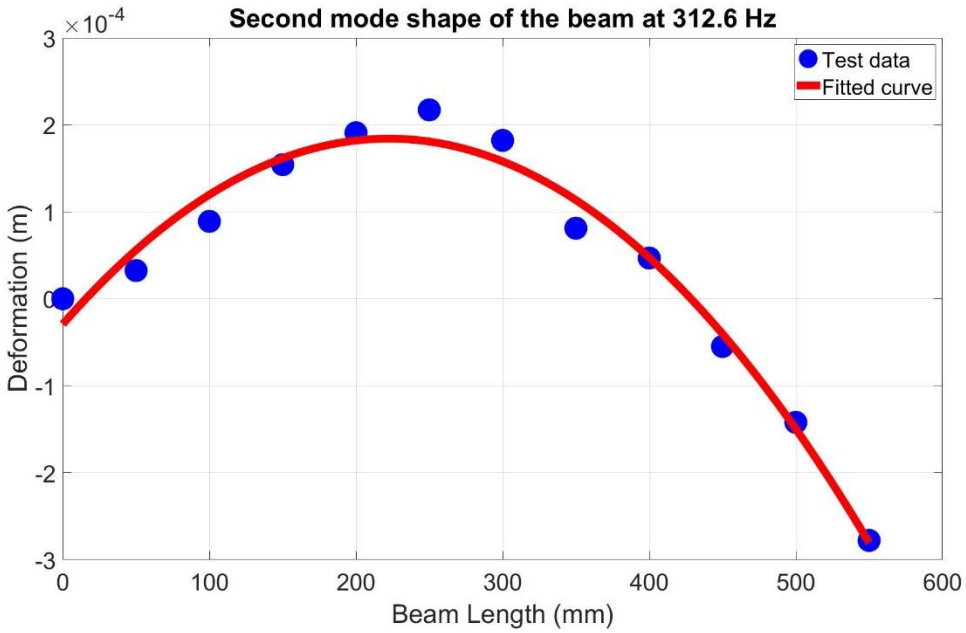

Figure 5.8 Test result for 2nd mode shape

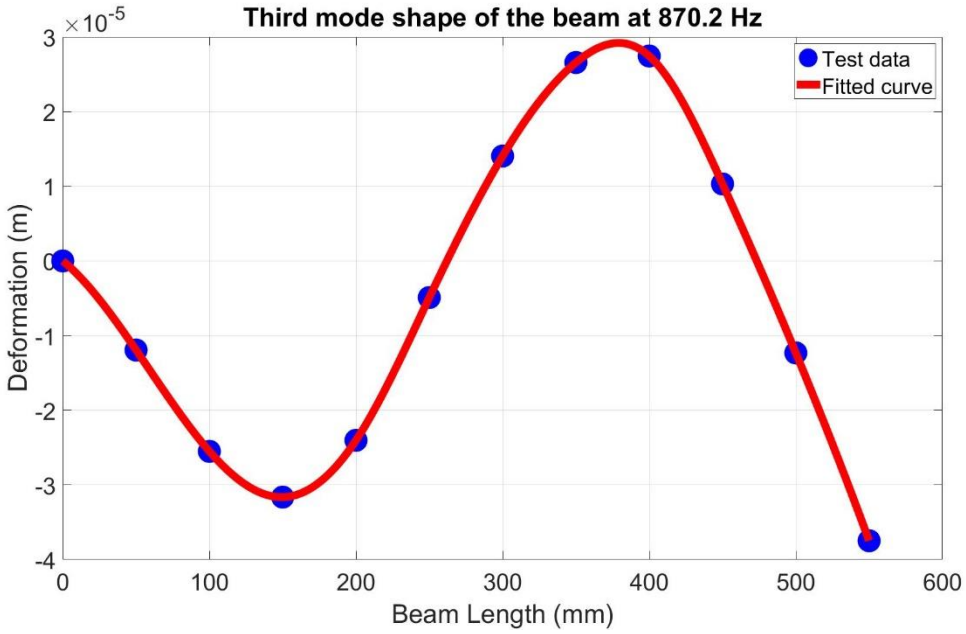

Figure 5.9 Test result for 3rd mode shape

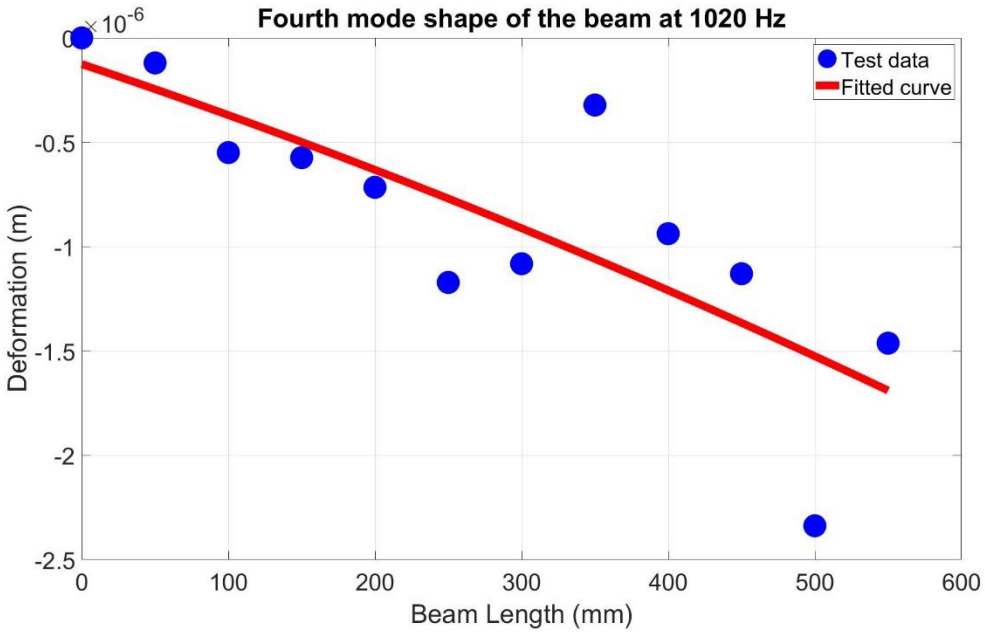

Figure 5.10 Test result for 4th mode shape

First three mode shapes are bending modes that match with the FEM results. Fourth mode shape does not appear as a bending mode in FEM results. After assessing the FEM results, it is seen that this mode shape is related with torsion rather than bending. Related torsion mode shape result from FEM results is given in Figure 5.11.

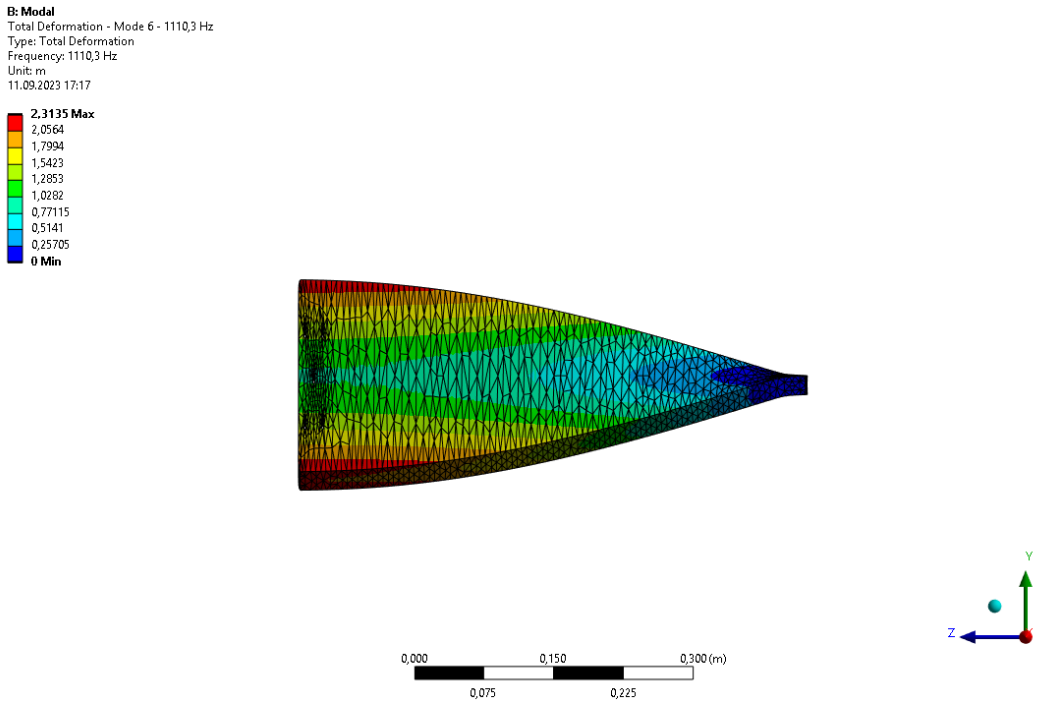

Figure 5.11 FEM result related with 4th mode shape of the cantilever beam test

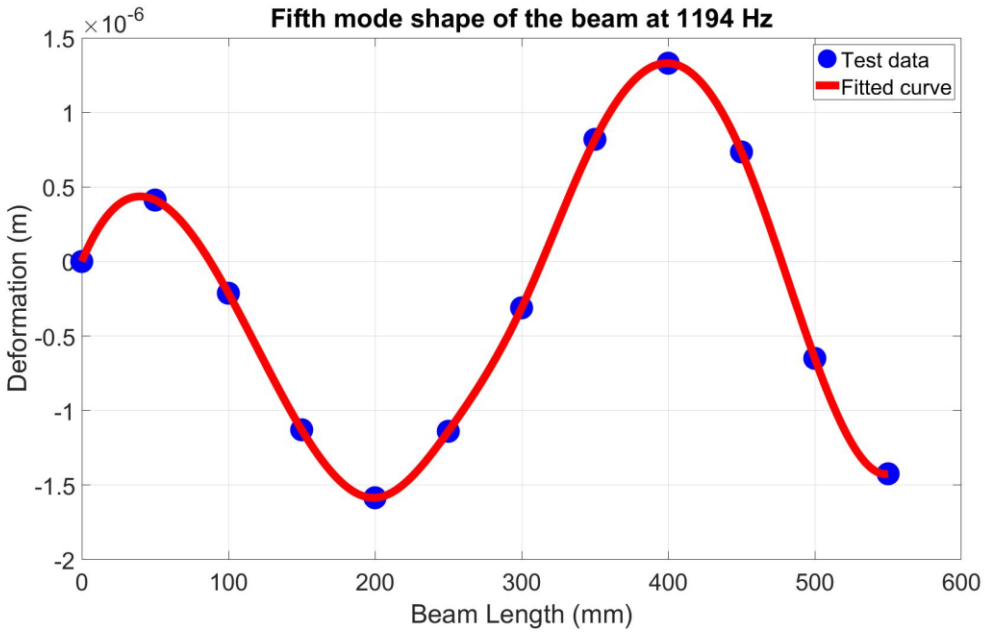

Figure 5.12 Test result for 5th mode shape

Fifth mode shape of the beam looks like the third mode shape, which is found to be third bending mode of the beam. No other mode shapes are found in proximity with this mode shape in FEM analyses. Because of this, FEM model is updated to include the test fixture to see the effects of the test fixture. It is found that given mode shape in Figure 5.13, which is a longitudinal and a bending mode shape, matches with fifth mode shape of the cantilever beam that is found in the tests.

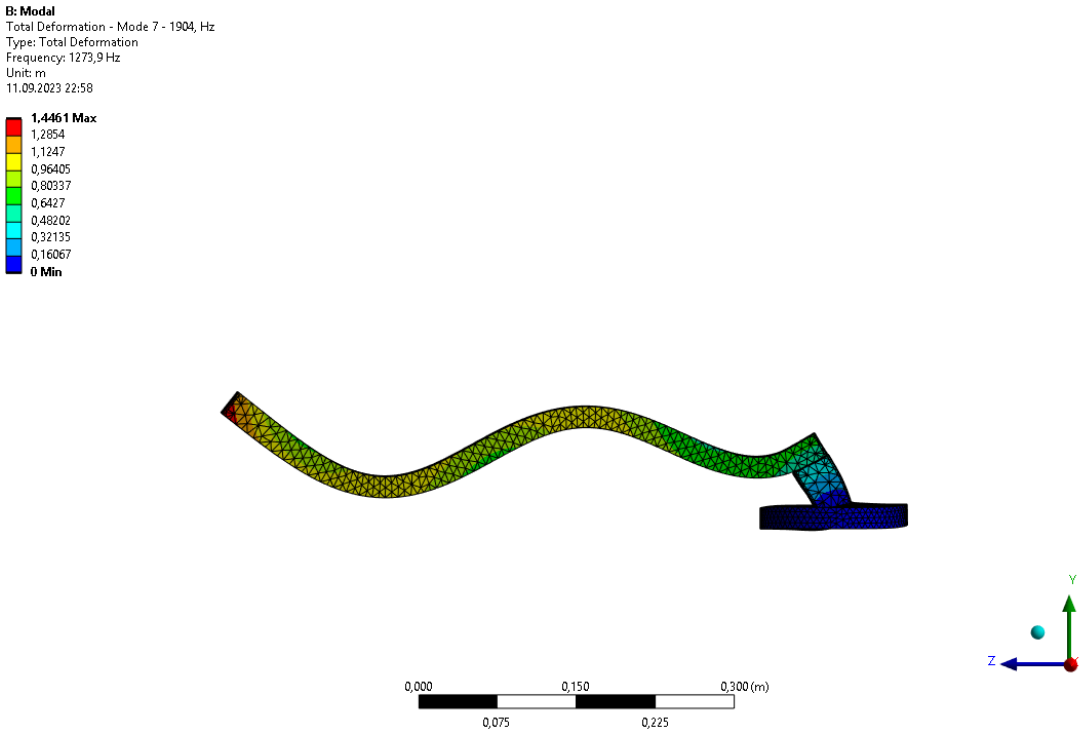

Figure 5.13 FEM result related with 5th mode shape of the cantilever beam test

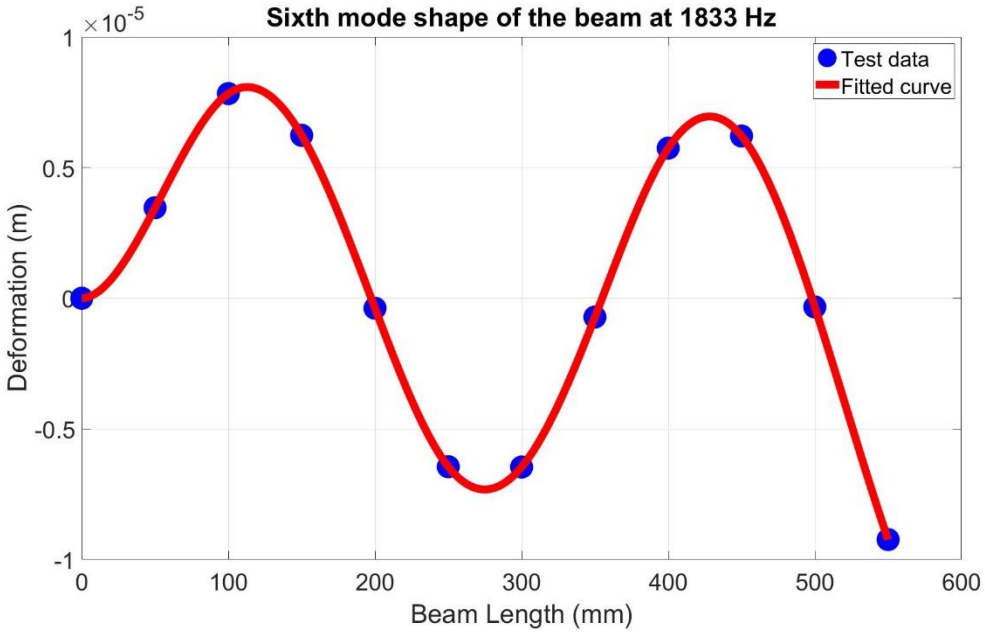

Figure 5.14 Test result for 6th mode shape of the cantilever beam

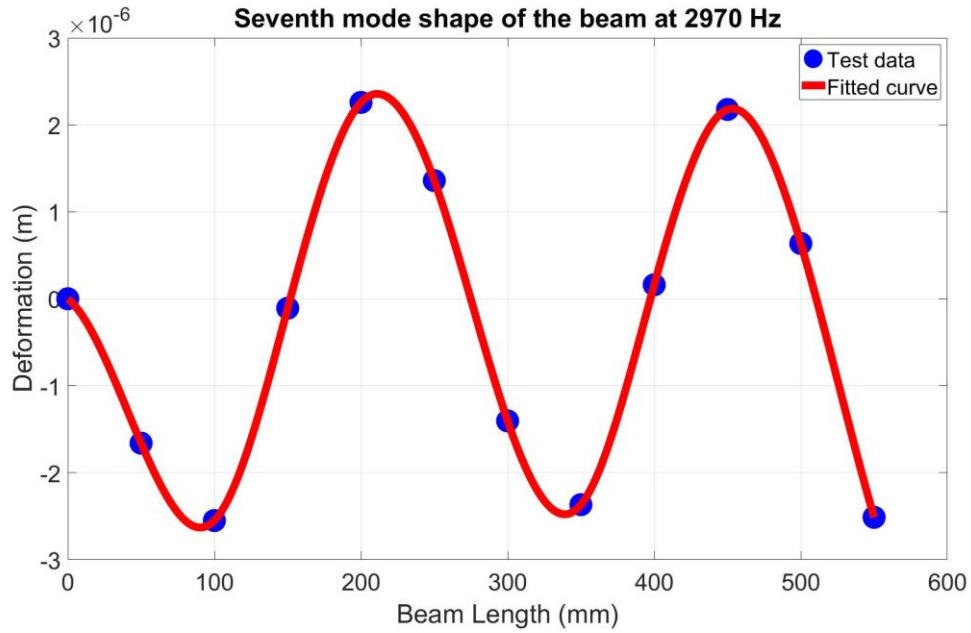

Figure 5.15 Test result for 7th mode shape of the cantilever beam

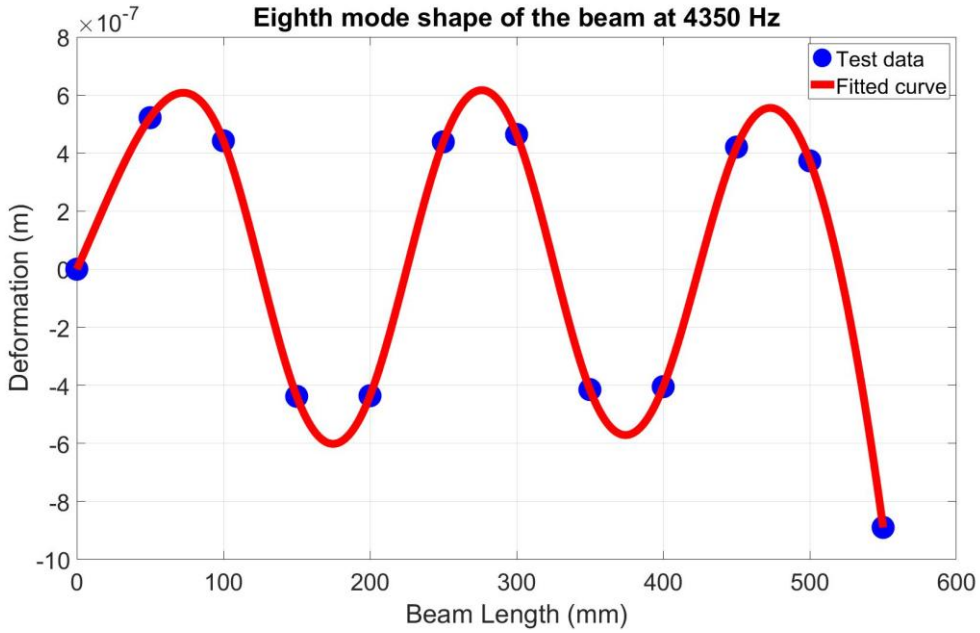

Figure 5.16 Test result for 8th mode shape of the cantilever beam

Sixth, seventh and eighth mode shapes are matching with fourth, fifth and sixth bending modes that are found in FEM results. Comparison of test results with FEM results are given in Table 5.7. It's found that error decreases as the frequency increases.

Table 5.7 Comparison of Test Results with FEM Results

Mode #	Error (%)

1	22.657
2	14.923
3	14.725
4	8.853
5	6.692
6	5.428
7	5.997
8	6.055

After modes and mode shapes are found, modal parameters of the mode shapes are extracted from the FRF's. Peak picking method is used in order to find these parameters [20]. Equations for peak picking method is given in Equation (5.6) to (5.9).

$$\zeta_{qi} = \frac{f_3 - f_2}{f_n} \tag{5.6}$$

$$k_{qi} = \frac{-1}{2A\zeta_{qi}} \tag{5.7}$$

$$m_{qi} = \frac{k_{qi}}{{w_n}^2} \tag{5.8}$$

$$c_{qi} = 2\zeta_{qi}\sqrt{m_{qi}k_{qi}} \tag{5.9}$$

Results of the peak picking method for the initial eight modes can be seen in Table 5.8.

Table 5.8 Modal parameters of cantilever beam

Case	Damping Ratio	Modal Stiffness (N/m)	Modal Mass (kg)	Modal Damping Coefficient (Ns/m)	Modal Frequency (Hz)
Mode 1	0.01559	3.53E+02	0.00406	0.03728	46.9
Mode 2	0.00352	4.70E+04	0.01221	0.16878	312.6
Mode 3	0.00239	1.08E+06	0.03619	0.95614	870.2
Mode 4	0.00147	7.58E+06	0.18454	3.47842	1020.00

Mode 5	0.00586	4.50E+06	0.07987	7.02586	1194.00
Mode 6	0.00218	1.06E+06	0.00800	0.40217	1833
Mode 7	0.00336	2.28E+06	0.00654	0.80977	2970
Mode 8	0.00253	5.92E+06	0.00793	1.07881	4350

It's found in results that the damping ratio of first mode is 5-7 times higher than the other modes' damping ratios.

5.3 Experimental Results of the Cantilever Beam Characterization While the TMD is off

After the beam is characterized using the modal analysis techniques, TMD is mounted on the beam while it's turned off and this configuration is tested to see the effects of the structure of the TMD to the cantilever beam. Photos of the TMD can be seen in Figure 5.17 - Figure 5.20.

Figure 5.17 Bottom view of the TMD.

Figure 5.18 Top view of the TMD.

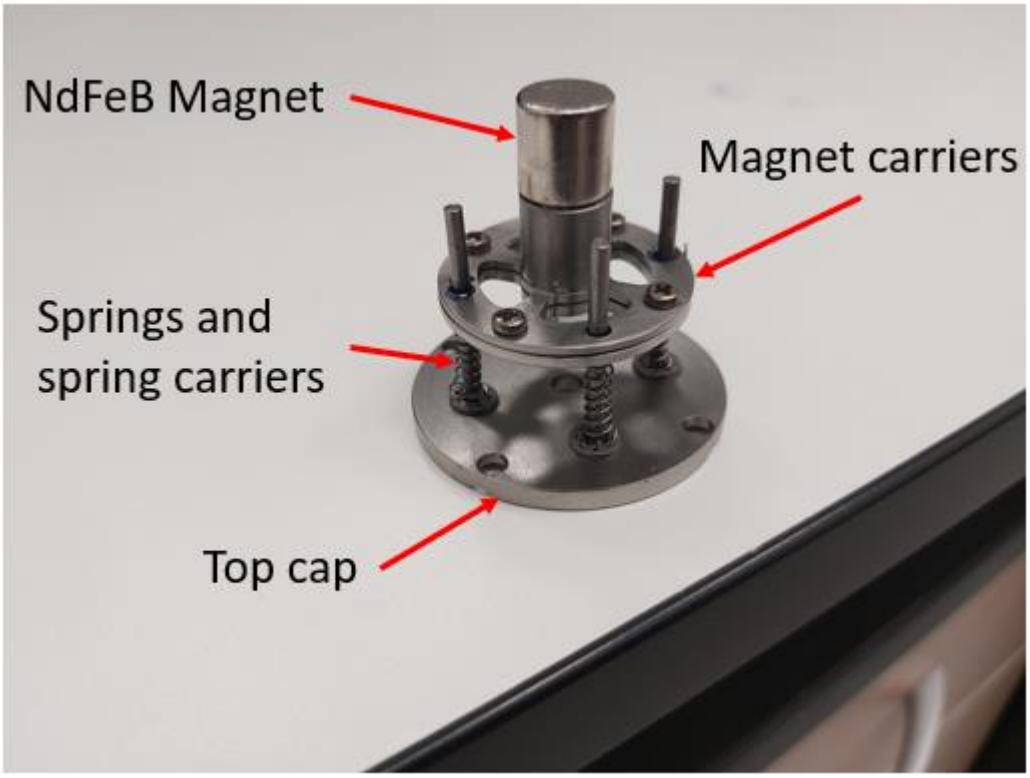

Figure 5.19 TMD's spring system which carries a permanent magnet.

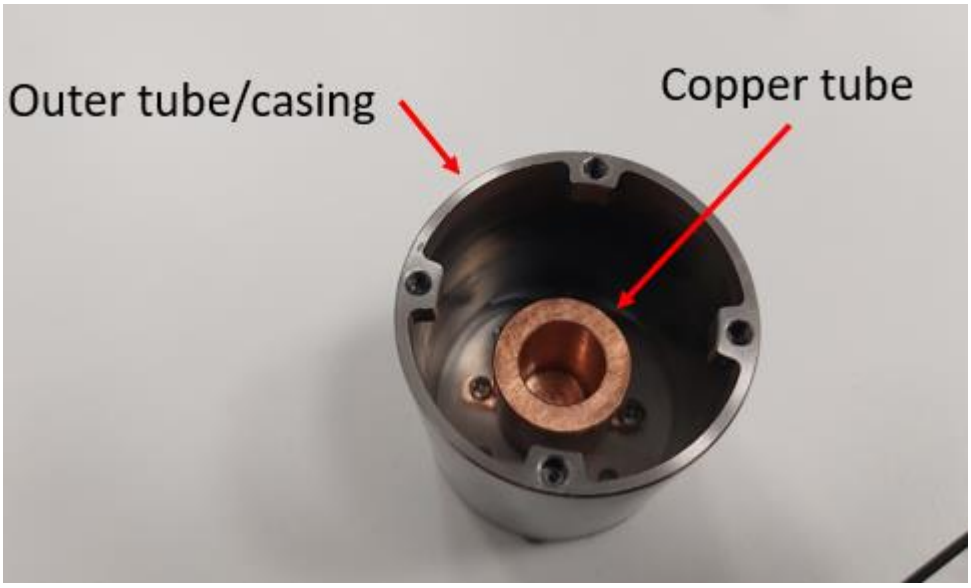

Figure 5.20 TMD's copper tube.

TMD’s mass is measured before the tests and it’s found as 117.9 grams, which is acceptable according to the analytical and 3D design models.

Before the beginning of the tests, TMD is turned off by using a polymer stopper which is shown in Figure 5.21.

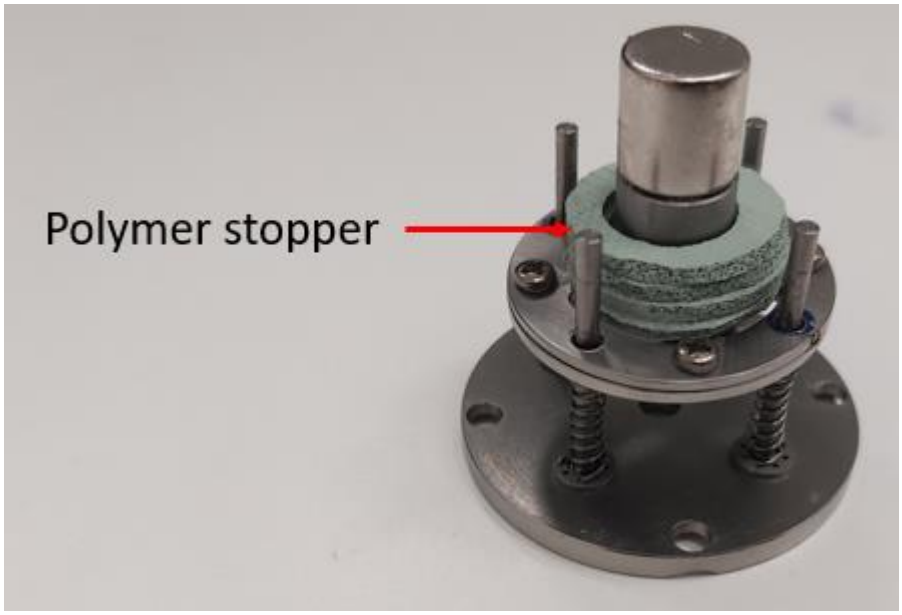

Figure 5.21 Polymer stopper (green) which is used to turn the TMD off

Since TMD is tuned at the first bending natural frequency of the cantilever beam which is 46.9 Hz, a low frequency band is the area of interest. Therefore, in order to excite this low frequency band a soft tip is used with impact hammer which can be seen in Figure 5.22. Test setup is given in Figure 5.23.

Figure 5.22 Impact hammer with soft tip

Figure 5.23 Cantilever beam characterization while the TMD is off test setup

In order to characterize the cantilever beam while the TMD is off, the beam is excited near its free-end three times and FRF of these excitations are gathered. These FRF's and average FRF are shown in Figure 5.24.

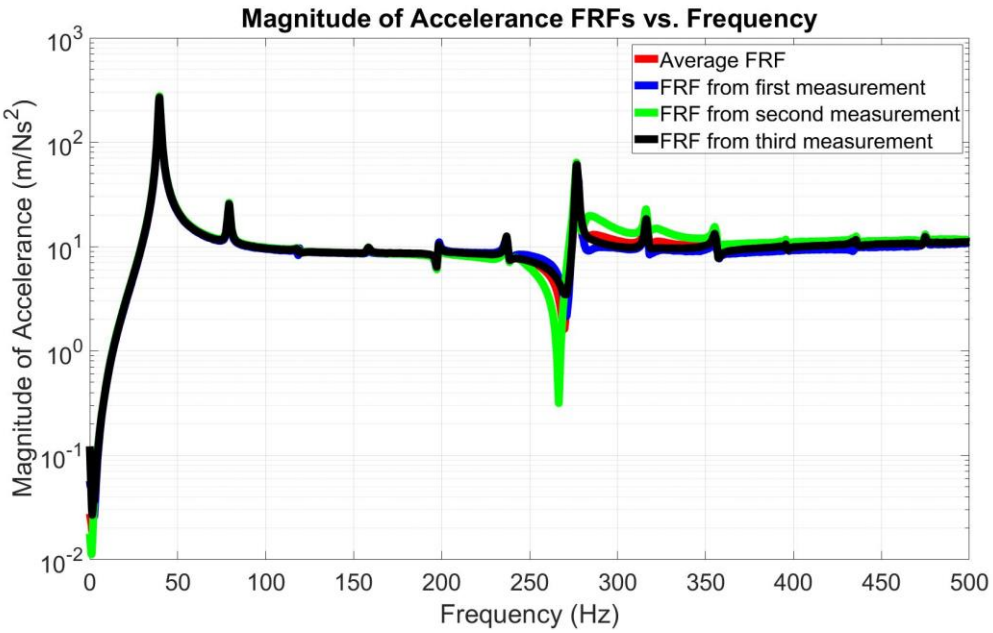

Figure 5.24 Magnitude of Accelerance FRFs vs. Frequency while TMD is off

It can be seen that all the FRF's are close in value except anti-resonances. In order to check this further and comment on repeatability of the measurements, coherence is found. Coherence and average FRF is plotted together in Figure 5.25. Also, natural frequencies are shown in red circles. Values of these natural frequencies are given in Table 5.9.

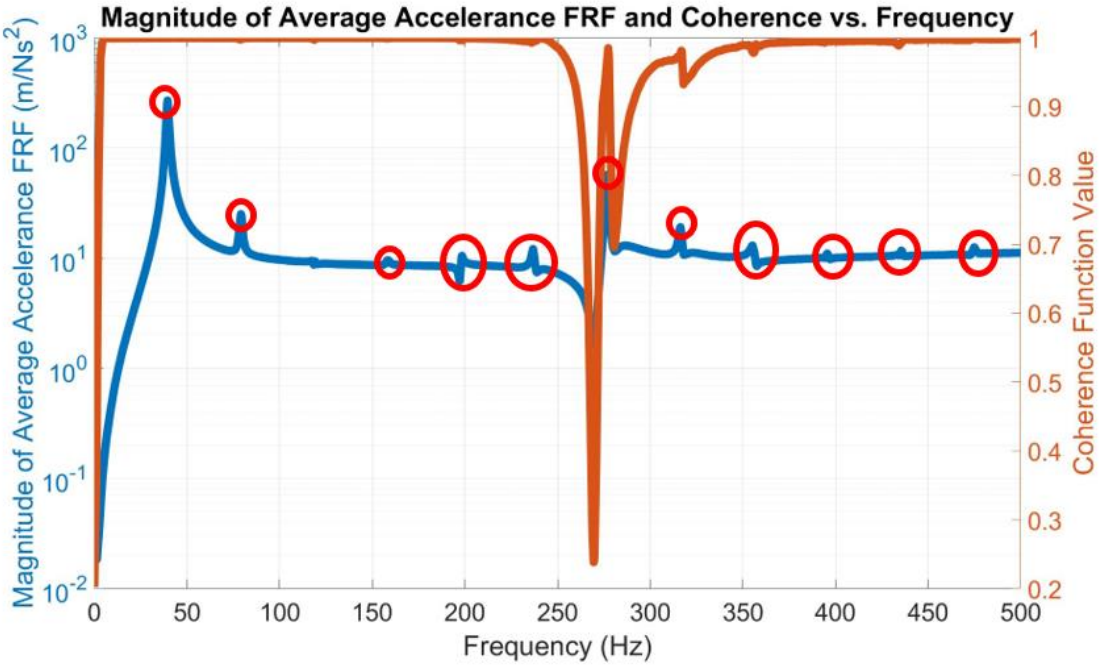

Figure 5.25 Magnitude of Average Accelerance FRF and Coherence vs. Frequency while TMD is off. Natural frequencies are marked in red circle

Table 5.9 Test results for natural frequencies of the cantilever beam while TMD is off

Mode #	Natural Frequency (Hz)
1	39.57
2	79.14
3	158.4
4	198.5
5	236.8
6	276.7
7	316.3
8	355.3
9	395.6
10	435.6
11	474.9

It is noted that all-natural frequencies are harmonics of the first natural frequency. Besides two large amplitude natural frequencies, there are nine low amplitude natural frequencies. In order to see if all of these natural frequencies are mode of the system, MIF is checked. MIF plot is given in Figure 5.26.

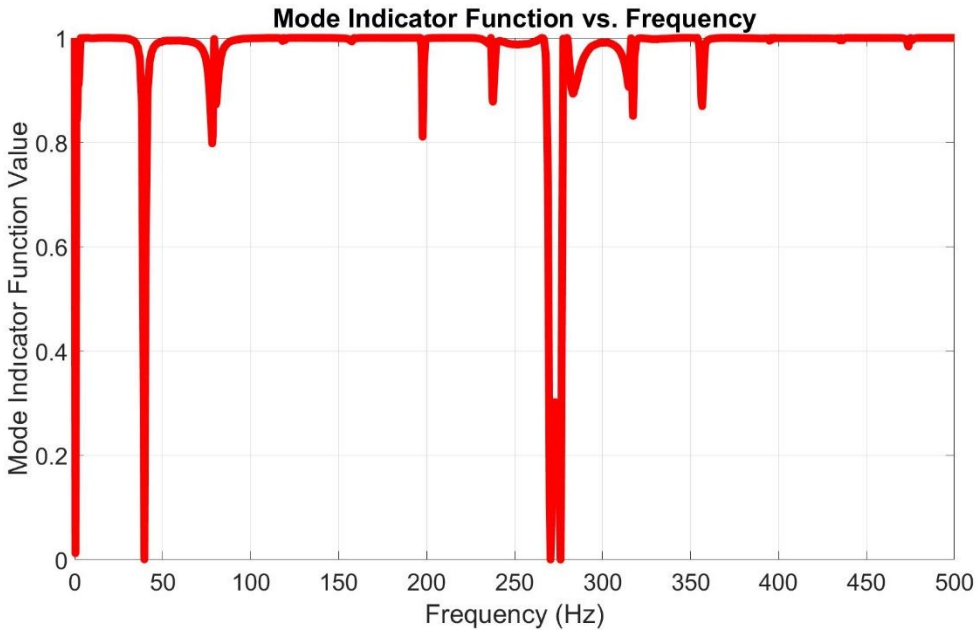

Figure 5.26 MIF vs. Frequency while TMD is off

It can be seen in Figure 5.26 that low amplitude harmonics do not fully represent the modes of the system, because MIF value is not zero at these frequencies. MIF value is zero at two large amplitude natural frequencies and anti-resonance region. It is concluded that low amplitude harmonics represent the modes related with springs of the TMD, not entire structure's modes. After this finding, stiffness of the spring system and cantilever beam is revisited. By assembling the TMD onto cantilever beam, spring system's stiffness is connected in series with cantilever beam's stiffness which can be seen in Figure 2.11. Equation (2.23) and Equation (2.30) and properties given in Table 4.5 are used to find the stiffness of the cantilever beam and spring system, which is given in Table 5.10.

Table 5.10 Stiffness properties of the spring system, cantilever beam and equivalent system in series

Parameter	Value (N/m)
Stiffness of the Spring System	1.26E+03
Stiffness of the Cantilever Beam	3.37E+04
Total Stiffness	1.22E+03

It can be seen from the Table 5.10 that the total stiffness is very close to the stiffness of the spring system. This means that the springs inside the TMD are the dominant stiffness-wise. Resulting harmonics are caused by this dominance of the spring system.

After founding the natural frequencies of the structure, corresponding mode shapes are found. In order to do that, cantilever beam is excited at several locations with an impact

hammer while an accelerometer is placed at the free end. Then, direct and cross FRF's are found to find mode shapes. Found mode shapes when TMD is off are shown in Figure 5.27 and Figure 5.28.

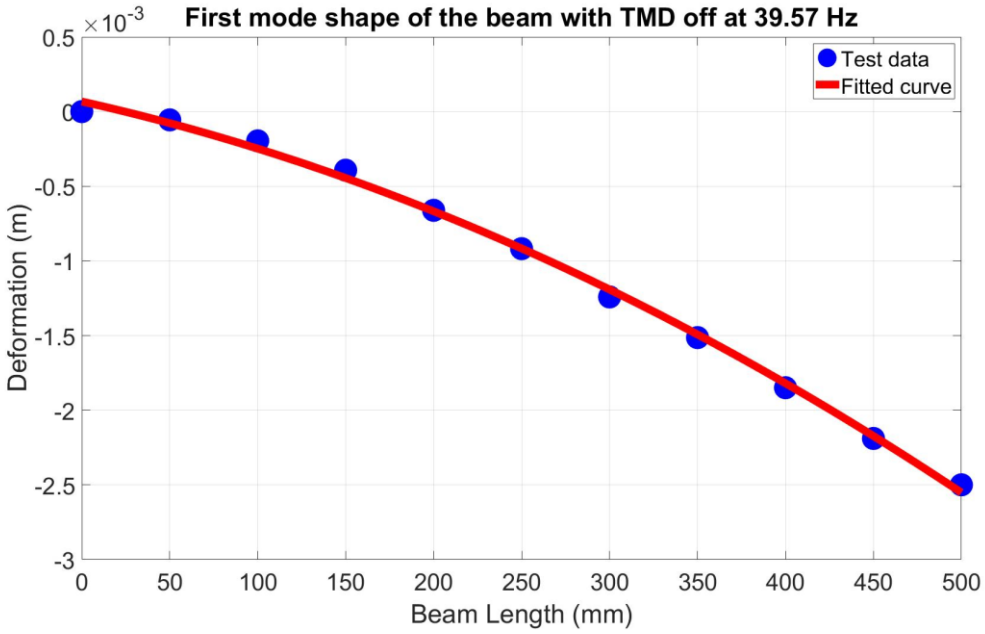

Figure 5.27 Test result for 1st mode shape of the cantilever beam while TMD is off

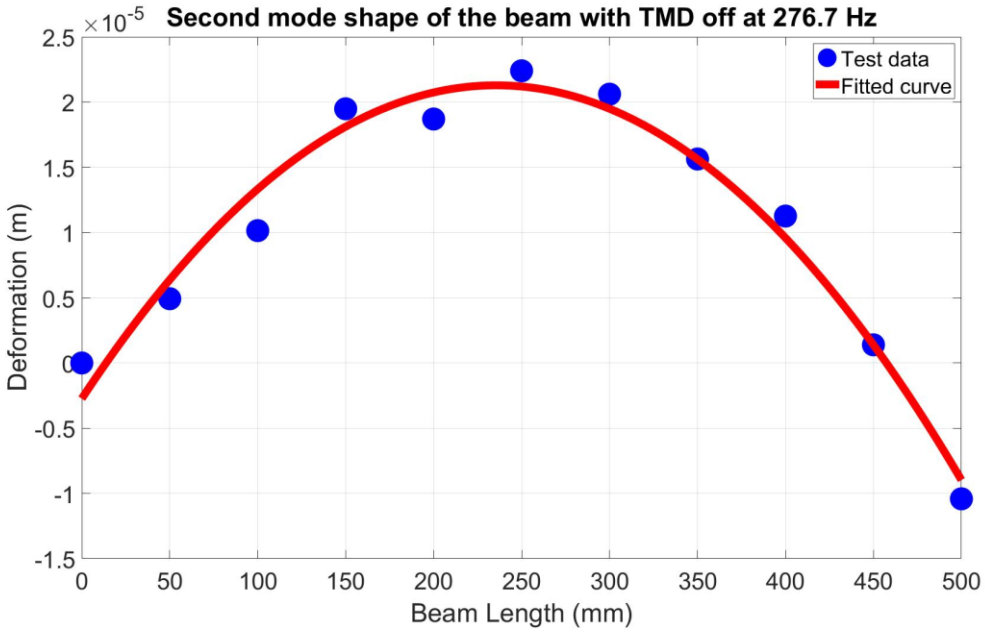

Figure 5.28 Test result for 2nd mode shape of the cantilever beam while TMD is off

After mode shapes have been found, modal parameters of these mode shape are extracted. In order to find these parameters, peak picking method is used [20]. Results of the peak picking method for the found two modes are shown Table 5.11.

Table 5.11 Modal parameters of the cantilever beam while TMD is off

Case	Damping Ratio	Modal Stiffness (N/m)	Modal Mass (kg)	Modal Damping Coefficient (Ns/m)	Modal Frequency (Hz)
Mode 1	0.01466	3.96E+02	0.00641	0.04671	39.57
Mode 2	0.00356	4.29E+05	0.14223	1.75225	276.7

It can be seen that damping ratio of the first mode is 4.1 times higher than the other mode's damping ratio.

5.4 Experimental Results of the Cantilever Beam Characterization While the TMD is on

After the beam is characterized while TMD is assembled to the free end while its off, the TMD is turned on by removing the polymer stopper and the same characterization procedure is followed for the TMD on case. An impact hammer with soft tip is used for the excitations. In order to characterize the cantilever beam while the TMD is off, the beam is excited near its free-end three times and FRF of these excitations are gathered. These FRF's and average FRF are given in Figure 5.29.

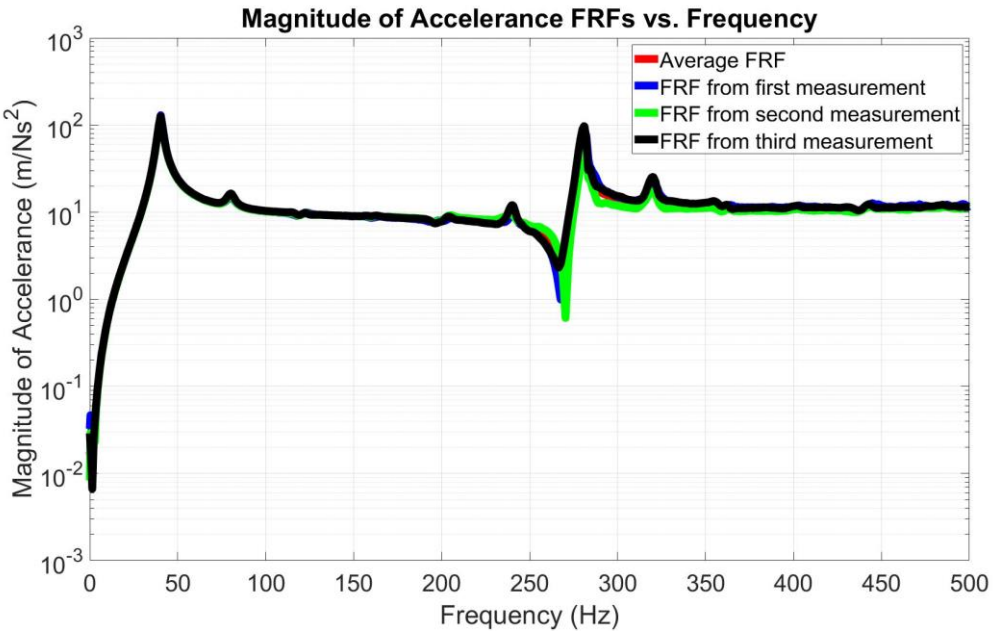

Figure 5.29 Magnitude of Accelerance FRFs vs. Frequency while TMD is on

It can be seen in Figure 5.29 that all the FRF's are close in value except anti-resonances. In order to check this further and comment on repeatability of the measurements, coherence is found. Coherence and average FRF is plotted together in Figure 5.30. Also,

natural frequencies are shown in red circles. Values of these natural frequencies are given in Table 5.12.

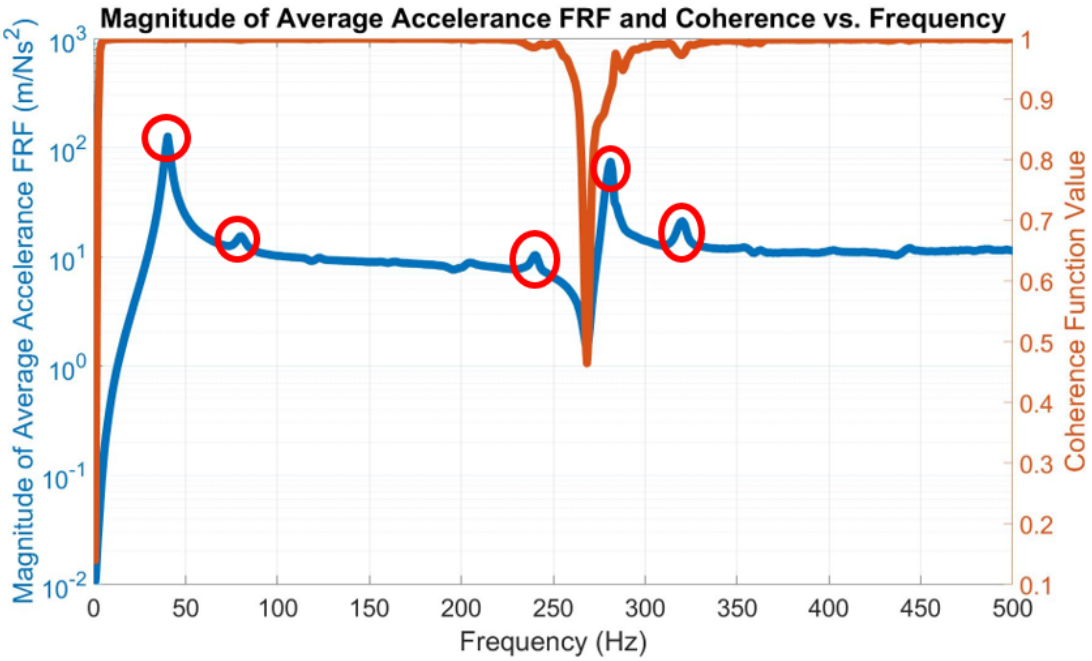

Figure 5.30 Magnitude of Average Accelerance FRF and Coherence vs. Frequency when TMD is on. Natural frequencies are marked in red circle

Table 5.12 Test results for natural frequencies of the cantilever beam while TMD is on

Mode #	Natural Frequency (Hz)
1	40.34
2	80.17
3	240.3
4	281.2
5	320.2

It is noted that all the natural frequencies are harmonics of the first natural frequency. Besides two large amplitude natural frequencies, there are three low amplitude natural frequencies. In order to see if all of these natural frequencies are mode of the system, MIF is checked. MIF plot is shown in Figure 5.31.

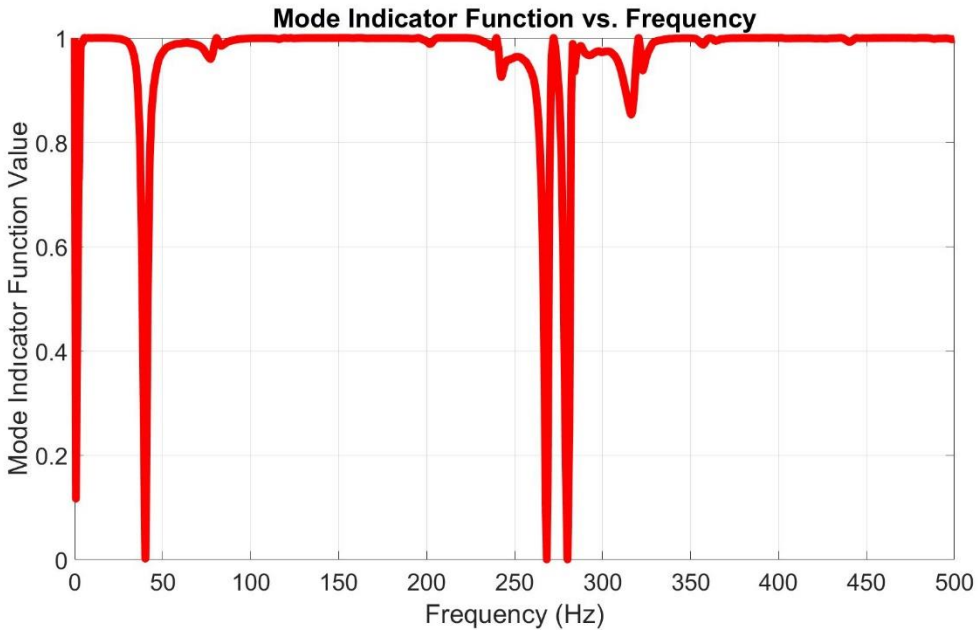

Figure 5.31 MIF vs. Frequency when TMD is on

It can be seen in MIF plot that low amplitude harmonics do not fully represent the modes of the system, because MIF value is not zero at these frequencies. MIF value is zero at two large amplitude natural frequencies and anti-resonance region. It is concluded that low amplitude harmonics represent the modes related with springs of the TMD, not entire structure's modes.

After founding the modes of the structure, corresponding mode shapes are found. In order to do that, cantilever beam is excited at several locations with an impact hammer while an accelerometer is placed at the free end. Then, direct and cross FRF's are found to find mode shapes. Found mode shapes when TMD is on are given in Figure 5.32 and Figure 5.33.

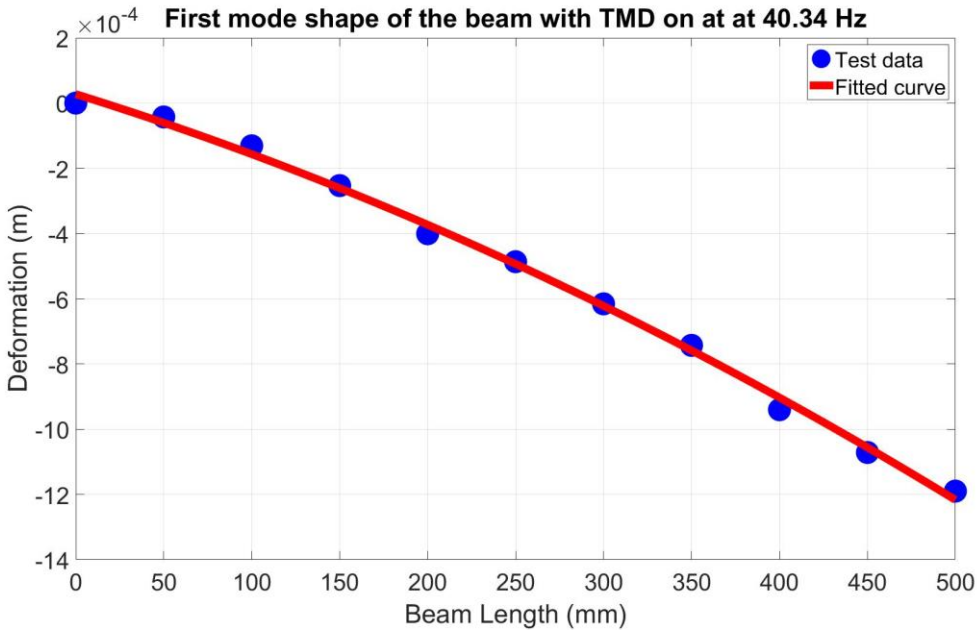

Figure 5.32 Test result for 1st mode shape of the cantilever beam when TMD is on

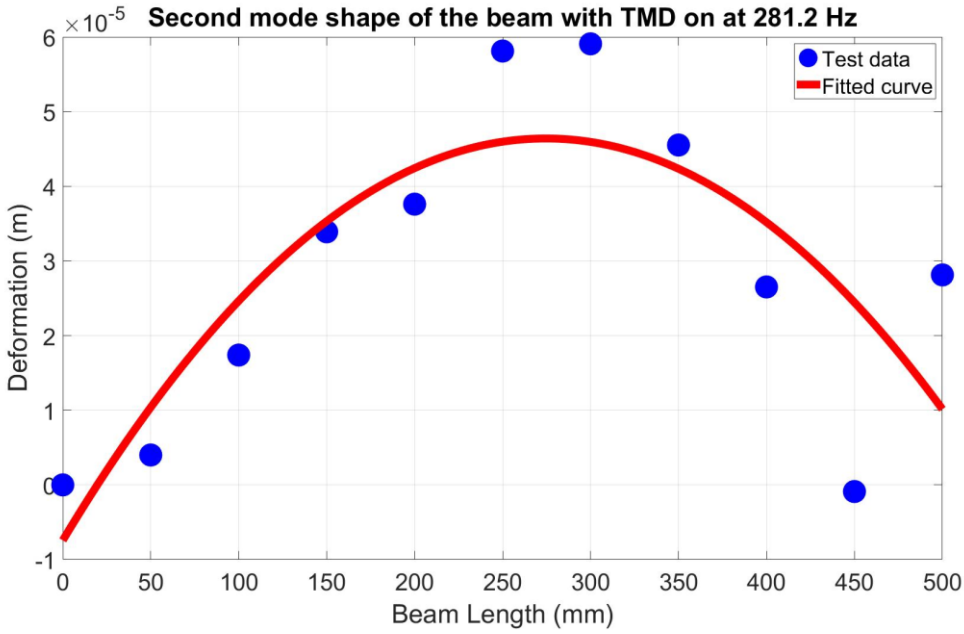

Figure 5.33 Test result for 2nd mode shape of the cantilever beam when TMD is on

After mode shapes have been found, modal parameters of these mode shape are found. In order to find these parameters, peak picking method is used. Results of the peak picking method for the found two modes can be seen in Table 5.13.

Table 5.13 Modal parameters of the cantilever beam while TMD is on

Case	Damping Ratio	Modal Stiffness (N/m)	Modal Mass (kg)	Modal Damping Coefficient (Ns/m)	Modal Frequency (Hz)

Mode 1	0.03623	3.55E+02	0.00556	0.10179	40.34
Mode 2	0.00707	1.68E+05	0.05393	1.36924	281.2

It can be seen in the results that damping ratio of the first mode is 5.1 times higher than the other mode's damping ratio.

5.5 Comparison Between Experiments with the Cantilever Beam, TMD off and TMD on Cases

Modal parameters for the first two natural frequencies of cantilever beam, cantilever beam with TMD off and cantilever beam with TMD on can be seen in Table 5.14 and Table 5.15. While damping ratio of cantilever beam and cantilever beam with TMD off are close, damping ratio is doubled as the TMD is turned on for both natural frequencies.

Table 5.14 Comparison for the first natural frequency

Case	Damping Ratio	Modal Stiffness (N/m)	Modal Mass (kg)	Modal Damping Coefficient (Ns/m)	Modal Frequency (Hz)
Cantilever Beam	0.01559	3.53E+02	0.00406	0.03728	46.9
Cantilever Beam with TMD off	0.01466	3.96E+02	0.00641	0.04671	39.57
Cantilever Beam with TMD on	0.03623	3.55E+02	0.00556	0.10179	40.34

Table 5.15 Comparison for the second natural frequency

Case	Damping Ratio	Modal Stiffness (N/m)	Modal Mass (kg)	Modal Damping Coefficient (Ns/m)	Modal Frequency (Hz)
Cantilever Beam	0.00352	4.70E+04	0.01221	0.16878	312.6
Cantilever Beam with TMD off	0.00356	4.29E+05	0.14223	1.75225	276.7

Cantilever Beam with TMD on	0.00707	1.68E+05	0.05393	1.3692	281.2

Accelerance plots for cantilever beam, TMD off and on cases are given together in Figure 5.34. As the TMD is introduced to the system while its off, natural frequencies of the system decrease. Response of the system at natural frequencies decrease as well. Reason for these changes is the addition of the tip mass. Although TMD's mass is only 10% of the cantilever beam's mass, assembling the TMD onto cantilever beam changes dynamic characteristics of the cantilever beam. Activation of the TMD reduces the vibration levels at first natural frequency of the structure and first harmonic natural frequency of the system. This region is given in Figure 5.35 with linear scaling. Amount of reduction is given in Table 5.16. Activation of TMD halves the accelerance levels at first natural frequency of the structure.

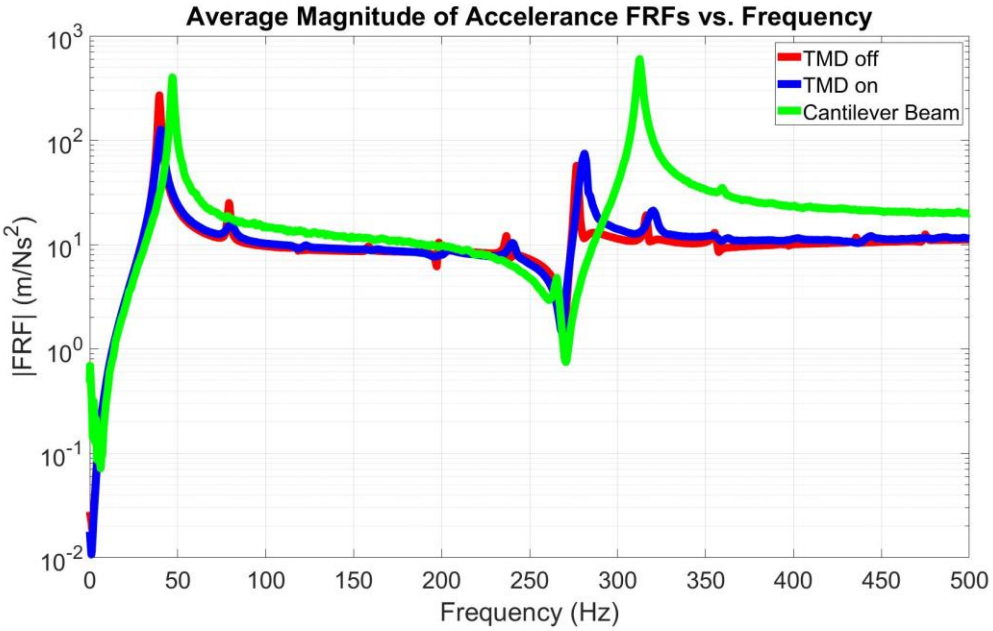

Figure 5.34 Comparison of cantilever beam, TMD off and on cases

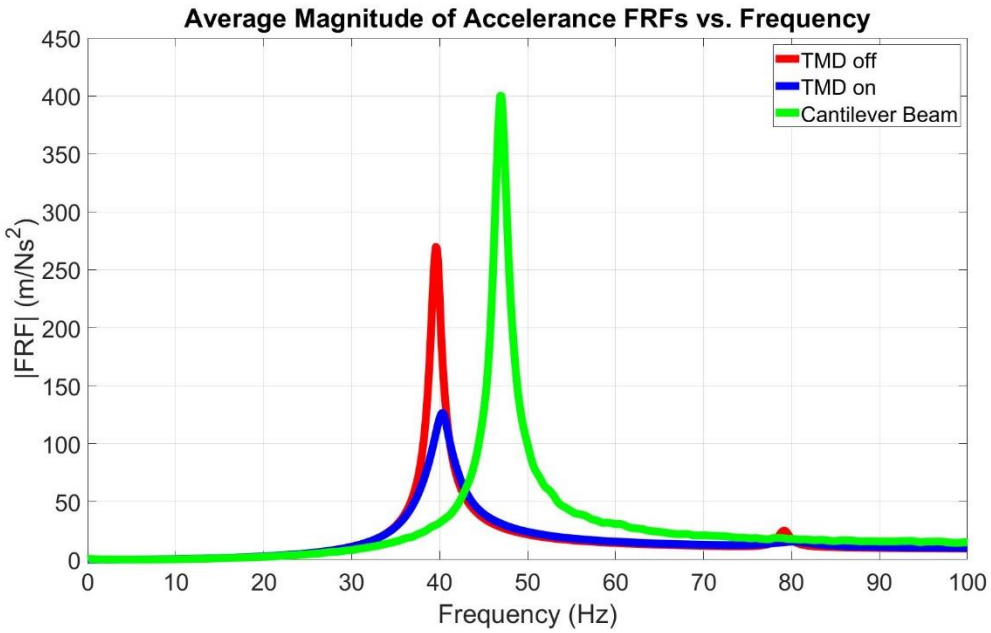

Figure 5.35 Comparison of cantilever beam, TMD off and on cases with linear scaling

Table 5.16 Reduction of vibration levels

Case	**Accelerance Magnitude Reduction**
First Natural Frequency of the Structure	2.13
First Harmonic Natural Frequency of Spring System	1.62

Besides the responses in frequency domain, responses in time domain are also given in Figure 5.36.

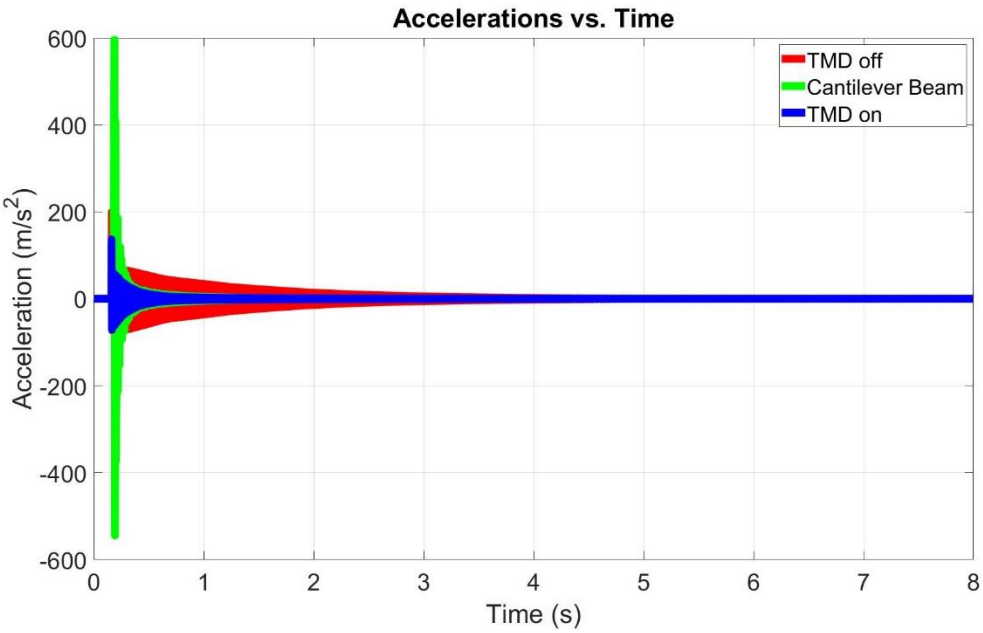

Figure 5.36 Comparison of cantilever beam, TMD off and on cases in the time domain

By using the measured values for damping ratio, length, width and height of the cantilever beam to update the response model given in Chapter 4.4, theoretical accelerance magnitude reduction is found to be 3.31 to 1. Theoretical system response while the TMD is off and on is shown in Figure 5.37.

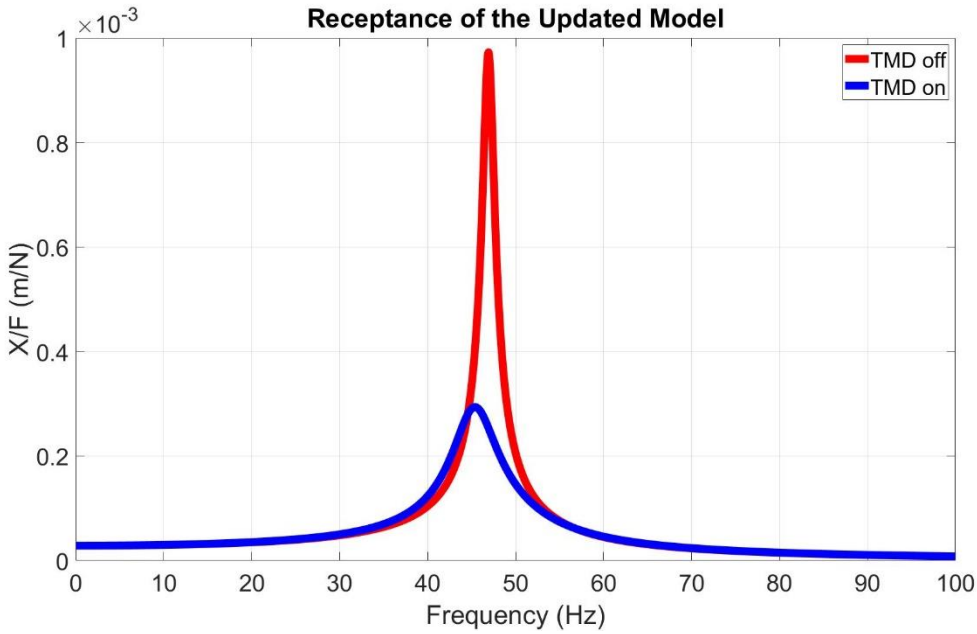

Figure 5.37 Theoretical system response with the measured parameters

Main source of error between theory and experimental results comes from the natural frequency shift of the system. TMD is tuned at 47 Hz theoretically. However, natural frequency of the structure is 39.57 Hz. Therefore, TMD is not working at its optimal

working conditions in experiments. Because of this, resulted error is found to be acceptable.

Although it is designed only for the first natural frequency of the structure, it can be seen from the results that it provides damping at first harmonic frequency of spring as well. As frequency increases and gets further away from TMD's tuned frequency, damping effect of the TMD decreases. At the second natural frequency of the structure, TMD increased the accelerance levels. Since it is further away from the tuned frequency of the TMD, TMD's disfunction at dampening accelerance levels is found to be acceptable.

At first and second natural frequency of the structure, activation of TMD increases the value of the natural frequency. It is concluded that as spring system of the TMD is activated, it tends to shift the natural frequency closer to its harmonic frequencies.

6. DISCUSSION AND CONCLUSION

All structures encounter vibration during their operation. A structure experiences the vibration load in an amplified manner at structure's natural frequency due to resonance. If the amplitude of vibration load is high enough, this may damage the structure. Tuned mass dampers (TMD's) are used as a passive vibration control strategy in order to prevent the failure.

A TMD, which may have a good applicability in space applications, is designed in this thesis work. Environmental effects of the space other than the mechanical loadings were out of context of this thesis. Only dynamic mechanical loadings were considered and assessed.

A TMD, which is designed to be used in the space applications, must be highly reliable. Because it operates in an environment which is hard to reach and apply maintenance. That's why, main concern in the TMD design was reliability. Literature survey about fundamentals of the TMD and types of TMD's was made and at the end of the survey a suitable concept of TMD for space applications was selected. This TMD concept was a classical TMD which is passively controlled and which utilizes eddy current damping (ECD) as the damping mechanism.

Classical TMD was chosen because of its simplicity. Chosen TMD was passively controlled because it does not require any means of an active control element and external power source to operate. These characteristics make passively controlled TMD concept highly simple and reliable. Eddy current damping mechanism was chosen to be used to create the damping effect because it creates the damping effect without the need of a physical contact. Instead of physical contact, it uses electromagnetic forces to create the damping effect. Electromagnetic forces are created by relative motion of a magnet near a conductive material. Also, since it does not contain any fluid, it does not have any sealing and packaging problems.

After the TMD concept was chosen to have ECD, details related how to achieve the ECD was investigated in the literature. Two different types to achieve ECD was found in the literature. These were placing permanent magnets directly across a conductive plate and placing permanent magnets inside of a conductive tube. Between these two types, placing permanent magnets inside of a conductive tube was chosen. Placing permanent magnets

inside of a conductive tube was a more suitable geometry than the contester because in the tube geometry the magnet is always at the same close proximity of the conductor.

After the TMD was selected, analytical model of the TMD was made. At first, analytical model for the damping coefficient was made. It was found on the literature that as the excitation frequency increases, the damping coefficient of the TMD decreases. Reason for that was found to be the skin effect. Because of this phenomenon, as the frequency increases effective thickness of the conductor decreases and this results with less damping. Therefore, a damping coefficient model which is a function of frequency was made. In order to do so, first a damping coefficient model for the steady-state damping coefficient was accomplished where no frequency effects are present and conductor's whole thickness is available to be used. Then, skin effect was introduced to this model and a model for dynamic damping coefficient was build-up.

After the dynamic coefficient model was presented, analytical and numerical models for the system were made. This system included a TMD and a structure which was to be controlled. Structure to be controlled was chosen to be a cantilever beam with rectangular cross section. TMD's and cantilever beam's models were made. At first the cantilever beam is investigated by itself in a wide frequency band by finding its natural frequencies and mode shapes. Then, frequency band narrowed down to first natural frequency. Mass, damping coefficient, stiffness and damped natural frequency for both of the structures were modeled for the first natural frequency. Coupling of these structures to simulate the assembly of these two structures were also modeled. Then, response of the coupled system under a harmonic sine sweep forcing excitation was modeled. To compare the structure with and without the TMD, response of the cantilever beam alone was also modeled.

Designs of the TMD, cantilever beam and experimental setups which were used for the experiments were made after preparing the models for the TMD. Two experiments were planned. These experiments were planned to validate steady-state damping coefficient and the system response.

Designs for the TMD, cantilever beam and experimental setups included the material selection and mechanical design of the TMD, the host structure (cantilever beam) and the experimental setups. In the TMD, magnet to be used was chosen to be a NdFeB N35

magnet because of its high magnetic flux density and its availability. Conductive material to be used was chosen to be copper because of its high electrical conductivity. Material for other supporting structures was chosen to be titanium because it has no magnetic properties and has low electrical conductivity. Because of this reason, its electromagnetic interference with the copper to interfere with the magnet was minimized. Material for the cantilever beam was chosen to be aluminum, since it is the most commonly used aerospace metal. Same material selection approach was repeated in the design of the experimental setups.

Mechanical design of the TMD was performed to maximize the damping effect generated by ECD. Magnet of the TMD has a diameter of 10 mm and a height of 10 mm. Copper tube of the TMD has an inner diameter of 11 mm and an outer diameter of 18 mm. Mechanical design of the cantilever beam includes mounting the interfaces with the TMD and test stand which was used for system response test. Mechanical design of the steady-state damping coefficient test included a copper tube which has same inner and outer diameter with the tube used in TMD and same magnet that was used in TMD. Mechanical design of the system response test comprised the system which is TMD assembled to the cantilever beam. An accelerometer was placed at the free end. Then, cantilever beam is assembled to test stand which is made of aluminum and the test stand assembled to a fixture.

After the system was modeled and designed, steady-state damping coefficient, dynamic damping coefficient and system response was found theoretically. In order to do that, MATLAB codes and FEM models were prepared. Steady-state damping coefficient was found to be 2.397 Ns/m. Dynamic damping coefficient was found in a frequency bandwidth of 0-500 Hz. Within this bandwidth, limit frequency in which skin effect becomes effective was found to be 357 Hz. Until this frequency, dynamic damping coefficient was found to be equal to the steady-state damping coefficient. After this frequency, dynamic damping frequency started to decrease. System response was found in both a wide frequency band and a narrow frequency band. FEM model to find natural frequency and mode shapes of the beam is prepared for frequency band up to 5 kHz. After that, two parametric studies were conducted in a narrower bandwidth. At first, damping ratio of the cantilever beam has changed and response of the system while the TMD is on and off were observed. It was found that as the damping ratio of the cantilever beam

increases, effect of the TMD increases. Then, damping coefficient of the TMD has changed and response of the system while the TMD is on and off were observed. It was found that low damping coefficient of the TMD has the lowest vibration amplitude at the natural frequency, but this caused two peaks around the natural frequency with large amplitude. As the damping coefficient of the TMD increases, two peaks formation fades away and response converge into the case where TMD is off.

After system response was found theoretically, experimental setups were prepared to validate the results experimentally. In order to validate theoretically found steady-state damping coefficient, a drop test was performed. NdFeB N35 magnet dropped inside of a copper conductive tube. Passed time was measured by a chronometer as the magnet drops. Ten experiments were made and steady-state damping coefficient was found by averaging the results of these ten experiments as 1.95 Ns/m. Percentagewise true error with respect to the theoretical result was found to be 18.8%. This error may be caused by the manufacturing errors of the parts and human error while measuring the past time. Damping coefficient was used to update the analytical model of the TMD system.

After finding steady-state damping by tests, test setups are prepared for system response test. At first cantilever beam's wide frequency dynamic characterization is made in system response tests in order to verify the cantilever beam. In these tests, an impact hammer with hard tip was used to excite to structure. Natural frequencies and mode shapes of the cantilever beam were found. Frequency band was 0-5 kHz due to equipment limitations. Although in FEM results, they were six bending natural frequencies within the band, eight natural frequencies were found. Measurements' repeatability was checked by the coherence function and found modes were validated by the MIF. Then, mode shapes of these natural frequencies are found by testing. It was verified by the FEM results that found six bending mode shapes matches with cantilever beam's bending mode shapes, one extra natural frequency was a torsional mode shape of the beam and the other one was a bending mode shape caused by the test fixture. Natural frequencies are found within 5.4-22.7% error. As the frequency increased, error decreased. This error is caused by manufacturing errors of the beam which result in a not ideal bent/twisted shape and measurement error which is caused by the test equipment. Modal parameters of these modes were found by peak picking method. It was observed that the damping ratio of the first bending mode of the system was 5-10 times higher than the other modes.

TMD was assembled while it's off to the cantilever beam, and same characterization process described above repeated. TMD turned off by inserting a polymer stopper to stop the movement of the springs. A soft tip used in the tests to excite low frequency band which first bending mode of the cantilever beam and tune frequency of the TMD was located. Frequency band was 0-500 Hz. Although in FEM results there were two bending modes within the band, nine other modes were also found. It was seen that all the modes are harmonics of the first mode. Cause of this was found that TMD's spring system's stiffness was more dominant in the system than cantilever beam's stiffness. This resulted with harmonics of the spring system's appearing in the FRF's. These harmonics were found not to be the system's modes by MIF. System's bending mode shapes matched with cantilever beam's bending mode shapes. Natural frequency of these modes dropped as expected by adding a tip mass to the system. Damping ratios of the modes of the system were not significantly changed after assembling the TMD. Damping ratio of the first bending mode was used to update the analytical model of the TMD system.

Then, TMD was activated by removing the polymer stopper and same procedure with TMD off case was repeated. Two bending modes and three harmonics of the spring system were found in the frequency spectrum. Effect of the TMD was observed clearly with a smaller number of harmonics. System's bending modes were matched with TMD off case. Damping ratio of the system modes were doubled. Three times of amplitude drop was expected by the activation of the TMD from the updated TMD model, but amplitude drop was seen to be 2 times at the first bending mode. Error in the amplitude drop was found to be acceptable, because the TMD was not working at its theoretically tuned frequency. It was seen in the results that as the frequency gets further away from tuning frequency, effect of the TMD decreases. Amplitude in the second bending mode increased as the TMD activated. Since natural frequency of the second mode was further away from TMD's tuned frequency, this result was found acceptable. It was expected that natural frequencies of these modes drop due to the increased damping, but natural frequency of these modes increased slightly. Reason for that was by activating the TMD, spring system tends to shift the natural frequency of the whole system to its tuned frequency and its harmonics.

At the end of the thesis study, a TMD based on ECD was successfully designed, analyzed and tested. Errors between theoretical and experimental results were found acceptable.

REFERENCES

[1] F. Yang, R. Sedaghati, E. Esmailzadeh, Vibration suppression of structures using tuned mass damper technology: A state-of-the-art review, Journal of Vibration and Control. 28 (2022) 812–836. https://doi.org/10.1177/1077546320984305.

[2] J. Ormondroyd, Theory of the Dynamic Vibration Absorber, in: 1928. https://www.semanticscholar.org/paper/Theory-of-the-Dynamic-Vibration-Absorber-Ormondroyd/db017dc2d8a73b61066212591675125cf68804a7 (accessed May 23, 2023).

[3] J.E. Brock, A Note on the Damped Vibration Absorber, Journal of Applied Mechanics. 13 (2021) A284. https://doi.org/10.1115/1.4009588.

[4] R. Lewandowski, Dynamic behaviour of composite mass damper for control of wind-excited vibration, (2003). https://www.academia.edu/25384687/Dynamic_behaviour_of_composite_mass_damper_for_control_of_wind_excited_vibration (accessed May 23, 2023).

[5] C. Li, B. Zhu, Estimating double tuned mass dampers for structures under ground acceleration using a novel optimum criterion, Journal of Sound and Vibration. 298 (2006) 280–297. https://doi.org/10.1016/j.jsv.2006.05.018.

[6] K. Xu, T. Igusa, Dynamic characteristics of multiple substructures with closely spaced frequencies, Earthquake Engineering & Structural Dynamics. 21 (1992) 1059–1070. https://doi.org/10.1002/eqe.4290211203.

[7] T. Igusa, K. Xu, Vibration Control Using Multiple Tuned Mass Dampers, Journal of Sound and Vibration. 175 (1994) 491–503. https://doi.org/10.1006/jsvi.1994.1341.

[8] M. Gu, H. Xiang, Optimization of TMD for suppressing buffeting response of long-span bridges, Journal of Wind Engineering and Industrial Aerodynamics. 42 (1992) 1383–1392. https://doi.org/10.1016/0167-6105(92)90146-2.

[9] T.-P. Chang, C.-Y. Chang, Vibration analysis of beams with a two degree-of-freedom spring-mass system, International Journal of Solids and Structures. 35 (1998) 383–401. https://doi.org/10.1016/S0020-7683(97)00037-1.

[10] S.J. Dyke, Acceleration Feedback Control Strategies for Active and Semi-Active Control Systems: Modelling, Algorithm Development and Experimental Verification, 1996.

[11] E. Diez-Jimenez, R. Rizzo, M.-J. Gómez-García, E. Corral-Abad, Review of Passive Electromagnetic Devices for Vibration Damping and Isolation, Shock and Vibration. 2019 (2019) e1250707. https://doi.org/10.1155/2019/1250707.

[12] J.-S. Bae, J.-H. Hwang, J.-S. Park, D.-G. Kwag, Modeling and experiments on eddy current damping caused by a permanent magnet in a conductive tube, J Mech Sci Technol. 23 (2009) 3024–3035. https://doi.org/10.1007/s12206-009-0819-0.

[13] T. van Beek, K. Pluk, H. Jansen, E. Lomonova, Optimisation and measurement of eddy current damping in a passive tuned mass damper, IET Electric Power Applications. 10 (2016) 641–648. https://doi.org/10.1049/iet-epa.2015.0445.

[14] C.S. MacLatchy, P. Backman, L. Bogan, A quantitative magnetic braking experiment, American Journal of Physics. 61 (1993) 1096–1101. https://doi.org/10.1119/1.17356.

[15] B. Irvine, M. Kemnetz, A. Gangopadhyaya, T. Ruubel, Magnet traveling through a conducting pipe: A variation on the analytical approach, American Journal of Physics. 82 (2014) 273–279. https://doi.org/10.1119/1.4864278.

[16] N. Derby, S. Olbert, Cylindrical magnets and ideal solenoids, American Journal of Physics. 78 (2010) 229–235. https://doi.org/10.1119/1.3256157.

[17] W.H. Hayt, Jr., J.A. Buck, Engineering Electromagnetics, 8th ed., McGraw-Hill, New York, 2012.

[18] Rao,Singiresu S., Mechanical Vibrations, 5th ed., Prentice Hall, 2010.

[19] R.G. Budynas, J.K. Nisbett, Shigley's Mechanical Engineering Design, 9th ed., McGraw-Hill, 2011.

[20] T.L. Schmitz, S.K. Smith, Mechanical Vibrations Modeling and Measurement, Springer, 2012.

[21] Samarium Cobalt Magnets, SmCo Magnets Datasheet, (2023). https://www.eclipsemagnetics.cn/site/assets/files/2418/samarium_cobalt_magnets_datasheet.pdf (accessed June 5, 2023).

[22] NdFeB Magnets, Neodymium Iron Boron Magnets Datasheet, (2023). https://www.eclipsemagnetics.com/site/assets/files/19485/ndfeb_neodymium_iron_boron-standard_ndfeb_range_datasheet_rev1.pdf (accessed June 5, 2023).

[23] Aluminum 6061-T6; 6061-T651, (2023). https://www.matweb.com/search/datasheet_print.aspx?matguid=1b8c06d0ca7c456694c7777d9e10be5b (accessed June 10, 2023).

[24] Oxygen-free electronic Copper, UNS C10100, (2023). https://www.matweb.com/search/datasheet_print.aspx?matguid=25cdd9bd3ebb4941be91cb0bee4cc661 (accessed June 10, 2023).

[25] Oxygen-free high conductivity Copper, Soft, UNS C10200, (2023). https://www.matweb.com/search/datasheet.aspx?matguid=a629b7c5643b44bfb25b9bba7f8140ab&ckck=1 (accessed June 10, 2023).

[26] Copper Alloy, UNS C10910, H02 Temper, Flat Products, (2023). https://www.matweb.com/search/datasheet.aspx?matguid=21f6a1ee0d6a49bf846735c607f15faa (accessed June 10, 2023).

[27] Electrolytic Tough Pitch (ETP) Copper, UNS C11000, OSO50 Temper flat products, rod, tube, shapes, (2023). https://www.matweb.com/search/datasheet_print.aspx?matguid=41a3ab3af15a4ca7b8d558b974d8eb51 (accessed June 10, 2023).

[28] Titanium Alloy UNS R50400, (2023). https://asm.matweb.com/search/SpecificMaterial.asp?bassnum=MTU020 (accessed June 10, 2023).

[29] Titanium Alloy UNS R56400, (2023). https://asm.matweb.com/search/SpecificMaterial.asp?bassnum=mtp641 (accessed June 10, 2023).

[30] Liang, Zach, Lee, George C., Random Vibration: Mechanical, Structural, and Earthquake Engineering Applications, 1st ed., Taylor & Francis Group, 2015.

[31] Nestorovic, Tamara, Trajkov, Miroslav, Patalong, Matthias, Identification of modal parameters for complex structures by experimental modal analysis approach, Advances in Mechanical Engineering. (2016). https://doi.org/10.1177/1687814016649110.